

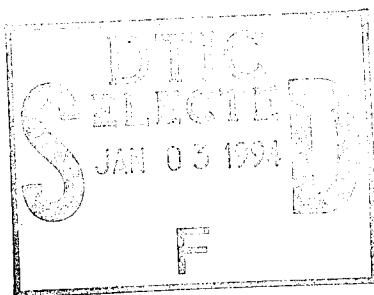
19941228 001

This document has been approved  
for public release and sale; its  
distribution is unlimited.

DEPARTMENT OF THE AIR FORCE  
AIR UNIVERSITY  
**AIR FORCE INSTITUTE OF TECHNOLOGY**

Wright-Patterson Air Force Base, Ohio

AFIT/GAP/ENP/94D-11



HIGH RESOLUTION FOURIER TRANSFORM  
SPECTROSCOPY OF THE FIRST OVERTONE OF  
THE N-O STRETCH IN NITROSYL BROMIDE

THESIS

Todd E. Wiest, Second Lieutenant, USAF  
AFIT/GAP/ENP/94D-11

Accession For	
NTIS CRA&I	<input checked="checked" type="checkbox"/>
DTIC TAB	<input type="checkbox"/>
Unannounced	<input type="checkbox"/>
Justification	
By	
Distribution/	
Availability Codes	
Dist	Avail and/or Special
A-1	

DTIC QUALITY INSPECTED 2

Approved for public release; distribution unlimited

The views expressed in this thesis are those of the author and do not reflect the official policy or position of the Department of Defense of the U. S. Government.

HIGH RESOLUTION FOURIER TRANSFORM  
SPECTROSCOPY OF THE FIRST OVERTONE OF  
THE N-O STRETCH IN NITROSYL BROMIDE

THESIS

Presented to the Faculty of the School of Engineering  
of the Air Force Institute of Technology  
Air University

In Partial Fulfillment of the  
Requirements for the Degree of  
Master of Science in Engineering Physics

Todd E. Wiest, B.S.  
Second Lieutenant, USAF

September 1994

Approved for public release; distribution unlimited

## *Preface*

This research is an investigation of the  $v_1 = 0 \rightarrow v_1 = 2$  transition of nitrosyl bromide to expand the understanding of the role this molecule plays in the depletion of the ozone layer and the  $\text{Br}^*/\text{NO}$  energy transfer laser. The most recent work done on this transition was completed almost two decades ago. With the improvements in technology, the resolution of this work is two orders of magnitude higher than the previous study. This exploration required knowledge in a plethora of subject fields from vacuum system construction to chemical kinetics to numerical analysis. Since this inquiry was done to study the rotational energy manifold on the vibrational transition, a knowledge of quantum mechanics and the interaction of light and matter proved essential. Even though this knowledge was obtained through class work, applying this "lecture" knowledge in the laboratory proved to be an exciting and sometimes vexing experience.

I would like to express my gratitude to my advisor, Major Glen P. Perram, for his open door policy, support, and encouragement throughout a research project which moved AFIT into a new realm of molecular study - asymmetric molecules. Thanks also go to Dr. David Weeks for the numerous hours of theoretical quantum mechanics discussions which lead to the understanding of the asymmetric top theory. Although Dr. Weeks showed me solutions for the UNIX enigma, Captain Charlie Brennan always took time out to steer me through the cold, iceberg-laden sea of this operating system. Finally, I owe a solid day of time and a big hug to my fiancée, Jerianne Shelton, who supported me through the long nights of computation and revision; thank you, Jerianne.

Todd E. Wiest

## *Table of Contents*

<b>Preface.....</b>	<b>ii</b>
<b>List of Figures .....</b>	<b>v</b>
<b>List of Tables .....</b>	<b>vii</b>
<b>Abstract.....</b>	<b>viii</b>
<b>1. Introduction.....</b>	<b>1</b>
1.1 Overview .....	1
1.2 Preliminary Considerations .....	4
1.3 Problem Statement.....	4
<b>2. Background .....</b>	<b>6</b>
2.1 Summary of Current Knowledge.....	6
2.2 Theory.....	9
2.3 Energy Level Approximation .....	19
2.3.1 Theoretical Development of the Approximation.....	19
2.3.2 Accuracy of the Approximation .....	22
<b>3. Experimental Apparatus and Procedures .....</b>	<b>26</b>
3.1 Fourier Transform Spectrometer .....	26
3.1.1 Theory of Operation .....	26
3.1.2 Bomem Fourier Transform Spectrometer .....	29
3.1.3 Data Collection and Spectrum Analysis Software .....	30
3.2 Vacuum System.....	31
3.3 Absorption Cell .....	32
3.4 Creation of ONBr .....	33
<b>4. Results .....</b>	<b>36</b>
4.1 Data Collection.....	36
4.2 Spectrum Analysis .....	38
4.3 Spectral Assignment.....	41
<b>5. Discussion .....</b>	<b>46</b>
5.1 Validation of Spectral Assignment.....	47
5.1.1 Limits of Analytical $\Delta_2$ Expressions .....	48
5.1.2 $\Delta_2$ Fits to $v_1 = 0 \rightarrow v_1 = 2$ Spectrum .....	51
5.2 Global Fitting Routine .....	57
5.2.1 Approach .....	57
5.2.2 Implementation.....	59
5.3 Determination of the Valid Range of J and the Rotational Constants.....	62
<b>6. Conclusion .....</b>	<b>70</b>
6.1 Summary.....	70
6.2 Recommendations for Future Work .....	73
<b>Bibliography .....</b>	<b>75</b>

<b>Appendix A: Simplification of the Rotational Hamiltonian .....</b>	<b>77</b>
<b>Appendix B: Second Difference Plots and Residuals .....</b>	<b>83</b>
<b>Appendix C: Mathematica<sup>®</sup> Codes .....</b>	<b>91</b>
<b>Appendix D: List of Transitions .....</b>	<b>98</b>
<b>Vita .....</b>	<b>105</b>

## List of Figures

<b>Figure 2-1.</b> Nitrosyl bromide in the $I'$ representation where the molecule lies in the <b>a-c</b> plane of the body fixed coordinate system.....	12
<b>Figure 3-1.</b> Michelson Interferometer. <i>a.</i> source, <i>b.</i> aperture, <i>c.</i> collimating mirror, <i>d.</i> beamsplitter, <i>e.</i> movable mirror, <i>f.</i> fixed mirror, <i>g.</i> focusing mirror, <i>h.</i> spectral filters, <i>i.</i> sample cell, and <i>j.</i> detector.....	26
<b>Figure 3-2.</b> Typical interference pattern produced by a monochromatic source.....	28
<b>Figure 3-3.</b> Vacuum system used to create nitrosyl bromide. <i>a.</i> distillation tubes to purify the $Br_2$ .....	31
<b>Figure 4-1.</b> Raw spectrum of 19.10 Torr of ONBr. Notice the somewhat linear trends in the intensity at both ends of the spectrum and the density of the spectral features. ...	37
<b>Figure 4-2.</b> Background spectrum taken to eliminate various absorption phenomena not connected to absorption by ONBr.....	38
<b>Figure 4-3.</b> Absorbance spectrum of ONBr where the spectral features (lines) corresponding to absorption transitions are positive. ....	39
<b>Figure 4-4.</b> Blow up of ONBr absorbance spectrum in the R branch. Lines above the spectral features depict the different $K_a, K_c$ lines for a particular $J$ . ....	40
<b>Figure 5-1.</b> Second difference data and curve fit for the trend from $J_{0,J}$ to $J_{2,J-2}$ as a function of $J$ for $J < 40$ . Transitions used to generate data points were obtained from Esposti <i>et al.</i> <sup>4</sup> Expression fit without distortion parameters in expression.....	49
<b>Figure 5-2.</b> Same $\Delta_2$ fit as above for $J < 70$ . ....	50
<b>Figure 5-3.</b> Curve fit for $\Delta_2$ trend from $J_{0,J}$ to $(J+1)_{0,(J+1)}$ . The fine balance between the parameters results in the fit of a twelfth order polynomial to a linear set of data without overfitting. ....	52
<b>Figure 5-4.</b> Residuals for trend shown in Figure 5-3. Note that the upper and lower bound of the residual axis is equal to the resolution of the spectrometer. Also note that all residuals lie within this region. ....	53
<b>Figure 5-5.</b> Example of overfitting in $v_1 = 0 \rightarrow v_1 = 2$ data resulting from the loss of the fine balance between rotational parameters in the approximate energy level expressions when the approximation breaks down.....	54
<b>Figure 5-6.</b> $\Delta_2$ trend fit with appropriate equation for valid region of $J$ . ....	55
<b>Figure 5-7.</b> Residuals of fit in Figure 5-6. All residuals are within $0.02 \text{ cm}^{-1}$ .....	55
<b>Figure 5-8.</b> Overfitting resulting from the apparent break down of the approximation for this trend which could be attributable to inappropriate expansion coefficients.....	56



<b>Figure 5-9.</b> Residuals of the P branch transitions. Dotted lines represent the resolution bounds and each symbol represents a different combination of $K_a$ and $K_c$ .	64
<b>Figure 5-10.</b> Residuals of $J_{0,J}$ transitions for the asymmetry expansion and diagonalization procedures. Rotational parameters used for both methods are found in Table 5-3.	65
<b>Figure 5-11.</b> Difference in the transitions calculated with the diagonalization method and the transitions obtained from the global fit based on the asymmetry approximation method. The smooth trend in this plot clearly shows the dynamic breakdown of the approximation for $J > 25$ .	66
<b>Figure B-1.</b> Second difference for the trend from $J_{0,J}$ to $J_{1,J}$ . Blending is the cause of the scattering of the locations in the region from $J = 6$ to $J = 13$ .	83
<b>Figure B-2.</b> Residuals of fit above. Even though the transition differences in the $J = 6$ to $J = 13$ range looked bad, the residuals are still within the resolution.	83
<b>Figure B-3.</b> Second difference for the trend from $J_{0,J}$ to $J_{2,J-1}$ . Once again, the effects of blending can be seen in the assignments.	84
<b>Figure B-4.</b> Residuals of second difference fit above.	84
<b>Figure B-5.</b> Second difference for the trend from $J_{0,J}$ to $J_{2,J-2}$ .	85
<b>Figure B-6.</b> Residuals of the $J_{0,J}$ to $J_{2,J-2}$ trend.	85
<b>Figure B-7.</b> Second difference from $J_{0,J}$ to $J_{3,J-2}$ in the P branch. Note the ability to fit these transitions for the reduced range of $J$ .	86
<b>Figure B-8.</b> Residuals from the fit above.	86
<b>Figure B-9.</b> Break down of the asymmetry approximation occurs for this trend above $J = 22$ . The transitions that were fit in Figure B-7 in the region between $J = 20$ and $J = 25$ are not fit well.	86
<b>Figure B-10.</b> Trend from $J_{0,J}$ to $J_{3,J-3}$ .	87
<b>Figure B-11.</b> Residuals for the trend fit above.	87
<b>Figure B-12.</b> Difference in assignments for the $J_{0,J}$ and $J_{4,J-4}$ levels.	88
<b>Figure B-13.</b> Distance from the fit to the differences in the transitions used above.	88
<b>Figure B-14.</b> Trend from $J_{0,J}$ to $J_{5,J-5}$ .	89
<b>Figure B-15.</b> Residuals from above fit.	89
<b>Figure B-16.</b> Fit for the $J_{0,J}$ to $J_{6,J-6}$ trend.	90
<b>Figure B-17.</b> Residuals for the above fit.	90

## *List of Tables*

<b>Table 2-1.</b> Bond lengths in ONBr as measured with different experimental techniques. <sup>5</sup>	6
<b>Table 2-2.</b> NO bond stretch frequencies in $\text{cm}^{-1}$ of ONBr for isotopes of N and O. <sup>5</sup>	7
<b>Table 2-3.</b> Force constants of ONBr. <sup>5</sup>	7
<b>Table 2-4.</b> Molecular constants for the $\nu_1$ fundamental band for both isotopomers. Band origins in $\text{cm}^{-1}$ , rotational constants in MHz. Standard errors in units of the last quoted digit are in parentheses for the fitted constants. *Both levels share common value. <sup>4</sup>	9
<b>Table 5-1.</b> Molecular constants for $\text{ON}^{79}\text{Br}$ for the $\nu_1$ fundamental band as published and determined by this research. All rotational parameters, band origins, and $\sigma$ 's in $\text{cm}^{-1}$ . Standard errors in units of the last quoted digit are given in parentheses for the constants.	61
<b>Table 5-2.</b> Rotational parameters obtained from fit to observed transitions for $J \leq 40$ . Rotational parameters, band origin, and $\sigma$ are given in $\text{cm}^{-1}$ and $\epsilon$ is unitless.	63
<b>Table 5-3.</b> Molecular constants for $\text{ON}^{79}\text{Br}$ . All values are in $\text{cm}^{-1}$ except the number of transitions. Numbers in parentheses represent the error in the last digit.	67

## *Abstract*

Infrared Fourier transform spectroscopy of the first overtone of the nitric oxide (NO) bond stretch in nitrosyl bromide (ONBr) has been performed at a resolution of  $0.02 \text{ cm}^{-1}$  to obtain the rotational parameters of the  $v_1 = 2$  energy level. On the order of 1000 transitions have been observed for rotational levels up to  $J = 80$  and  $K_a = 7$ . The calculation of the complete set of rotational energy levels of this asymmetric molecule requires the numerical diagonalization of four, tridiagonal matrices for each  $J$ . A non-linear least squares fit of observed transitions with  $J \leq 40$  was accomplished using an approximation for the energy levels. From this fit, the maximum  $J$  value accurately approximated was determined to be twenty-four. The fit was reaccomplished for  $J \leq 24$  and the following rotational parameters were obtained:  $\nu_o = 3563.03442 \pm 0.00092$ ,  $A = 2.793526 \pm 0.000055$ ,  $B = 0.1264969 \pm 0.0000056$ ,  $C = 0.1207390 \pm 0.0000022$ ,  $\Delta_J = (1.649 \pm 0.038) \times 10^{-7}$ ,  $\Delta_{JK} = (-2.23 \pm 0.17) \times 10^{-6}$ ,  $\Delta_K = (1.577 \pm 0.025) \times 10^{-4}$ , and  $\delta_J = (1.22 \pm 0.29) \times 10^{-8} \text{ cm}^{-1}$ . Monte Carlo techniques were used to determine the errors in the reported constants, and this analysis suggests the need to use higher  $J$  levels to determine the distortion constants.

# HIGH RESOLUTION FOURIER TRANSFORM SPECTROSCOPY OF THE FIRST OVERTONE OF THE N-O STRETCH IN NITROSYL BROMIDE

## 1. Introduction

### *1.1 Overview*

Nitrosyl bromide, ONBr, is a member of the nitrosyl halide family of molecules. This family also contains nitrosyl fluoride (FNO), nitrosyl chloride (ONCl), and nitrosyl iodide (INO). There are two major reasons to investigate these molecules: the halogens in these compounds have been linked to the chemical reactions believed to describe the ozone depletion cycle<sup>1</sup> and the nitrosyl halides are a constituent produced in the reactions of possible infrared laser sources that rely on the transfer of energy from an electronic energy level of an excited halogen (F, Cl, I, Br) to a vibrational energy level in nitric oxide (NO).<sup>2</sup> Much spectroscopic work has been completed on the other nitrosyl halides (FNO, ONCl, INO) to understand their vibrational and rotational structure, but only limited work has been reported for nitrosyl bromide. This research seeks to increase the knowledge of the energy levels of nitrosyl bromide to help provide an understanding of the role of the molecule in the two applications mentioned above.

The depletion of the ozone layer over Antarctica has been linked to chlorofluorocarbons (CFCs). These chemicals contain halogens that deplete the ozone through reactions:<sup>1</sup>



where X represents the halogen (Cl, F, Br, or I). These three reactions have the net effect of ozone depletion:<sup>1</sup>



Notice that in reaction (1.2) the halogen appears on the right side of the reaction which implies that it may react as shown in (1.1). If, however, this halogen encounters a nitric oxide molecule produced from reaction (1.3), the halogen in (1.2) may react with the NO molecule to form the nitrosyl halide:



where ONX is the nitrosyl halide. This reaction would limit the concentration of the halogen and thus assist in decreasing the rate of ozone depletion.

The other reason to investigate these halides arises from an Air Force requirement to develop an airborne, laser-based countermeasure system. This system would be mounted either internal or external and be required to use limited power from the aircraft.<sup>2</sup> Other requirements of the system include the power of the infrared (IR) laser to be in the kilowatt-class with wavelength tunability in the 3 to 5  $\mu\text{m}$  region to prevent simple filtering as a counter-countermeasure.<sup>2</sup> To achieve the power required over distances at

which the system would be used, minimal divergence is desired, and the cavity configuration must allow for operation on the vibrating aircraft.<sup>2</sup>

One of the possible candidates for this system is the Br\*/NO energy transfer laser in which the excited bromine (Br\*) transfers its electronic energy to vibrational energy in the NO. This places the NO in the second vibrational energy level which relaxes to the first vibrational state with the emission of a photon in the IR region. This photon results from a transition which meets the appropriate selection rules from one of approximately thirty rotational energy levels in the second vibrational state to a rotational energy level in the first vibrational state. The large number of possible energy differences produced in the transitions creates photons of many different wavelengths and thus provides the tunability required. The main complication involved in creating this system arises from the fact that Br<sub>2</sub> and NO will react spontaneously to form ONBr when the mixture is allowed to equilibrate under room lights.<sup>3</sup> Since the formation of this molecule drastically depletes the populations of NO and Br, it appears that the creation of this molecule severely limits the system performance, however, it has been reported that photolysis of a cell containing Br<sub>2</sub> and NO may create Br which can then react with the ONBr:<sup>3</sup>



to increase the population of the NO and generate more Br<sub>2</sub> which can then be converted to Br\*. To understand this reaction, the potential energy curves of ONBr must be known. The creation of the ONBr potential energy curves requires a knowledge of the molecular constants for rotation and vibration.

The most recent work on nitrosyl bromide was accomplished by Esposti *et al*<sup>4</sup> using a Fourier transform spectrometer to study the absorption of IR light by ONBr. This study refined the molecular coefficients found by Laane *et al*<sup>5</sup> for the fundamental band ( $\nu_1 = 0 \rightarrow \nu_1 = 1$ ) of the NO bond stretch frequency in nitrosyl bromide. To gain more understanding of the rotational levels of the molecule, this research will study the first overtone ( $\nu_1 = 0 \rightarrow \nu_1 = 2$ ) of the NO bond stretch in the molecule.

## 1.2 Preliminary Considerations

The NO bond in nitrosyl bromide first absorbs IR light at a wavelength of approximately 5.5  $\mu\text{m}$  ( $\nu_1 = 0 \rightarrow \nu_1 = 1$ ), and the next absorption band of this stretch ( $\nu_1 = 0 \rightarrow \nu_1 = 2$ ) occurs in the 2.8  $\mu\text{m}$  region. These two regions also contain the absorption of light by nitric oxide, 5.3  $\mu\text{m}$  for the  $\nu = 0 \rightarrow 1$  and 2.7  $\mu\text{m}$  for the  $\nu = 0 \rightarrow 2$ . In both of these regions, the presence of nitric oxide can cause a difficulty in the assignment of the nitrosyl bromide spectrum. Much work has been done to characterize the energy levels of nitric oxide by Nichols *et al*<sup>6</sup> and Olman *et al*.<sup>7</sup> These studies, along with a study completed as part of this research, aided in the removal of any spectral features resulting from unreacted nitric oxide. The removal of these lines subsequently aided in the proper assignment of the absorption lines of nitrosyl bromide.

## 1.3 Problem Statement

In the past few years, a considerable amount of work has been done at the Air Force Institute of Technology (AFIT) on the possible development and characterization of a Br\*/NO energy transfer laser to meet the Air Force airborne laser countermeasure

requirement. Also, as the Air Force and the world grow more environmentally oriented, the reactions involved in the depletion of the ozone layer have become an important issue. To understand the role of the nitrosyl bromide in both of these applications, the potential energy curves of the molecule must be known. However, the complete curves cannot be created until a firm understanding of the different vibrational bands are known. Since only the fundamental vibrational band of the NO bond stretch has been documented, it is the goal of this research to expand the knowledge of this molecule to the first overtone of the NO bond stretch. To accomplish this goal, ONBr must be created from NO and distilled Br<sub>2</sub>, a spectrum of the first overtone of the NO bond stretch in ONBr must be recorded, and this spectrum must be analyzed to determine the molecular constants governing the motion of the molecule.



## 2. Background

### 2.1 Summary of Current Knowledge

One of the earliest studies done to understand nitrosyl bromide was completed by Laane *et al.*<sup>5</sup> This work studied the fundamental and combination vibrational bands of the three vibrations of nitrosyl bromide, the NO bond stretch ( $\nu_1$ ), the bending of the molecule ( $\nu_2$ ), and the NBr stretch ( $\nu_3$ ), and determined the force constants associated with the general quadratic valence force field (GQVFF) constants. These values were obtained for all possible combinations of the isotopes of bromine ( $^{81}\text{Br}$  and  $^{79}\text{Br}$ ), oxygen ( $^{16}\text{O}$  and  $^{18}\text{O}$ ), and nitrogen ( $^{14}\text{N}$  and  $^{15}\text{N}$ ). Also, this paper discussed and tabulated the potential energy distribution, mean amplitudes, coriolis constants, and inertial defect data for specific isotope combinations.

The information applicable to this research includes the NO bond stretch frequencies and the cited bond lengths and bond angle. The bond lengths appear in Table 2-1, the NO stretch frequencies in Table 2-2, and Table 2-3 contains the force constants obtained from the study.

**Table 2-1.** Bond lengths in ONBr as measured with different experimental techniques.<sup>5</sup>

<i>Bond</i>	<i>Microwave (Å)</i>	<i>e- Diffraction (Å)</i>
N - O	1.15	1.15
N - Br	2.14	2.14
Br - O	2.81	2.85
Bond Angle	No Data	117°

**Table 2-2.** NO bond stretch frequencies in  $\text{cm}^{-1}$  of ONBr for isotopes of N and O.<sup>5</sup>

	$^{16}\text{O}^{14}\text{NBr}$	$^{16}\text{O}^{15}\text{NBr}$	$^{18}\text{O}^{14}\text{NBr}$	$^{18}\text{O}^{15}\text{NBr}$
$\nu_1$	1799.0	1768.3	1751.5	1719.5
$2\nu_1$	3562.1	3503.1	3470.9	3408.1
$3\nu_1$	5296	5206	5158	5066
$4\nu_1$	6994	6878	No Data	6695

**Table 2-3.** Force constants of ONBr.<sup>5</sup>

	Calculated Value
$F_{\text{NO}}$	$15.25 \pm 0.04 \text{ md/\AA}$
$F_{\text{NBr}}$	$1.13 \pm 0.05 \text{ md/\AA}$
$F_{\alpha}$	$1.13 \pm 0.02 \text{ md \AA/rad}^2$
$F_{\text{NO,NBr}}$	$1.47 \pm 0.36 \text{ md/\AA}$
$F_{\text{NO},\alpha}$	$0.11 \pm 0.20 \text{ md \AA/rad}$
$F_{\text{NBr},\alpha}$	$0.10 \pm 0.02 \text{ md \AA/rad}$

These values were obtained by the analysis of spectral data collected at  $2 \text{ cm}^{-1}$  resolution. The experimental equipment included a Perkin-Elmer 521, Beckman IR 11, and a Cary 14 for the spectral regions of  $4000\text{-}300 \text{ cm}^{-1}$ ,  $300\text{-}200 \text{ cm}^{-1}$ , and  $>4000 \text{ cm}^{-1}$ , respectively.

Since the above study was done at  $2 \text{ cm}^{-1}$  resolution, Esposti *et al* studied the NO stretch for the  $\nu_1 = 0 \rightarrow \nu_1 = 1$  transition again at  $0.0045 \text{ cm}^{-1}$ .<sup>4</sup> This study focused on determining the band origin and rotational constants for this transition and used this

information to determine the cubic force constants for both isotopomers ( $\text{ON}^{79}\text{Br}$  and  $\text{ON}^{81}\text{Br}$ ).

To study this transition, Esposti *et al* prepared nitrosyl bromide by mixing NO and gaseous bromine at room temperature in a 20 cm long glass cell equipped with calcium fluoride ( $\text{CaF}_2$ ) windows.<sup>4</sup> The  $\nu_1$  spectrum of the 2 mbar sample was recorded with a Bruker IFS 120HR Fourier transform spectrometer at the aforementioned resolution. A globar source was used with a potassium bromide (KBr) beamsplitter, and the spectrum was recorded with a mercury cadmium telluride (HgCdTe) detector. Calibration of the spectrum was accomplished by comparing the location of absorption lines due to residual water in the spectrometer with the reported locations as cited in the *Handbook of Infrared Standards*.<sup>8</sup> This research observed only a-type transitions ( $\Delta K_a = 0$ ) where the P and R branches were dominant with a weaker Q branch feature found on the shoulder of the P branch. Transitions for rotational levels up to  $J = 70$  and  $K_a = 10$  were observed in the very dense structure for both isotopomers. The band origins and rotational constants for  $\text{ON}^{79}\text{Br}$  and  $\text{ON}^{81}\text{Br}$  obtained by this research appear in Table 2-4.

**Table 2-4.** Molecular constants for the  $\nu_1$  fundamental band for both isotopomers. Band origins in  $\text{cm}^{-1}$ , rotational constants in MHz. Standard errors in units of the last quoted digit are in parentheses for the fitted constants. \*Both levels share common value.<sup>4</sup>

	$\text{ON}^{79}\text{Br}$		$\text{ON}^{81}\text{Br}$	
	$\nu_1 = 0$	$\nu_1 = 1$	$\nu_1 = 0$	$\nu_1 = 1$
$\nu_0$	1798.751285(53)		1798.742722(57)	
A	85500.4620	84720.73(11)	85482.944	84703.09(11)
B	3747.07053	3762.6039(44)	3722.34778	3737.8017(47)
C	3585.98785	3598.9833(39)	3563.30894	3576.2520(43)
$\Delta_J (10^{-3})$	2.852185	2.88560(37)	2.816479	2.84996(39)
$\Delta_{JK} (10^{-2})$	-5.69179	-5.6952(27)	-5.66109	-5.6676(31)
$\Delta_K$	4.8255	4.7272(12)	4.8052	4.7096(13)
$\delta_J (10^{-4})$	1.57887	1.6145(47)	1.54934	1.5881(51)
$\delta_K (10^{-2})^*$	1.9859		1.938	
$\Phi_J (10^{-10})^*$	4.068		4.068	
$\Phi_{JK} (10^{-7})^*$	1.2012		1.1179	
$\Phi_{KJ} (10^{-5})^*$	-2.9615		-2.9315	
$\Phi_K (10^{-10})^*$	2.149		2.149	

## 2.2 Theory

The Schrödinger equation for a molecule, neglecting translation, is given by:

$$\hat{H}_{s,v,r}\psi = E_{s,v,r}\psi \quad (2.1)$$

where  $\hat{H}_{s,v,r}$  is the Hamiltonian describing the motion of the molecule and  $E_{s,v,r}$  is the energy of the molecule which can be broken into the following:<sup>9</sup>

$$E_{s,v,r} = E_s + E_v + E_r \quad (2.2)$$

where  $E_s$  is the electronic energy,  $E_v$  is the vibrational energy, and  $E_r$  is the rotational energy of the molecule. By using the Born-Oppenheimer approximation, the electronic energy can be found by solving the Schrödinger equation for the motion of the electrons. This solution yields values for the electronic energy which are dependent upon the nuclear separation. These electronic energy eigenvalues can then be used to generate the potential energy surfaces for the ground and excited states of the molecule. With the potential energy surfaces known, the nuclear motion can be studied by solving for the vibrational energy eigenvalues from the Schrödinger equation for this motion. To complete the solution of the Schrödinger equation in (2.1), the rotational energy eigenvalues must be computed.

For triatomic molecules like nitrosyl bromide, the computation of the eigenvalues for the rotational energy levels is difficult. This difficulty begins with three different principle moments of inertia resulting from the unequal distribution of the mass of the nuclei (the ratio of the atomic weights being 5.70:1.14:1.00 for Br:O:N). The computation of eigenvalues is further complicated by the rotationally induced distortion of the molecule, particularly at high values of angular momentum.

The classification of an asymmetric molecule, or rotor, is dependent upon the values of the three principle moments of inertia. These moments of inertia can be labeled as  $I_a$ ,  $I_b$ , and  $I_c$  where  $I_c$  denotes the largest moment of inertia,  $I_b$  the next largest moment, and  $I_a$  the smallest. The inverse of these quantities, when multiplied by the appropriate constants, yield the rotational constants of the rotor:<sup>10</sup>

$$B_{\alpha} = \frac{\hbar^2}{2hcI_{\alpha}} \quad (2.3)$$

where  $\alpha$  is either a, b, or c. The body fixed axes can then be labeled **a**, **b**, **c** and the notation A, B, C is then used to denote  $B_a$ ,  $B_b$ , and  $B_c$ , respectively.<sup>10</sup> The body fixed system is used to describe the molecular orientation since the moments of inertia are constant, with the classification of the symmetry of the rotor being defined by the value of B.

A rotor is classified as asymmetric when the values of the rotational parameters are such that  $A \neq B \neq C$ . The bounds of the value of B are given by the A and C values. When  $A = B$ , the rotor is symmetric and classified as oblate while the prolate symmetric case is one in which  $B = C$  for the rotor. There are numerous formulas that can be used to determine the degree of asymmetry associated with the rotor when  $A \neq B \neq C$ , but the asymmetry of any rotor can be found by:<sup>11</sup>

$$\kappa = \frac{2B - A - C}{A - C} \quad (2.4)$$

where  $\kappa$  is the asymmetry parameter and takes on the value of 1 for the oblate case and -1 for the prolate case.

Nitrosyl bromide is nearly prolate ( $B \approx C$ ) with an asymmetry parameter of -0.996.<sup>4</sup> By using the  $\Gamma$  representation given in Watson,<sup>10</sup> all molecules are represented as shown in Figure 2-1.

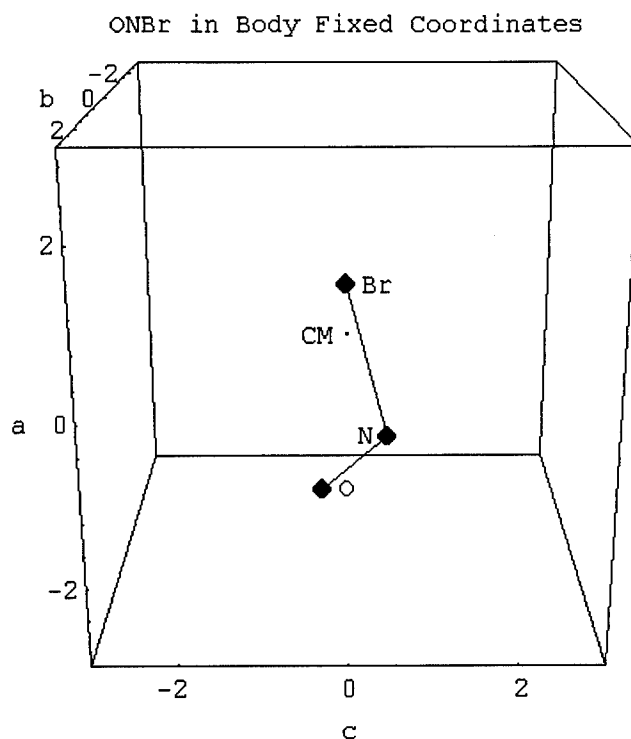


**Figure 2-1.** Nitrosyl bromide in the  $I^r$  representation where the molecule lies in the **a-c** plane of the body fixed coordinate system.

The initial form of the Hamiltonian describing the rotational motion of ONBr can be found by invoking the rigid rotor approximation. The Hamiltonian for this approximation is:<sup>10</sup>

$$\hat{H}_{\text{rigid}} = B\hat{J}_b^2 + C\hat{J}_c^2 + A\hat{J}_a^2 \quad (2.5)$$

where  $\hat{J}_b$ ,  $\hat{J}_c$ , and  $\hat{J}_a$  are the angular momentum operators about the **b**, **c**, and **a** axes, respectively. This Hamiltonian does not properly deal with the asymmetric nature of the rotor, however, since in the quantum-mechanical representation the matrices are not diagonal. The Hamiltonian in (2.5) can be rewritten for the prolate ( $B = C$ ) symmetric molecule as:

$$\hat{H}_{\text{rigid}} = C(\hat{J}_b^2 + \hat{J}_c^2 + \hat{J}_a^2) - C\hat{J}_a^2 + A\hat{J}_a^2 \quad (2.6)$$

The diagonalization of the Hamiltonian can be accomplished by invoking the following operator transformation:<sup>10</sup>

$$\begin{aligned} \bar{J}^2 &= \hat{J}_b^2 + \hat{J}_c^2 + \hat{J}_a^2 \\ \hat{J}_a &= \hat{J}_a \end{aligned} \quad (2.7)$$

Since  $B = C$ , the  $C$  parameter in (2.6) can be written as  $C = \frac{1}{2}(B + C)$  without loss of generality. With this substitution and the operator transformation in (2.7), the rigid rotor Hamiltonian for the symmetric case is:

$$\hat{H}_{\text{rigid}} = \frac{1}{2}(B + C)\bar{J}^2 + \left[ A - \frac{1}{2}(B + C) \right] \hat{J}_a^2 \quad (2.8)$$

where  $J$  is the total angular momentum and  $k$  is the projection of  $J$  along an axis fixed in space with the eigenvalues:

$$\begin{aligned} \langle J, k | \bar{J}^2 | J, k \rangle &= J(J + 1) \\ \langle J, k | \hat{J}_a^2 | J, k \rangle &= k^2 \end{aligned} \quad (2.9)$$

where the allowed ranges of these eigenvalues are  $J = 0, 1, 2, \dots$  and  $k = -J, -J+1, \dots, J-1, J$ .<sup>10</sup>

For the asymmetric molecule,  $B \neq C$  and instead of (2.6), we find the Hamiltonian for the asymmetric rigid rotor is:

$$\begin{aligned} \hat{H}_{\text{rigid}} &= \frac{1}{2}(B + C)\{\hat{J}_b^2 + \hat{J}_c^2 + \hat{J}_a^2\} + \frac{B}{2}\{\hat{J}_b^2 - \hat{J}_c^2\} \\ &\quad - \frac{C}{2}\{\hat{J}_b^2 - \hat{J}_c^2\} + \left[ A - \frac{B}{2} - \frac{C}{2} \right] \hat{J}_a^2 \end{aligned} \quad (2.10)$$

By using the transformation in (2.7) and noting that:



$$\frac{B}{2}\{\hat{j}_b^2 - \hat{j}_c^2\} - \frac{C}{2}\{\hat{j}_b^2 - \hat{j}_c^2\} = \left[A - \frac{B}{2} - \frac{C}{2}\right] \left(\frac{B-C}{2A-B-C}\right) \{\hat{j}_b^2 - \hat{j}_c^2\} \quad (2.11)$$

and:

$$A - \frac{B}{2} - \frac{C}{2} = A - \frac{1}{2}(B+C) \quad (2.12)$$

the rotational Hamiltonian for the asymmetric rigid rotor is:

$$\hat{H}_{\text{rigid}} = \frac{1}{2}(B+C)\bar{J}^2 + \left[A - \frac{1}{2}(B+C)\right] \left\{ \hat{j}_a^2 + \frac{B-C}{2A-B-C} (\hat{j}_b^2 - \hat{j}_c^2) \right\} \quad (2.13)$$

To model the distortion of the molecule as it rotates, a Hamiltonian with quartic and sextic centrifugal distortion terms is used where:<sup>10</sup>

$$\begin{aligned} \hat{H}_{\text{rot}}^{(A)} = & \mathcal{B}\hat{j}_b^2 + \mathcal{C}\hat{j}_c^2 + \mathcal{A}\hat{j}_a^2 - \Delta_J(\hat{j}^2)^2 - \Delta_{JK}\bar{J}^2\hat{j}_a \\ & - \Delta_K\hat{j}_a^4 - \frac{1}{2}\left[\delta_J\bar{J}^2 + \delta_K\hat{j}_a^2, \hat{j}_+^2 + \hat{j}_-^2\right]_+ + \Phi_J(\bar{J}^2)^3 \\ & + \Phi_{JK}(\bar{J}^2)^2\hat{j}_a^2 + \Phi_{KJ}\bar{J}^2\hat{j}_a^4 + \Phi_K\hat{j}_a^6 \\ & + \frac{1}{2}\left[\phi_J(\bar{J}^2)^2 + \phi_{JK}\bar{J}^2\hat{j}_a^2 + \phi_K\hat{j}_a^4, \hat{j}_+^2 + \hat{j}_-^2\right]_+ \end{aligned} \quad (2.14)$$

The  $\Delta_i$  and  $\delta_i$  coefficients represent the quartic effects of the centrifugal distortion, the  $\Phi_i$  and  $\phi_i$  coefficients represent the sextic effects to the centrifugal distortion, the operators are given by:

$$\begin{aligned} \bar{J}^2 &= \hat{j}_b^2 + \hat{j}_c^2 + \hat{j}_a^2 \\ \hat{j}_+ &= \hat{j}_b + i\hat{j}_c \\ \hat{j}_- &= \hat{j}_b - i\hat{j}_c \end{aligned} \quad (2.15)$$

the (A) superscript denotes the use of the inverse asymmetry parameter in (2.4) where A and B are interchanged to reduce the representation of the system to a more convenient

form, and with this choice of representation, the A, B, and C parameters are transformed to the  $\mathcal{A}$ ,  $\mathcal{B}$ , and  $\mathcal{C}$  parameters using the following transformation:

$$\begin{aligned}\mathcal{A} &= A + 2\Delta_J \\ \mathcal{B} &= B + 2\Delta_J + \Delta_{JK} - 2\delta_J - 2\delta_K \\ \mathcal{C} &= C + 2\Delta_J + \Delta_{JK} + 2\delta_J - 2\delta_K\end{aligned}\tag{2.16}$$

The matrix elements of this Hamiltonian in the  $|J, k\rangle$  basis are given as:<sup>10</sup>

$$\begin{aligned}E_{k,k} &= \langle J, k | \hat{H}_{\text{rot}}^{(A)} | J, k \rangle = \frac{1}{2}[\mathcal{B} + \mathcal{C}]J(J+1) + \left\{ \mathcal{A} - \frac{1}{2}[\mathcal{B} + \mathcal{C}] \right\} k^2 \\ &\quad - \Delta_J J^2(J+1)^2 - \Delta_{JK} J(J+1)k^2 - \Delta_K k^4 + \Phi_J J^3(J+1)^3 \\ &\quad + \Phi_{JK} J^2(J+1)^2 k^2 + \Phi_{KJ} J(J+1)k^4 + \Phi_K k^6 \\ E_{k\pm 2,k} &= \langle J, k \pm 2 | \hat{H}_{\text{rot}}^{(A)} | J, k \rangle = \left( \frac{1}{4}[\mathcal{B} + \mathcal{C}] - \delta_J J(J+1) \right. \\ &\quad \left. - \frac{1}{2}\delta_k [(k \pm 2)^2 + k^2] + \phi_J J^2(J+1)^2 \right. \\ &\quad \left. + \frac{1}{2}\phi_{JK} J(J+1)[(k \pm 2)^2 + k^2] + \frac{1}{2}\phi_K [(k \pm 2)^4 + k^4] \right) \\ &\quad \times \left\{ [J(J+1) - k(k \pm 1)][J(J+1) - (k \pm 1)(k \pm 2)] \right\}^{\frac{1}{2}}\end{aligned}\tag{2.17}$$

Notice that the  $|J, k\rangle$  basis does not diagonalize the Hamiltonian of the asymmetric molecule as can be seen in (2.17) where an expression for off diagonal terms is given.

The angular momentum does not have a component with a constant direction along a *body-fixed* axis of the rotating asymmetric molecule.<sup>11</sup>

Since the  $|J, k\rangle$  basis almost diagonalizes the rotational Hamiltonian for the asymmetric case and has physical meaning for the symmetric molecule, the definition of the required quantum numbers is almost determined. With the asymmetric case being the continuum between the symmetric prolate and oblate cases, the quantum numbers used are J, the total angular momentum,  $K_a$ , the quantum number used to label the energy

levels of the prolate symmetric top, and  $K_c$ , the quantum number used to label the energy levels of the oblate symmetric top. With these quantum numbers, the energy levels are labeled according to their possible  $k$  values for either the prolate or oblate case. This labeling is written as  $J_{K_a K_c}$ .

Physically, with the existence of two separate “ $k$ ” quantum numbers, the energy levels for any angular momentum are found to split as a result of the “ $k$ ” dependence of the matrix elements in (2.17). This phenomenon, known as *K-doubling*, is similar to the  $\Lambda$ -doubling found in linear molecules. For the asymmetric molecule,  $K$ -doubling results since angular momentum is not conserved along a particular body fixed direction.

The diagonalization of the matrices generated by evaluating the expressions given in (2.17) can be simplified as shown in Appendix A. By writing the matrix form of the Hamiltonian for the system for a specific  $J$ , one obtains a non-adjacent, tridiagonal matrix (A.1) with matrix entries given by (2.17) as a function of  $k$ . This matrix can be simplified by noting that the matrix must be Hermitian to obtain real eigenvalues and the matrix is independent of the ordering of  $k$  such that  $E_{k',k} = E_{k,k'}$ . This allows one to consider only the lower half of the non-adjacent, tridiagonal matrix. By using the transformation first derived by Wang:<sup>12</sup>

$$\begin{aligned} |J, O^+\rangle &= |J, 0\rangle \\ |J, k^+\rangle &= \frac{1}{\sqrt{2}}(|J, k\rangle + |J, -k\rangle) \\ |J, k^-\rangle &= \frac{1}{\sqrt{2}}(|J, k\rangle - |J, -k\rangle) \end{aligned} \tag{2.18}$$

the matrix can be transformed into a regular tridiagonal matrix that is of a block diagonal form (A.6). The eigenvalues of each of the submatrices of the block diagonal matrix in (A.7) can be found independently, and the method of labeling given in (A.8) can be used to denote the rotational quantum number, the  $k$  value of the prolate symmetric molecule energy level, and the  $k$  value of the oblate symmetric molecule energy level.

Since nitrosyl bromide is asymmetric, much time and effort has been placed in describing the implications of this asymmetry. Due to this asymmetry, angular momentum is not conserved about a particular body fixed axis. This produces a phenomenon known as K-doubling. Mathematically, the implication of asymmetry is a system with a non-adjacent, tridiagonal matrix representation for the rotational Hamiltonian. The phenomenon of K-doubling requires new quantum numbers that will retain the physical situation of a rotating molecule yet simplify the mathematics. The quantum numbers chosen for this situation are  $J$ , the rotational quantum number,  $K_a$ , the quantum number used in the prolate case, and  $K_c$ , the quantum number used in the oblate case. With this selection of quantum numbers and the Wang transformation (2.18), a block diagonal matrix can be used to represent this system. This block diagonal matrix can be separated into four tridiagonal matrices which can be diagonalized independently to yield the eigenvalues which correspond to the rotational energy levels, labeled as  $J_{K_a K_c}$ , for nitrosyl bromide.

Even though the energy levels can be labeled, these levels cannot be measured for a quantum mechanical system. What is measurable are transitions between these energy levels. These transitions are the spectral lines seen when a spectrum has been recorded.

The type of spectroscopy being done determines which spectral features are important. If one is looking for the locations at which a sample emitted radiation, the important features in the unmodified spectrum are peaks. If absorption spectroscopy is being done, the key spectral features appear as valleys in the raw spectrum.

For this research, absorption spectroscopy was completed for nitrosyl bromide. In absorption spectroscopy of molecules, the valleys in the recorded spectrum result from three types of possible rotational transitions which can take place between different vibrational energy levels. These transitions result from the absorption of incident energy that raise the molecular energy from a lower level,  $J''$ , to a higher level,  $J'$ . The rotational quantum number of the higher level, due to the selection rules of the system, must be such that  $J' - J'' = \pm 1$  or 0. If heading is neglected and the rotational quantum number changes such that  $\Delta J = +1$ , the transition will be located at a higher energy than the energy difference between the vibrational levels. These transitions are labeled as R branch transitions. Transitions which are found at lower energies than the energy difference between the vibrational levels, once again neglecting the heading phenomenon, obey the selection rule  $\Delta J = -1$  and are labeled P branch transitions. The transitions which follow the selection rule  $\Delta J = 0$  are Q branch transitions, and these transitions would occur at the same energy as the energy difference between vibrational levels if the molecule did not distort and stretch while it rotated.

Since nitrosyl bromide is an asymmetric top molecule, selection rules for the  $K_a$  and  $K_c$  values must also be followed. These rules further restrict the transitions allowed. For nitrosyl bromide, the selection rules governing these "quantum numbers" are  $\Delta K_a = 0$  and

$\Delta K_c = 1$ . Therefore, the only transitions observed for nitrosyl bromide can occur between rotational energy levels such that  $K_a' = K_a''$  and  $K_c' = K_c'' + 1$  while  $\Delta J$  may be  $\pm 1$  or 0.

If the  $|J, k\rangle$  basis diagonalized the Hamiltonian of the system in the *body-fixed* coordinate system, analytical expressions could be written for the energy levels which implies that expressions for the locations of the transitions in each branch of the spectrum could be obtained analytically. These analytic expressions could then be used to determine the rotational parameters of the molecule. Because of the asymmetry and the lack of “good” quantum numbers, this luxury is not available with this technique, however, an approximation can be made to generate analytical expressions for the energy levels.

### **2.3 Energy Level Approximation**

For a general asymmetric molecule, there is not an approximation. However, ONBr is nearly prolate, so a power series expansion in terms of  $J$ ,  $K$ , and an asymmetry parameter is applicable. The use of this approximation can be twofold: (1) analytical expressions can be used to determine the validity of the spectral assignment by fitting the assigned transitions to the expressions and (2) the approximate expressions can be used to calculate the energy levels in a global fitting routine.

#### **2.3.1 Theoretical Development of the Approximation**

To generate an approximation that will represent the asymmetry of a rigid rotor, recall that the rotational Hamiltonian for a near-prolate asymmetric top is given by:

$$\begin{aligned}\hat{H}_{\text{rigid}} &= B\hat{J}_b^2 + C\hat{J}_c^2 + A\hat{J}_a^2 \\ &= \frac{1}{2}(B+C)\bar{J}^2 + \left[A - \frac{1}{2}(B+C)\right] \left\{ \hat{J}_a^2 + \frac{B-C}{2A-B-C}(\hat{J}_b^2 - \hat{J}_c^2) \right\}\end{aligned}\quad (2.13)$$

where  $\hat{J}_a$ ,  $\hat{J}_b$ , and  $\hat{J}_c$  are defined as in (2.5),  $\bar{J}^2$  is defined as in (2.7), and  $A$ ,  $B$ , and  $C$  are defined as in (2.3).

In the representation which diagonalizes  $\bar{J}^2$  and  $\hat{J}_a$ , the matrix elements that do not vanish in (2.13) are:<sup>13</sup>

$$\begin{aligned}\langle J, k | \bar{J}^2 | J, k \rangle &= J(J+1), \\ \langle J, k | \hat{J}_a | J, k \rangle &= k, \\ \langle J, k | \hat{J}_b^2 - \hat{J}_c^2 | J, k \pm 2 \rangle &= \frac{1}{2} \left\{ [J(J+1) - k(k \pm 1)] [J(J+1) - (k \pm 1)(k \pm 2)] \right\}^{\frac{1}{2}}\end{aligned}\quad (2.19)$$

where  $J$  is defined as above and  $k$  is the prolate rotor quantum number,  $K_a$ , for ONBr.

The expression in (2.13) can be rewritten as:

$$\hat{H}_{\text{rigid}} = \hat{H}_{\text{sym}} + \hat{H}_{\text{asym}} \quad (2.20)$$

where  $\hat{H}_{\text{sym}}$  is the rotational Hamiltonian for the symmetric top derived in (2.8) and:

$$\begin{aligned}\hat{H}_{\text{asym}} &= \left[ A - \frac{1}{2}(B+C) \right] \left\{ \frac{B-C}{2A-B-C} (\hat{J}_b^2 - \hat{J}_c^2) \right\} \\ &= \left[ A - \frac{1}{2}(B+C) \right] \left\{ 2\epsilon (\hat{J}_b^2 - \hat{J}_c^2) \right\}\end{aligned}\quad (2.21)$$

where a different asymmetry parameter,  $\epsilon$ , has been chosen as:<sup>13</sup>

$$\epsilon = \frac{B-C}{2(2A-B-C)} \quad (2.22)$$

which is related to the asymmetry parameter in (2.4) by:<sup>11</sup>

$$\epsilon = -\frac{1}{2} \frac{\kappa + 1}{\kappa - 3} \quad (2.23)$$

The eigenvalues of the rotational Hamiltonian in (2.20) can be calculated by treating  $\hat{H}_{\text{asym}}$  as a perturbation. The energy levels obtained from the perturbation study are labeled in the same fashion as above and are calculated from a power series of the form:<sup>13</sup>

$$F(J_{K_a, K_c}) = \frac{1}{2}(B+C)J(J+1) + \left[ A - \frac{1}{2}(B+C) \right] k^2 + \left[ A - \frac{1}{2}(B+C) \right] \left\{ k^2 \sum_{n=2}^{\infty} c_{0n} \epsilon^n + \sum_{m=1}^{\infty} J^m (J+1)^m \sum_{n=m}^{\infty} c_{mn} \epsilon^n \right\} \quad (2.24)$$

where  $F(J_{K_a, K_c})$  denotes the energy of the  $J_{K_a, K_c}$  level and the  $c_{mn}$  are the numerical expansion coefficients that describe the effect of asymmetry on the energy levels which are tabulated in Polo<sup>13</sup> for  $m = 1, 2, \dots, 6$ . Thus the maximum number of terms that can be used in the series expansion in  $m$  is seven, one for the  $k^2$  term and six for the  $J^m (J+1)^m$  term.

The energy levels calculated from (2.24) apply only to the rigid rotor. Centrifugal distortion terms must be included to explain the stretching of the molecule as it rotates. The energy level dependent equations for the distortion are listed in Polo's paper without splitting for  $K_a > 3$  and with splitting for the  $K_a = 0, 1, 2$ , and 3 levels. Below is the  $J$  dependent distortion contribution to the  $J_{1,J}$  energy levels:<sup>13</sup>

$$F(J_{1,J}) = [-D_K + 10R_6 - 30R_5\epsilon] + [-D_{JK} - 4R_6 - 2R_5 + (3R_6 + 20R_5 + 3\delta_J)\epsilon] J(J+1) + [-D_J + \delta_J - (2R_6 + \frac{5}{2}R_5 + 2\delta_J)\epsilon] J^2(J+1)^2 + \left[ \frac{1}{4}(R_6 + \delta_J)\epsilon \right] J^3(J+1)^3 \quad (2.25)$$



where  $D_J$ ,  $D_{JK}$ ,  $D_K$ ,  $\delta_J$ ,  $R_5$ , and  $R_6$  are the coefficients used to describe the quartic centrifugal distortions and, for  $J_{1,J-1}$ , the sign of the underscored terms must be reversed. The distortion constants above are related to the quartic distortion constants in the diagonalization theory by the following transformation:<sup>10</sup>

$$\begin{aligned}
 \Delta_J &= D_J - 2R_6 \\
 \Delta_{JK} &= D_{JK} + 12R_6 \\
 \Delta_K &= D_K - 10R_6 \\
 \delta_J &= \delta_J \\
 \delta_K &= -2R_5 - \frac{2}{\epsilon} R_6
 \end{aligned} \tag{2.26}$$

where  $\epsilon$  is the asymmetry parameter defined in (2.22).

By adding these expansions to the rigid rotor energy levels given in (2.24), the approximation can be used to determine the location of the transitions to aid in the assignment of the spectrum and to calculate the energy levels in a global fitting routine.

### 2.3.2 Accuracy of the Approximation

Since equation (2.24) contains a power series expansion that must be truncated at  $m = 6$ , the maximum  $J$  for which this approximation held was investigated. Since the expansion is in  $\epsilon$ , the contribution to the energy level of the first term in the power series in  $n$  for the  $m = 6$  (i.e.,  $n = 6$  term) was used to determine the limitations of the approximation.

The maximum  $J$  value which could be approximated was determined by setting the  $n = m = 6$  term equal to the resolution of the spectrometer since any deviation of this amount in a calculated energy level would result in a calculated transition that would

deviate by the same quantity. Hence, the maximum rotational level that could be approximated was given by:

$$J_{\text{upper}} \approx \sqrt[12]{\frac{RES}{\left[A - \frac{1}{2}(B + C)\right]c_{66}\epsilon^6}} \quad (2.27)$$

where  $c_{66} = \frac{1002401}{79626240}$  as given by Polo,<sup>13</sup>  $\epsilon = 5.04718 \times 10^{-4}$ ,  $A = 2.82628 \text{ cm}^{-1}$ ,  $B = 0.125520 \text{ cm}^{-1}$ ,  $C = 0.120062 \text{ cm}^{-1}$  for the  $\nu_1 = 1$  level, and the resolution of the spectrometer,  $RES$ , is  $0.02 \text{ cm}^{-1}$ . The  $\nu_1 = 1$  level constants were used since the rotational constants for the  $\nu_1 = 2$  level were sought by this research and consequently unknown. By substituting the values listed, the approximate upper bound of  $J$  was calculated to be:

$$J_{\text{upper}} \approx 42 \quad (2.28)$$

To ensure that the upper bound for the  $\nu_1 = 2$  level was not too high, the transitions studied with the approximation were limited to an upper bound of  $J = 40$  following the trend between the approximate upper bounds calculated from the  $\nu_1 = 0$  and  $\nu_1 = 1$  parameters ( $J_{\text{upper}}$  for the  $\nu_1 = 0$  level was found to be forty-three).

To calculate the location to truncate the power series in  $n$ , the second term in the  $n$  series for  $m = 1$  ( $n = 2$  term) was calculated at the upper bound as:

$$\left[A - \frac{1}{2}(B + C)\right] \left(J_{\text{upper}}(J_{\text{upper}} + 1)\right) c_{12}\epsilon^2 = 1.24 \times 10^{-3} \text{ cm}^{-1} \quad (2.29)$$

where  $A$ ,  $B$ ,  $C$ ,  $J_{\text{upper}}$ , and  $\epsilon$  are the same as in (2.27) and  $c_{12} = 1$ . Therefore, only the  $n = m$  (first) term for the power series in  $n$  needs to be retained.

To determine the error in truncating the power series expansion in  $m$  for nitrosyl bromide, the contribution of the  $n = m = 7$  term to the energy level was investigated at  $J_{\text{upper}}$  and found to be:

$$\left[ A - \frac{1}{2}(B + C) \right] \left( J_{\text{upper}}^7 (J_{\text{upper}} + 1)^7 \right) c_{66} \epsilon^7 = 0.01779 \text{ cm}^{-1} \quad (2.30)$$

where  $A$ ,  $B$ ,  $C$ ,  $c_{66}$ ,  $J_{\text{upper}}$ , and  $\epsilon$  are the same values as in (2.27) with the use of  $c_{66}$  was required since a numerical value for the  $c_{77}$  coefficient was not published in the paper by Polo.<sup>13</sup> Since the  $n = m = 7$  term contribution was on the order of the resolution of the spectrometer, the contribution of the  $n = m = 8$  term was investigated by calculating (2.30) where all the values of seven are replaced with eight. This calculation showed that the  $n = m = 8$  term would contribute  $0.01622 \text{ cm}^{-1}$ . Hence, the truncation of the power series in  $m$  at  $m = 6$  contains a truncation error at  $J_{\text{upper}}$  that is larger than the resolution of the spectrometer. This implies that the largest value of the rotational quantum number that can be approximated by this perturbational technique may be far removed from the value calculated in (2.27).

The determination of the actual upper bound for  $J$  is critical since any erroneous calculation of the energy levels would produce a calculated transition that would not be within  $0.02 \text{ cm}^{-1}$  of the correct location. Hence, any calculation completed with that transition would result in residuals that were larger than the resolution of the spectrometer.

Even though the above calculation was accomplished with the  $v_1 = 1$  constants to determine the validity and the error of the approximation, the trend in the approximate rotational energy levels properly predicted from the zero to first vibrational level should

hold well enough to be able to determine the approximate upper bound for the  $v_1 = 2$  level as  $J = 40$ . However, the actual upper bound must be determined before an appropriate set of constants can be reported.

### 3. Experimental Apparatus and Procedures

#### 3.1 Fourier Transform Spectrometer

##### 3.1.1 Theory of Operation

The Fourier transform spectrometer (FTS) is one of the instruments used for data collection in absorption spectroscopy experiments. The primary component of this instrument is the optical design used to obtain the signal. In this research, the FTS used employed a Michelson interferometer design as shown in Figure 3-1.

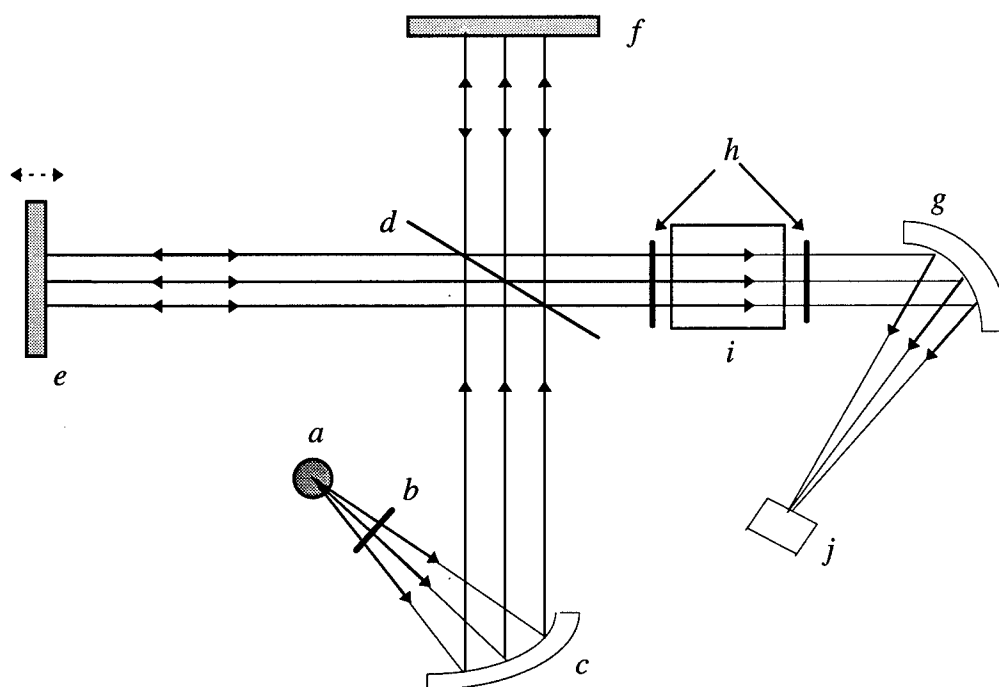


**Figure 3-1.** Michelson Interferometer. *a.* source, *b.* aperture, *c.* collimating mirror, *d.* beamsplitter, *e.* movable mirror, *f.* fixed mirror, *g.* focusing mirror, *h.* spectral filters, *i.* sample cell, and *j.* detector.

The light from the source of the interferometer passes through an aperture which limits the intensity of the light passing through the interferometer to the detector. This aperture also localizes the beam to improve the resolution obtainable from the spectrometer.

After the light has left the aperture, the light is still diverging. Since this divergence is not desirable, a curved mirror is placed into the path of the beam to collimate it. A mirror is used instead of a lens for three reasons: (1) the loss of light intensity upon reflection from a mirror is less than the loss of light intensity upon passing through a lens, (2) the use of a mirror allows the beam to be reversed in direction and a more compact system can be built, (3) since mirrors reflect almost any wavelength of light incident on them, the interferometer can be used for a larger range of the electromagnetic spectrum without changing the collimating optical component, and (4) no chromatic aberrations are present. With the beam collimated, the entire amount of light passing through the aperture can be used to collect data.

After the light is collimated, the light enters the components which comprise the Michelson interferometer. The collimated light is incident on a beamsplitter which splits the light intensity into beams of equal intensity to provide the greatest contrast. The light that is reflected travels toward the movable mirror while the transmitted light passes through the beamsplitter and travels toward the fixed mirror.

The light that is transmitted through the beamsplitter is incident on a fixed mirror which reflects the light directly back toward the beamsplitter. Since the distance traveled

by the light in this arm of the interferometer never changes, this arm can be referred to as the reference arm.

The light that is reflected from the beamsplitter is incident on a movable mirror. As this mirror is moved, the distance traveled by the light changes. Since the path length of the light changes, this arm of the interferometer can be referred to as the test arm. Upon reflection of the light from the movable mirror, the light passes back through the front surface of the beamsplitter and is recombined with the light that traveled through the test arm.

Because light from both arms of the interferometer have passed through the same amount of beamsplitter material, the only phase difference between the two beams of light results from the difference between the length of the test arm and the length of the reference arm. With the light traversing each arm twice, once to the mirror and once from the mirror, the optical path difference is twice the length difference for the two arms. This optical path difference creates a sinusoidal varying intensity pattern at the beamsplitter as shown in Figure 3-2 when the source of light is monochromatic.

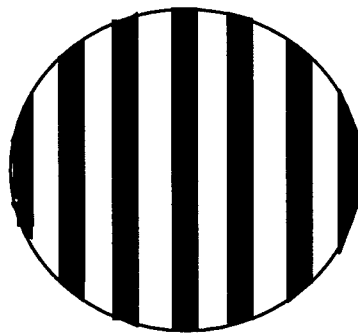


**Figure 3-2.** Typical interference pattern produced by a monochromatic source.

The interference pattern produced by the recombination of the light propagates through the sample cell to the focusing mirror. Once again, a mirror is chosen to focus the interference pattern for the same reasons listed for collimation. This mirror focuses the light from the interference pattern onto an intensity sensitive detector.

### **3.1.2 Bomem Fourier Transform Spectrometer**

For this research, a Bomem DA-8 FTS was used. This spectrometer contains a Michelson interferometer with a movable mirror that could translate up to 50 cm and two possible light sources. The 50 cm translation allowed for resolution as low as  $0.02\text{ cm}^{-1}$  while the sources available produce either visible or infrared, non-monochromatic radiation. For this research, the globar source was used to produce the required infrared radiation. This choice was driven by the location of the absorption region of the  $\nu_1 = 0 \rightarrow \nu_1 = 2$  transition of nitrosyl bromide.

Since this source is non-monochromatic, a continuous distribution of wavelengths is produced. Each of these wavelengths travels through the Michelson interferometer shown in Figure 3-1, where the beamsplitter chosen was made from calcium fluoride ( $\text{CaF}_2$ ). Upon recombination at the beamsplitter, each wavelength of the light produces a unique interference pattern similar to the pattern shown in Figure 3-2. This infinite number of interference patterns produces an interferogram, and this interferogram is focused onto the detector. By Fourier analyzing the interferogram recorded by the detector, the signal recorded can be broken into components where each component results from a different wavelength.<sup>14</sup>



For this research, a cell containing nitrosyl bromide was placed internal in the FTS in the sample chamber. This placed the cell before the focusing mirror and a Belov Technology Co., Inc. HgCdTe detector with an operating range of  $800\text{-}5000\text{ cm}^{-1}$ . As the infrared beam passed through the cell, photons of the appropriate energies were absorbed by the nitrosyl bromide. The absorption of these photons resulted in an interference pattern of reduced intensity for that wavelength. When the Fourier transform of this modified interferogram was taken, the wavelengths of light with reduced intensity were minimums.<sup>14</sup> To improve the signal to noise ratio of the interferogram, spectral filters made by Corion, a  $2.5\text{ }\mu\text{m}$  long pass and a  $3.0\text{ }\mu\text{m}$  short pass, were chosen to eliminate wavelengths emitted by the source that would not be absorbed by the  $\nu_1 = 0 \rightarrow \nu_1 = 2$  transition in ONBr.

### **3.1.3 Data Collection and Spectrum Analysis Software**

The FTS used was controlled via ethernet connection by an in-lab, IBM 486/DX50 computer. The software package used for this task was the Bomem PC-DA Version 1.1a. This package allowed numerous settings for the aperture, resolution, gain, the number of scans to be taken, the beamsplitter material, and the source used with typical settings of  $1.5\text{ mm}$ ,  $0.02\text{ cm}^{-1}$ , sixteen, sixty-four,  $\text{CaF}_2$  beamsplitter, and globar source, respectively. This software also contained menus that could start different experiments on the FTS. The experiments utilized for this research included the phase and the raw spectrum. In the phase experiment, the spectrometer finds the zero path length difference of the two arms of the interferometer while in the raw spectrum experiment, the spectrometer records the detector response to the intensity change of each interference pattern in the interferogram.

When the data had been collected for a particular experiment, the PC-DA software had the capability to take the numerical Fourier transform of the data.

To view the Fourier transform of the data, the spectrum analysis software, GRAMS 386 Version 2.03B by Galactic Industries Corporation, was used. This software was designed for use with the PC-DA software so file conversion was not required. Upon viewing a spectrum, there are numerous numeric techniques and several options in the software which can be implemented. For this research, the background ratio option, the "Absorbance" numerical technique, and the peak picking option were used. These three items will be discussed in Chapter 4.

### 3.2 Vacuum System

Since nitrosyl bromide is not readily available for purchase, the gas had to be created using nitric oxide (NO) and bromine ( $\text{Br}_2$ ) in gaseous states. These gases were mixed in a vacuum system constructed in the lab. The schematic diagram of this system appears in Figure 3-3.

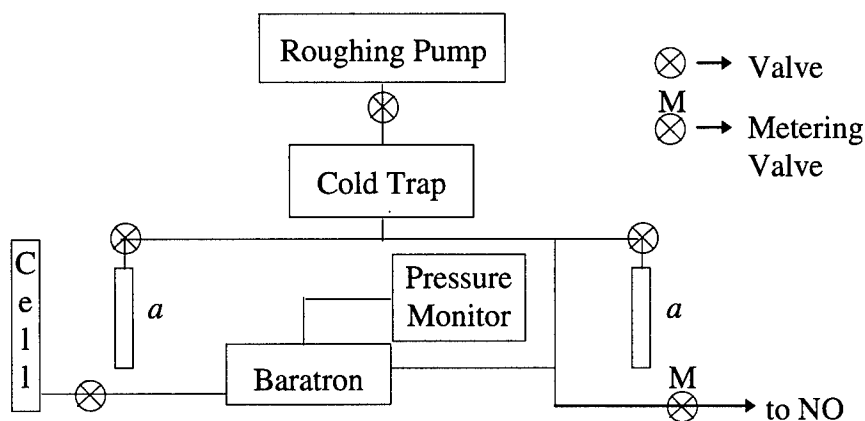


**Figure 3-3.** Vacuum system used to create nitrosyl bromide.  
a. distillation tubes to purify the  $\text{Br}_2$ .

When the construction of the vacuum system was complete, the vacuum system was brought down to less than 0.01 Torr with the roughing pump, and leak tests were performed. The vacuum system was considered sealed when the data from the fifth leak test showed a leak rate of 0.7 mTorr per minute.

When the vacuum system was sealed, the liquid bromine, obtained from Spectrum Chemical Manufacturing Corp., was transferred from storage to the vacuum system. Since the bromine could contain impurities resulting from prolonged storage time, the roughing pump was used to bring the system down to less than 0.01 Torr, and the natural, isotopic abundance bromine was purified. This purification was accomplished through three freeze/pump/thaw cycles in which the empty distillation tube in Figure 3-3 was chilled to 77° Kelvin, the valve on the tube containing the bromine was opened, and the pure bromine vapor was cryogenically pumped into the chilled distillation tube. Both tubes were sealed, and the frozen liquid bromine in the initially full tube was allowed to thaw to room temperature to create more bromine vapor in that tube. One cycle of this process was complete when most of the bromine from the full distillation tube had been pumped to the other tube.

The NO used for this experiment was obtained from Matheson Gas Products, Inc. This bottled gas was placed in the gas cabinet in the lab, and a tube made of Teflon was connected from the outlet of the gas bottle to the vacuum system.

### ***3.3 Absorption Cell***

In order to obtain a spectrum of the gaseous mixture produced in the vacuum system, an absorption cell was designed. This cell consisted of a 20 cm Pyrex glass tube of 2"

outer diameter. At 5 cm from one end of the cell, a 1" piece of 1/2" outer diameter Pyrex tubing was attached by a glass blower to obtain a port which could connect the cell to the vacuum system. On both ends of the cell, 2" diameter calcium fluoride ( $\text{CaF}_2$ ) windows made by Ealing were attached. These windows allowed visible and IR light to pass through the cell with minimal absorption. The windows were attached to the end of the cell with Torr Seal and allowed to dry for one day. Torr Seal was chosen since it exhibited the least amount of bromine absorption in previous experiments.<sup>14</sup>

### 3.4 Creation of ONBr

Previous research has shown that nitrosyl bromide can be formed by the following reaction:<sup>5</sup>



The rate at which equilibrium is established for this reaction has been reported as  $2.6 \times 10^9 \text{ cm}^6 \text{ mole}^{-1} \text{ sec}^{-1}$  which implies that ONBr will be formed in one to four hours. However, when NO and  $\text{Br}_2$  are placed in a sample chamber under room lights, equilibrium occurs more rapidly by the following reactions:<sup>15</sup>



where  $h\nu$  represents the energy of a photon of light and M is a third body needed to conserve energy. The equilibrium rate constant for the second reaction in (3.2) is  $8.7 \times 10^{-33} \text{ cm}^6 \text{ molecule}^{-2} \text{ sec}^{-1}$ .<sup>16</sup>

For this experiment, ONBr was created by initially releasing bromine into the vacuum system and cell by opening the valve of the distillation tube which contained the

liquid bromine. Due to its vapor pressure, gaseous bromine was also in the tube, and this gas was introduced when the valve was opened. The valve remained open until 30.54 Torr of bromine was contained in the vacuum system. Nitric oxide was introduced after the bromine tube had been sealed. Since the NO was under pressure, none of the bromine currently in the system entered the NO line. The NO was added until the pressure of the system was 61.40 Torr. By the law of partial pressures, 30.86 Torr of NO was present. The cell was then closed off from the rest of the system, and a halogen light was shined down the axis of the absorption cell to act as a catalyst for the reactions in (3.2). To guarantee that the reaction had reached equilibrium, the laboratory lights were left on, and the sample was allowed to equilibrate under these conditions for one day.

The amount of ONBr actually present in the cell at equilibrium can be determined from:

$$K_{eq} = \frac{[\text{ONBr}]_{eq}^2}{[\text{NO}]_{eq}^2 [\text{Br}_2]_{eq}} \quad (3.3)$$

$$[\text{NO}]_o = [\text{NO}]_{eq} + [\text{ONBr}]_{eq} \quad (3.4)$$

$$2[\text{Br}_2]_o = [\text{ONBr}]_{eq} + 2[\text{Br}_2]_{eq} \quad (3.5)$$

where  $K_{eq}$  is the equilibrium constant ( $2.6 \times 10^9 \text{ cm}^6 \text{ mole}^{-1} \text{ sec}^{-1}$ ),  $[\text{NO}]_o$  and  $[\text{Br}_2]_o$  are the initial concentrations of nitric oxide and bromine, respectively, and  $[\text{NO}]_{eq}$ ,  $[\text{Br}_2]_{eq}$ , and  $[\text{ONBr}]_{eq}$  are the equilibrium concentrations of nitric oxide, bromine, and nitrosyl bromide, respectively. By solving these equations, a relationship between the  $[\text{Br}_2]_o$  and the  $[\text{ONBr}]_{eq}$  can be found as a function of the  $[\text{NO}]_o$ . Upon substituting the initial

pressures of the gases, the amount of ONBr present in the cell was 29.93 Torr with roughly 0.04 Torr of NO remaining in the cell.

To verify the presence of nitrosyl bromide in the sample, the absorption cell was placed into the sample chamber of the Bomem FTS and a low resolution,  $4\text{ cm}^{-1}$ , spectrum was taken from  $3500 - 3650\text{ cm}^{-1}$ . This spectrum showed absorption due to nitrosyl bromide, however, there was a section of the P branch which had only seven percent transmission. With this minimal amount of transmission, detector noise could result in intensity fluctuation in the recorded data. When the Fourier transform of this data would be taken, these noise fluctuations would produce non-physical spectral features. To eliminate this possible problem, 11.17 Torr of the sample was removed leaving a total of 19.10 Torr of ONBr in the cell. The absorption spectrum of the sample was taken again, and this time seventeen percent transmission was recorded for the same section of the P branch. This amount of transmission reduced any detector noise problems while still obtaining significant absorption to allow data collection for spectral features resulting from high rotational energy transitions.

## 4. Results

### 4.1 Data Collection

The spectrum of the  $\nu_1 = 0 \rightarrow \nu_1 = 2$  transition in ONBr was obtained by placing the sample cell containing 19.10 Torr of nitrosyl bromide in the Bomem FTS sample chamber and evacuating the sample and source chambers to 0.23 Torr to remove as many air-based water and carbon dioxide molecules as possible. This spectrum was taken at high resolution,  $0.02 \text{ cm}^{-1}$ . The region of interest,  $3500 - 3625 \text{ cm}^{-1}$ , was scanned sixty-four times and coadded. The aperture was set to 1.5 mm diameter to obtain the high resolution required while supplying a sufficient signal, a mirror speed of 0.2 cm/s was used, and no apodization, named boxcar in the PC-DA software, was used to cancel any “ringing” effects that can occur.

These “ringing” effects can be traced to the mathematical problem of taking a Fourier transform of a signal that is of finite extent. The extent of this signal is limited by the translation of the movable mirror. When the mirror reaches the position of maximum translation, the data, which can be represented by a smoothly varying function up to that point, abruptly stops. When the Fourier transform of this data is taken, this abrupt stop of the data causes spurious effects in the spectrum that can be seen next to sharp absorption peaks.

By viewing the spectrum in the GRAMS/386 software, one immediate feature can be noticed: both ends of the spectrum exhibit linear trends in the intensity transmitted. This is clearly shown in Figure 4-1.

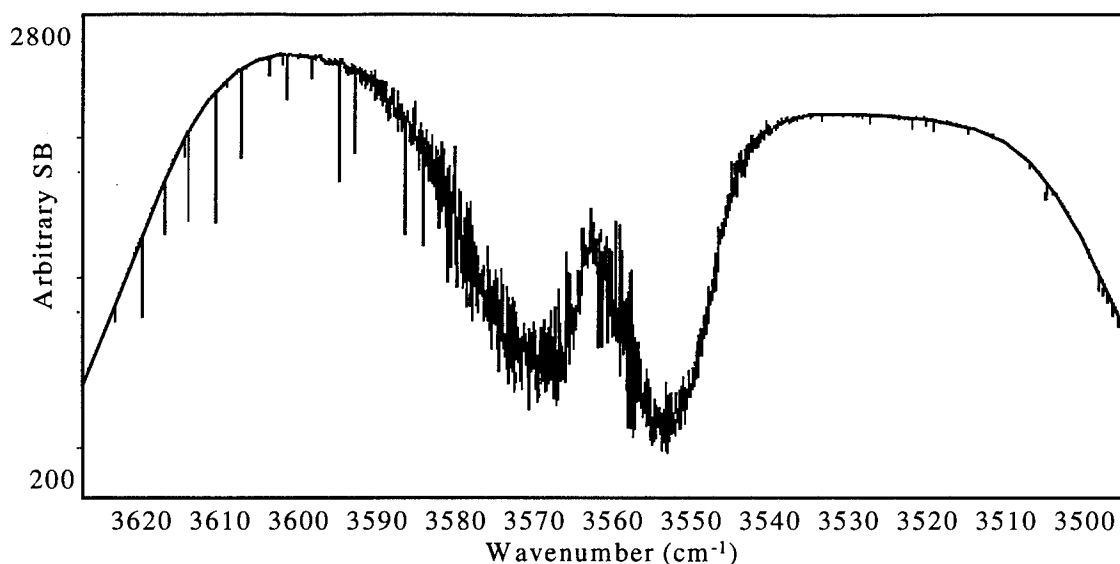


**Figure 4-1.** Raw spectrum of 19.10 Torr of ONBr. Notice the somewhat linear trends in the intensity at both ends of the spectrum and the density of the spectral features.

The trends at the edges of the spectrum and across the center region do not allow for a consistent baseline. Since the intensity can be used to help understand the physics governing the transition, a changing baseline is not desirable.

Not only does the spectrum require modification to correct the sloping baseline, the spectrum in Figure 4-1 represents the absorption of all elements in the sample chamber, i.e., any item between the interferometer and the detector. To generate the appropriate modifications to the raw spectrum in Figure 4-1, a background spectrum was recorded with an evacuated cell and spectral filters in the sample chamber of the FTS. This guaranteed that the only difference between the spectrum in Figure 4-1 and the background spectrum would be absorption due to the presence of ONBr. The background spectrum obtained is shown in Figure 4-2.



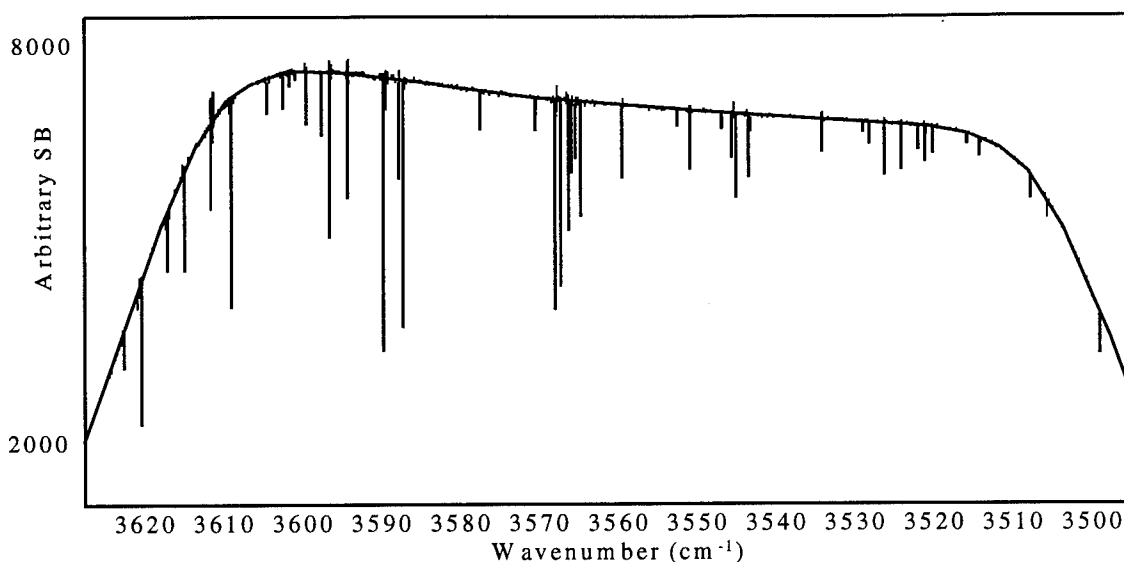


**Figure 4-2.** Background spectrum taken to eliminate various absorption phenomena not connected to absorption by ONBr.

The spectrum in Figure 4-2 was taken at  $0.1 \text{ cm}^{-1}$  resolution with 64 coadds, no apodization, an aperture setting of 1.5 mm, and a mirror speed of 0.50 cm/s. The pressure of the source and sample chambers was 0.32 Torr.

The most notable difference between the two raw spectra shown in Figure 4-1 and Figure 4-2 is in the region between  $3530 \text{ cm}^{-1}$  and  $3600 \text{ cm}^{-1}$ . The only difference between the spectrum in Figure 4-1 and the one in Figure 4-2 is the presence of ONBr in the absorption cell, therefore the absorption of light in this region must be caused by ONBr.

#### **4.2 Spectrum Analysis**

With the background spectrum taken, the data collection was complete, and the two spectra needed to be combined to produce the desired spectrum which will represent only

absorption by ONBr. To eliminate the background in Figure 4-1, the “Absorbance” mathematical procedure was used where the new spectrum is calculated from:<sup>17</sup>

$$\text{Absorbance file} = -\log \frac{\text{Sample file}}{\text{Background file}} \quad (4.1)$$

where the *Absorbance file* is the new spectrum produced, the *Sample file* is the raw spectrum taken with ONBr in the cell, and the *Background file* is the raw spectrum taken with the evacuated cell and spectral filters.

With the background taken out of the raw spectrum in Figure 4-1 the only features left are spectral features describing the absorption of IR light by ONBr. The resulting absorbance spectrum is shown in Figure 4-3.

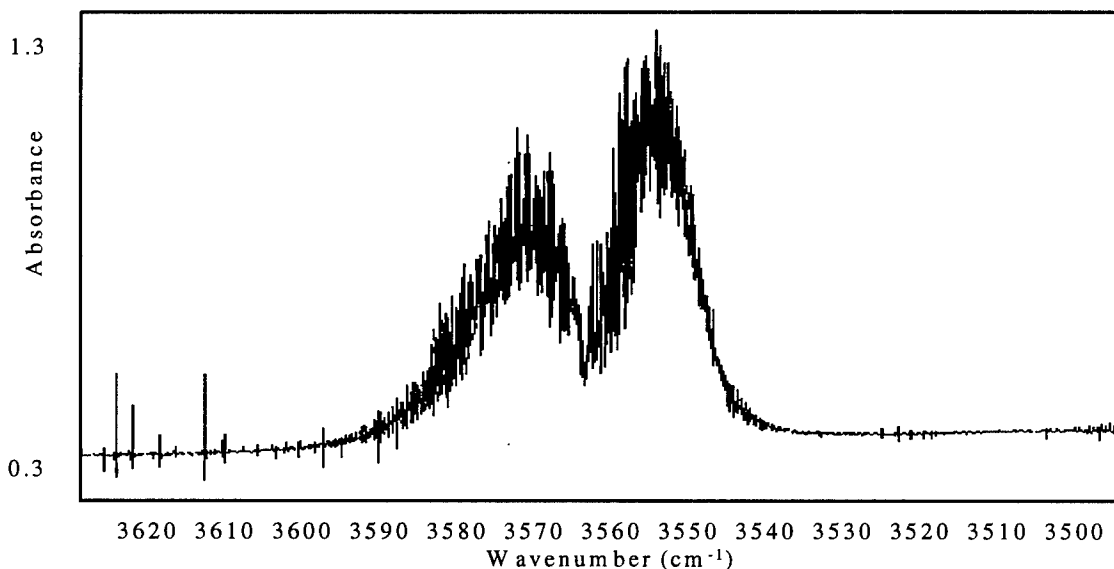


**Figure 4-3.** Absorbance spectrum of ONBr where the spectral features (lines) corresponding to absorption transitions are positive.

Not only did the use of the “Absorbance” routine make the spectrum more understandable, it also allowed the use of the peak picking routine in the software package. This package can be used with either default or user-defined settings. The latter

were opted for since a comprehensive listing of the spectral peaks was desired. The user-defined settings included peak location methods which relied on the change in the slope of the line to find a peak in the spectrum and decide where it was located. Also, sensitivity settings could be used to define a threshold for peaks that were not intense enough. Figure 4-4 shows a piece of the spectrum in Figure 4-3 from the R branch with lines to distinguish the different  $K_a$ ,  $K_c$  combinations for a particular rotational level.

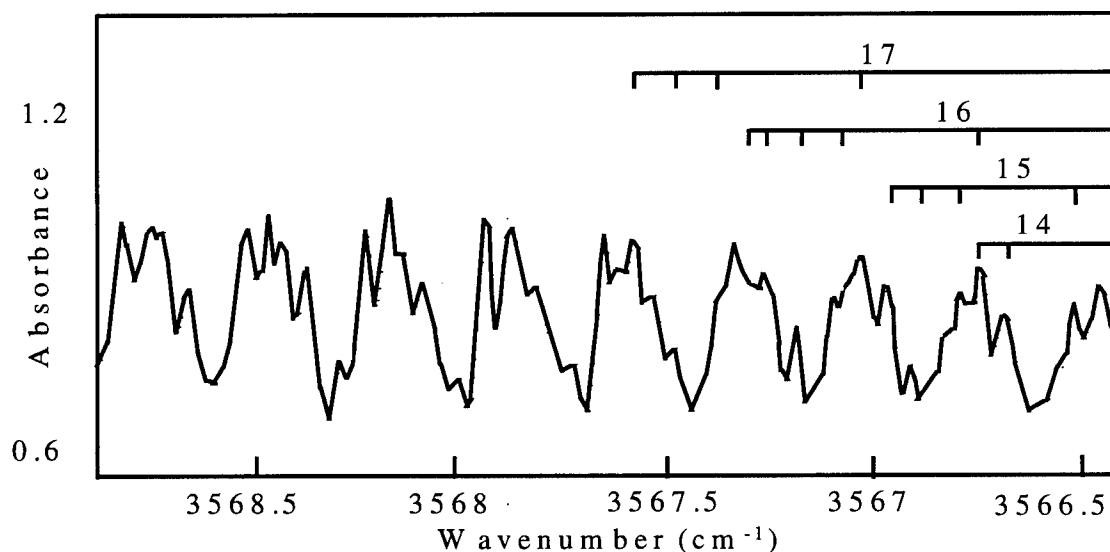


**Figure 4-4.** Blow up of ONBr absorbance spectrum in the R branch. Lines above the spectral features depict the different  $K_a$ ,  $K_c$  lines for a particular  $J$ .

Once the peaks were found, the energy location in  $\text{cm}^{-1}$ , the intensity, and the label of the peak were output to a file and printed. For those peaks that were not labeled, labels were added by hand through the use of the GRAMS/386 software which could be used to find points where the slope changed. This method was not as precise and a lot more tedious than the peak picking routine, however, it proved extremely useful in determining the width of the spectral lines.

The width of a spectral feature can be used to determine if there is too much of the sample in the absorption cell. If this is the case, the spectral features will broaden, referred to as pressure broadening, to a width much larger than the resolution and the percent of the light transmitted will be low as discussed previously. The spectral features shown in Figure 4-4 are clearly broader than the resolution,  $0.02\text{cm}^{-1}$ , however, only the bases of these peaks are wide. The features, often three or more, on top of these broad bases are on the order of the resolution. This implies the broadening of the spectral peaks is not due to pressure broadening but to a blending of spectral peaks.

Blending occurs where one transition peak reaches the maximum absorption as another peak begins to exhibit some absorption. As the first peak begins to disappear the second peak has gotten closer to the maximum and the two peaks intensities superimpose to produce a value even higher than both peaks at that point. When numerous peaks lie within resolution of each other, this blending becomes very severe and the recorded peaks appear as one, substantially wider peak.

### ***4.3 Spectral Assignment***

The most difficult part of spectroscopy is the assignment of the transitions corresponding to the peaks. This assignment process is critical in the determination of the physical parameters,  $\mathcal{A}$ ,  $\mathcal{B}$ ,  $\mathcal{C}$ , etc. If the assignment is not done properly, the determined values for these parameters will not represent the physical situation and this is the sole purpose for studying the rotational transitions of a molecule.

Typically, there are numerous methods which can be employed to determine the transition responsible for a given peak. Since the physical situation resulting in the

spectrum is the rotation of a molecule, the molecular forces and structure of the molecule can be used to aid in the spectral assignment. This procedure, however, relies heavily on previously reported force constants or approximations to these constants made from other, similar molecules. If any of these constants, either reported or approximated, are wrong, the corresponding assignment will be inappropriate, and the entire experiment will not produce new constants consistent with the physical interpretation.

A second method which can be employed to assign the spectrum relies on the trends between different spectral features. These trends can be determined without the use of previously reported numbers and plots can be made to graphically reinforce and improve the spectral assignment. These trends represent the difference between two transitions that have a change in one of the quantum numbers, i. e., either  $J$  is changed by one for the second transition and the other quantum numbers stay fixed or the  $J$  is held fixed for both transitions and one of the other quantum numbers is changed for the second transition. Since this method relies on the difference between transitions and the transitions are obtained through a difference in energy levels, this method is called the *second-difference*,  $\Delta_2$ , method. The best way to explain the formulation of the  $\Delta_2$  equations is by considering a linear molecule under the rigid rotor approximation since the equations for the energy levels of this molecular type are tractable and the procedure is analogous for other molecular types.

The rotational energy level of a linear molecule can be written as:

$$F(J) = B_v J(J+1) \quad (4.2)$$

where  $F(J)$  denotes the energy level as a function of the rotational quantum number and  $B_v$  is the rotational parameter as defined in (2.3) where the subscript  $v$  denotes that the  $B$  parameter is dependent on the vibrational level. To represent the upper vibrational level of a transition, the  $J$  and  $B_v$  are denoted as  $J'$  and  $B_v'$ , respectively. Similarly, the representation for the lower vibrational level is  $J''$  and  $B_v''$ .

By using the notation above, a P branch transition of a diatomic molecule can be represented by:

$$P(J) = v_o + B_v' J'(J' + 1) - B_v'' J''(J'' + 1) \quad (4.3)$$

where the  $P(J)$  is used since the equation represents a P branch transition, the  $v_o$  is the difference between the two vibrational levels in question (referred to as the band origin) for the transition, and the lower energy level is subtracted from the upper energy level. Recall that the P branch transitions follow the selection rule  $\Delta J = -1$  which implies that  $J' - J'' = -1$ . Hence, (4.3) can be simplified by setting  $J' = J'' - 1$ . The new equation is only in terms of  $J'$  so  $J'$  is set to  $J$ . The corresponding P branch transition becomes:

$$P(J) = v_o - (B_v' + B_v'')J + (B_v' - B_v'')J^2 \quad (4.4)$$

As stated previously, the  $\Delta_2$  is formed between two transitions with a change in one quantum number. Since the only quantum number in (4.4) is  $J$ , the only  $\Delta_2$  that can be formed is one in which  $J$  is changed. The most logical choice for this change is  $+1$ , thus we have:

$$P(J+1) - P(J) = \left[ v_o - (B_v' + B_v'')(J+1) + (B_v' - B_v'')(J+1)^2 \right] - \left[ v_o - (B_v' + B_v'')J + (B_v' - B_v'')J^2 \right] \quad (4.5)$$

This equation can be simplified to produce the following relation:

$$\Delta_2 P = -2B_V'' + 2(B_V' - B_V'')J \quad (4.6)$$

where  $\Delta_2 P$  is used to denote that the second difference formed is for the P branch. By a similar procedure, both the Q and R branch  $\Delta_2$  expressions can be obtained by substituting  $J' = J''$  and  $J' = J'' + 1$ , respectively, where the  $J' = J'' - 1$  simplification was invoked.

After obtaining a fit of a  $\Delta_2$  equation to the corresponding  $\Delta_2$  data with physically realistic values for the parameters, the residuals can be viewed to determine the quality of each data point. When a  $\Delta_2$  data point has a residual which lies outside the resolution of the spectrometer, the two transitions creating the  $\Delta_2$  data point must be reviewed. Upon reviewing the transitions creating this errant  $\Delta_2$  data point, the label(s) of the transition(s) can either be moved to an adjacent spectral feature that does not disrupt the rest of the data or considered misassigned and subsequently removed from the data set.

Since the  $\Delta_2$  data used to obtain these fit parameters is only a small subset of the data, these values are not precise. However, the values can be used as the initial guesses to a global fitting routine which calculates the best rotational constants for the entire data set. Through the use of various second differences, the entire spectral assignment can be made and validated quite readily. When all the  $\Delta_2$  fits yield spectral constants of roughly the same value, the spectrum has been properly assigned. This guarantees that the transitions sent to a global fitting routine will be a valid assignment representing the

physical situation, and the  $\Delta_2$  method can supply initial guesses for the rotational parameters.



## 5. Discussion

The goal of this research was to find the set of rotational parameters that accurately replicate the observed rotational transitions for the  $v_1 = 0 \rightarrow v_1 = 2$  transition in ONBr. The validity of these constants are heavily dependent on the assignments made to the observed transitions. To assign the spectrum properly, the constants should be known. Thus a circular argument is created.

This circular argument can be circumvented by using the appropriate  $\Delta_2$  expressions to find trends in the data. The formulation of these equations is dependent on analytical expressions for the energy levels. Since ONBr is asymmetric, the exact energy levels could not be expressed analytically, however, an approximation for the energy levels does exist.

Up to this point, the exact region of validity for the approximation has not been determined. The approximate upper bounds for  $J$  in the  $v_1 = 0$  and  $v_1 = 1$  levels have been calculated, and an approximate upper bound for  $J$  in the  $v_1 = 2$  level has been determined. However, the errors in these upper bounds were calculated with the largest  $K_a$ -dependent expansion coefficient for the highest order term in the series that is published.<sup>13</sup> While this calculation does not properly reflect the contribution of the terms that have been truncated, this series converges very slowly. Therefore, the exact  $J$  value which can be approximated to within the resolution must be determined before the rotational constants describing the  $v_1 = 2$  rotational energy levels can be accurately reported.

The asymmetry approximation has been used to generate the  $\Delta_2$  trends to aid in the spectral assignment and in a global fitting routine. It is quite possible that the exact upper bound for J can be determined from the application of either of these uses of the approximation.

### 5.1 Validation of Spectral Assignment

As previously discussed, second difference equations can be used to verify the spectral assignment and the parameters obtained after fitting these equations to the appropriate second difference data can be used as initial guesses to a global fitting routine. For ONBr, the number of  $\Delta_2$  equations that could be investigated was large. This is clear when the definition of the  $\Delta_2$  method is recalled. As both quantum numbers, J and  $K_a$ , can be changed,  $\Delta_2$  equations in which  $K_a$  is held fixed for both transitions and J is changed by one (same method as derived in Chapter 4.3) or J held fixed and  $K_a$  allowed to change are applicable to this study. In view of the information that can be obtained from a fit to the  $\Delta_2$  data by the corresponding equation, the selection of the correct  $\Delta_2$  trend was important. The  $\Delta_2$  trends studied were:

- 1) The trend in the difference between  $J_{0,J}$  and  $(J+1)_{0,(J+1)}$ .
- 2) The trends in the difference between  $J_{0,J}$  and  $J_{m,J-m+1}$  where  $m = 1, 2, \text{ or } 3$ .
- 3) The trends in the difference between  $J_{0,J}$  and  $J_{n,J-n}$  where  $n = 1, 2, \dots, 6$ .

where J will be used here and throughout the rest of the paper to represent the rotational quantum number of the lower energy level in a transition unless otherwise indicated.

The actual assignment of the spectrum becomes an iterative process in which the parts of the spectrum are assigned, the  $\Delta_2$  for the above trends are calculated, and the appropriate  $\Delta_2$  equation is fit to the data. The data points with residuals greater than the resolution are removed, and the fit is reaccomplished until all the residuals were within the resolution. This procedure is repeated for each trend in the branch until approximately all the spectral features of the branch are labeled with the corresponding transition.

Before the curve fitting procedure could be implemented for the spectrum, some possible difficulties needed to be addressed. These difficulties include the consequence of trying to extend the approximation past the upper bound and the number of parameters kept in the analytic  $\Delta_2$  expressions to properly represent the data in the valid region of the approximation.

By determining the consequence of extending the approximation past the upper bound, the characteristics of the breakdown of the approximation can be studied. An understanding of these characteristics may prove vital in the determination of the exact J value that can be approximated.

### **5.1.1 Limits of Analytical $\Delta_2$ Expressions**

To examine the validity of the  $\Delta_2$  equations and the types of erroneous curve fits that do not result from a faulty spectral assignment, the  $\Delta_2$  expressions obtained from the approximation were fit to previously published data. The  $v_1 = 0 \rightarrow v_1 = 1$  data obtained from Esposti *et al* was used to accomplish this validation.<sup>4</sup>

As a result of the validity of these published transitions, the only pitfalls encountered resulted from the inability of the approximation to replicate the data. In Figure 5-1 the second difference fit obtained for the trend in the  $J_{0,J}$  to  $J_{2,J-2}$  transitions in the R branch as a function of the rotational quantum number is plotted. In this and all subsequent  $\Delta_2$  plots, the nomenclature used gives the  $K_a$  value of the first transition and the  $K_a$  value for the second transition in the superscript, the branch analyzed by the data and the curve fit, and the  $K_c$  value for the second transition, e.g.  $\Delta_2^{0,2}R (K_c = J - 2)$  represents the second difference formed from the transitions  $J_{0,J}$  and  $J_{2,J-2}$  where the  $K_c$  value of the second transition is  $J - 2$  and  $J$  denotes the lower energy level for each transition.

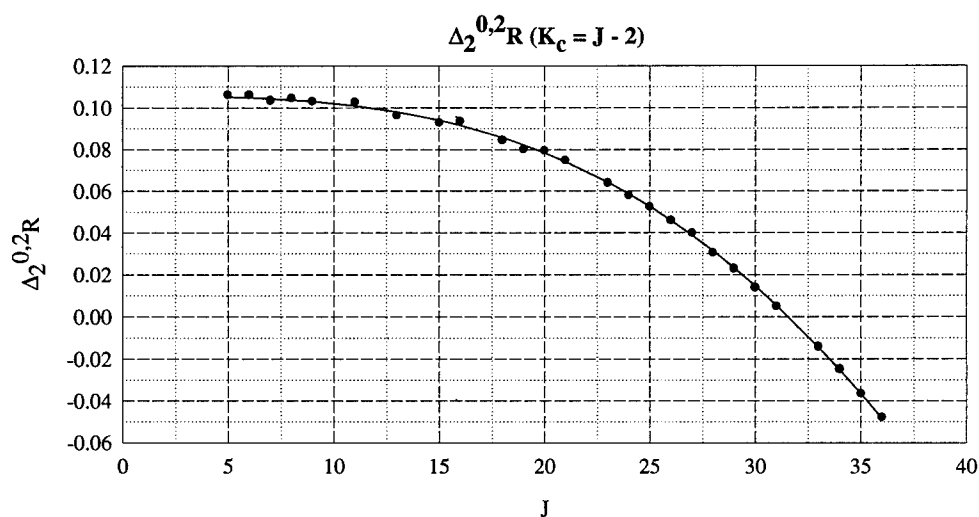


**Figure 5-1.** Second difference data and curve fit for the trend from  $J_{0,J}$  to  $J_{2,J-2}$  as a function of  $J$  for  $J < 40$ . Transitions used to generate data points were obtained from Esposti *et al.*<sup>4</sup> Expression fit without distortion parameters in expression.

The data in Figure 5-1 is well represented by the  $\Delta_2$  equation used for the fit.

However, this fit does not reveal any information about the exact  $J$  limit of the

approximation for the  $v_1 = 0 \rightarrow v_1 = 1$  transition since the parameters of this fit were within 0.2 percent of the values published by Esposti *et al.*<sup>4</sup>

To determine the effect of trying to use the approximation at values higher than the upper bound, the data used in Figure 5-1 was extended to include data up to  $J = 70$ . The resulting  $\Delta_2$  fit to this data appears in Figure 5-2.

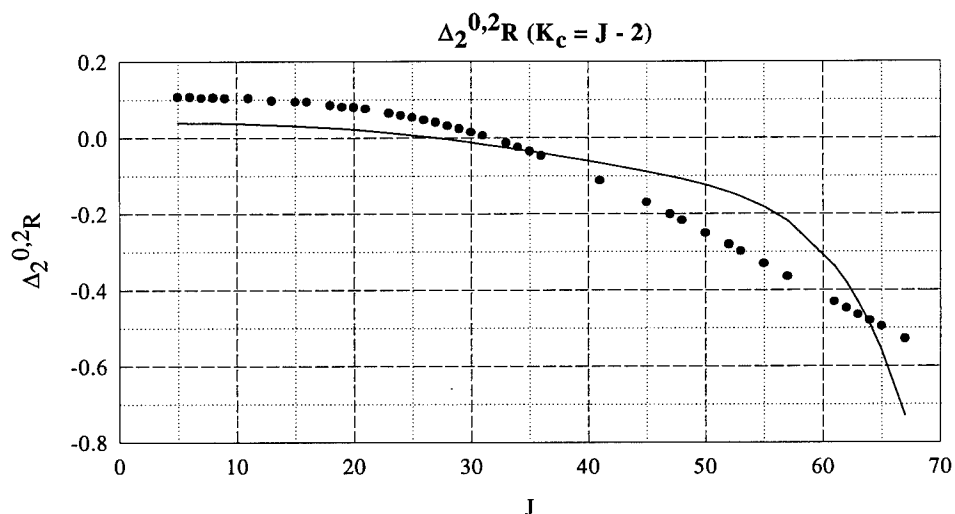


**Figure 5-2.** Same  $\Delta_2$  fit as above for  $J < 70$ .

This fit does show what will happen when the approximation breaks down.

However, without the distortion terms included in the  $\Delta_2$  fit in Figure 5-2, the inability of the approximation to represent the data was not conclusively caused by the breakdown of the asymmetry expansion. To determine the cause of the poor fit in Figure 5-2, the centrifugal terms were included in the analytical expression for the  $\Delta_2$  data plotted in the figure above, and this equation was fit to the same data. A good fit was obtained, but the values of the fit parameters representing the distortion constants showed liberal differences from the published constants with the largest of these differences being an

order of magnitude. This lead to the assumptions that the approximation had broken down and that the analytic  $\Delta_2$  expression containing the distortion parameters was somewhat parametric and consequently fit the data well.

The inability to reproduce the published distortion values from a fit to the data for  $J > 40$  lead to the assumption that the asymmetry approximation breaks down above the approximate upper bound. However, the requirement of distortion parameters in the  $\Delta_2$  expression was still not determined for the  $J \leq 40$  range. This was resolved by fitting the  $\Delta_2$  data in Figure 5-1 using the  $\Delta_2$  expression with the distortion parameters included. The fit obtained was better than the fit in Figure 5-1 which can be expected since there are more parameters used. In spite of a better fit, the accuracy obtained in the values of the fit parameters was only on the order of  $0.01 \text{ cm}^{-1}$ . Any global fitting routine used should be able to find the best set of constants with initial guesses that are moderately close, so the difference of  $0.01 \text{ cm}^{-1}$  in the values of the parameters does not necessitate the use of these parameters in the analytic  $\Delta_2$  expressions.

### **5.1.2 $\Delta_2$ Fits to $v_1 = 0 \rightarrow v_1 = 2$ Spectrum**

With the knowledge of the pitfalls that result from using data above the approximate upper bound, the assignments made for the P branch of the  $v_1 = 0 \rightarrow v_1 = 2$  transition were investigated with analytical  $\Delta_2$  expressions that contained only the A, B, and C rotational parameters. All of the second difference plots and the subsequent residuals, the distance from each data point to the curve fit to the data, that are not discussed herein

appear in Appendix B. There are two plots which require a discussion of noteworthy features.

The feature exhibited by the first set of plots is the overfitting of data. Although the actual overfitting occurs for a range of  $J$  values that are not appropriate for the approximation, the fine balance between the parameters of the fit for  $J$  values less than the approximate upper bound can be appreciated by viewing an extension of the approximation. In Figure 5-3 the  $\Delta_2$  trend  $J_{0,J}$  to  $(J+1)_{0,(J+1)}$  is shown for the  $v_1 = 0 \rightarrow v_1 = 2$  transition.

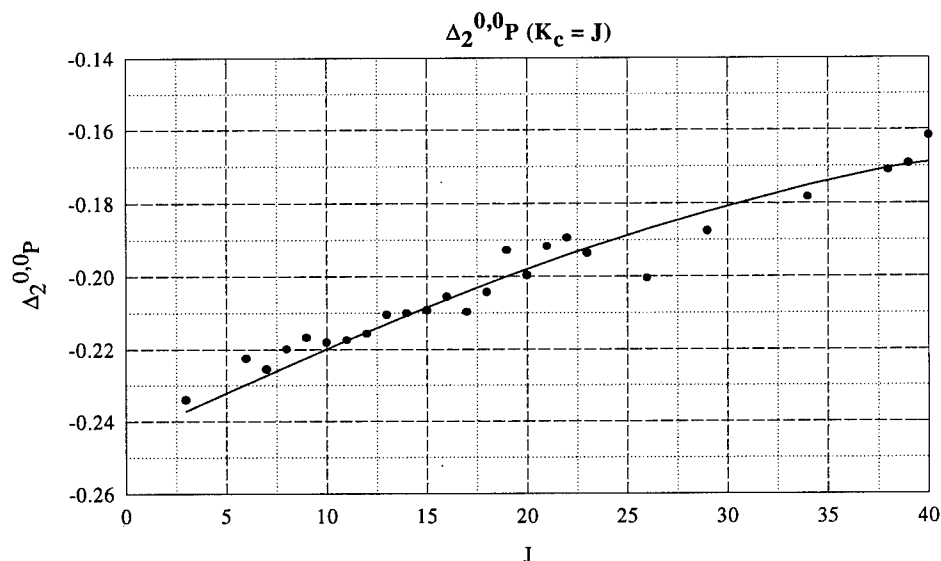


**Figure 5-3.** Curve fit for  $\Delta_2$  trend from  $J_{0,J}$  to  $(J+1)_{0,(J+1)}$ . The fine balance between the parameters results in the fit of a twelfth order polynomial to a linear set of data without overfitting.

The equation fit in this plot is a twelfth order polynomial in  $J$ . This high order polynomial was generated by the  $\Delta_2$  of the approximate analytical energy level expressions and, amazingly, it fits the somewhat linear data rather nicely as can be seen in

Figure 5-4 where the residuals of the fit above are plotted. With all of the residuals of the data within the resolution of the spectrometer in Figure 5-4 and physically realistic values for the fit parameters, it is clear that these spectral features follow an appropriate trend.

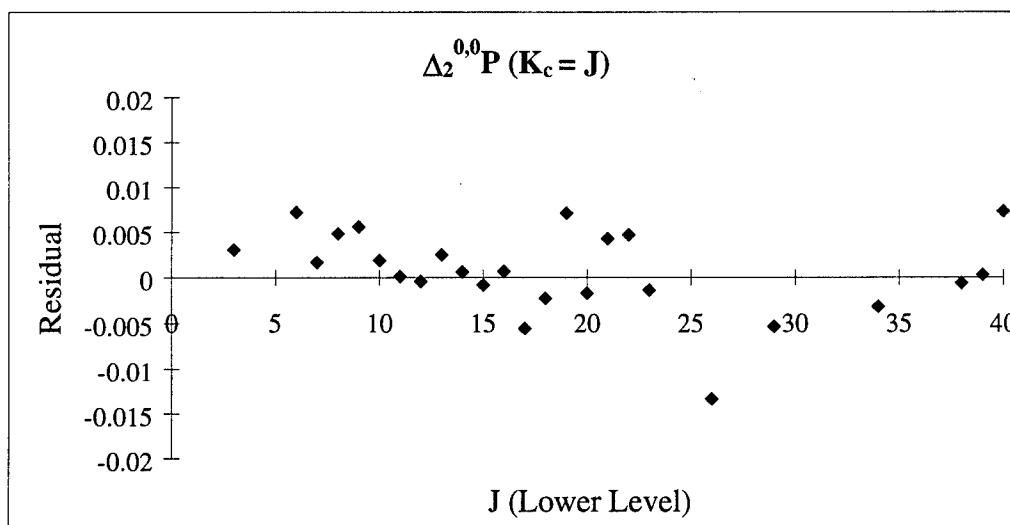


**Figure 5-4.** Residuals for trend shown in Figure 5-3. Note that the upper and lower bound of the residual axis is equal to the resolution of the spectrometer. Also note that all residuals lie within this region.

When the range of  $J$  is increased for the plot in Figure 5-3 not only is the range of  $J$  increased above the approximate upper bound, but the fit shows the expected overfitting of a high order polynomial. This occurs because the fine balance that allowed the data to be fit in Figure 5-3 has been lost with a clear breakdown of the asymmetry approximation. The overfitting is shown in Figure 5-5.



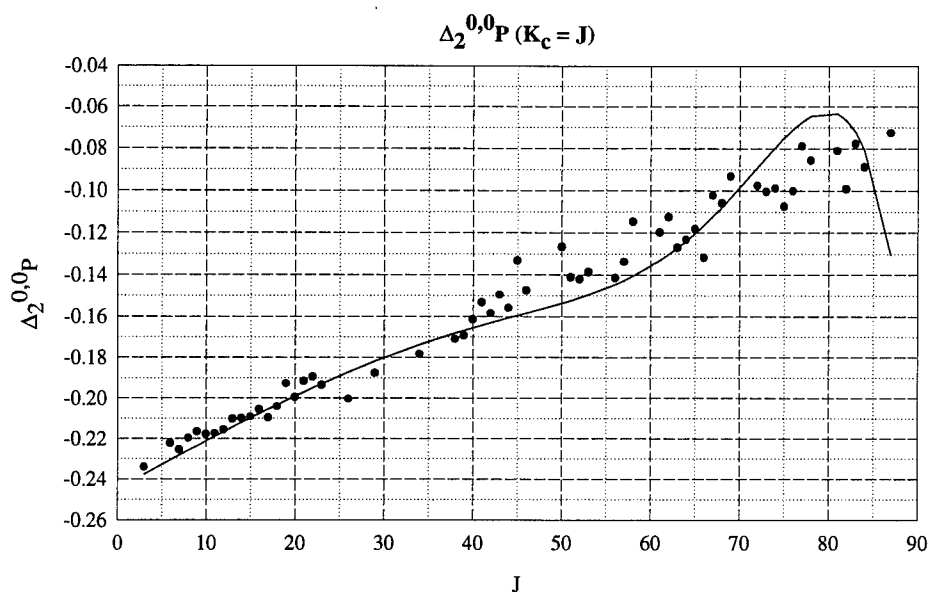


**Figure 5-5.** Example of overfitting in  $v_1 = 0 \rightarrow v_1 = 2$  data resulting from the loss of the fine balance between rotational parameters in the approximate energy level expressions when the approximation breaks down.

The second feature of the curve fits that was observed originated in the  $\Delta_2$  trend from  $J_{0,J}$  to  $J_{1,J-1}$ . This peculiarity resembled the overfitting found in Figure 5-5, but the  $J$  value at which the approximation seemed to breakdown was eighteen. The  $\Delta_2$  data for  $J < 18$  for the trend is fit with the corresponding  $\Delta_2$  expression in Figure 5-6. The residuals for this fit appear in Figure 5-7, and the  $\Delta_2$  data for  $J \leq 40$  for the trend is fit with the same expression in Figure 5-8.

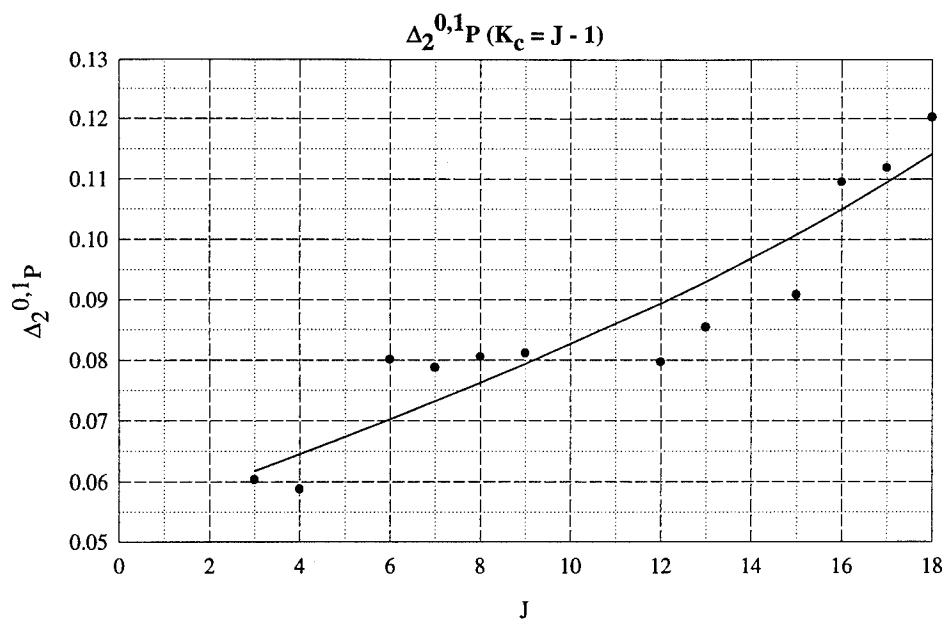


**Figure 5-6.**  $\Delta_2$  trend fit with appropriate equation for valid region of  $J$ .

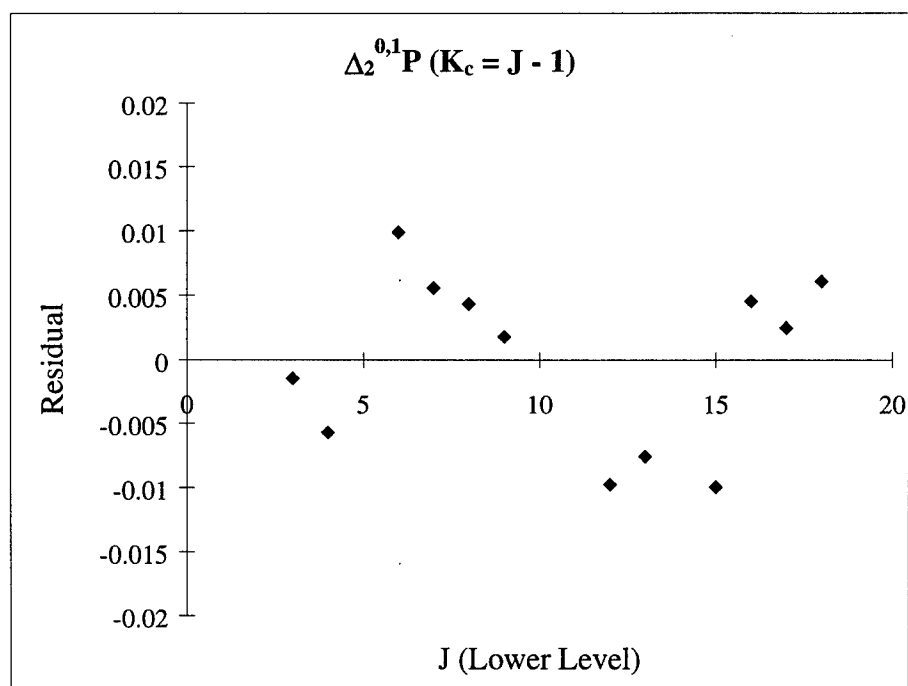


**Figure 5-7.** Residuals of fit in Figure 5-6. All residuals are within  $0.02 \text{ cm}^{-1}$ .

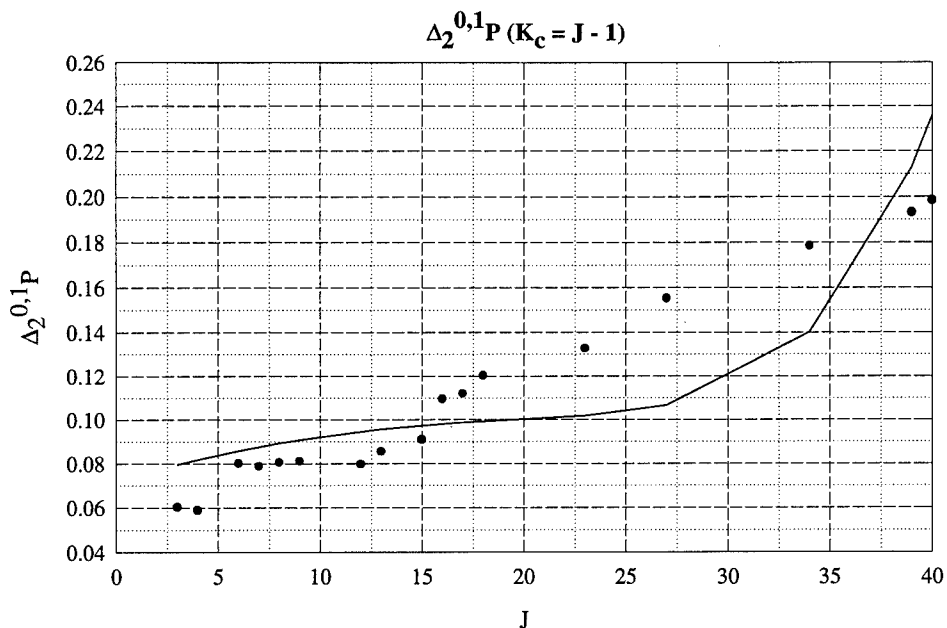


**Figure 5-8.** Overfitting resulting from the apparent break down of the approximation for this trend which could be attributable to inappropriate expansion coefficients.

The overfitting shown in Figure 5-8 was also witnessed in the fit to the  $\Delta_2^{0,3}P$  ( $K_c = J - 2$ ) data for  $J > 25$ . This apparent overfitting in these two particular cases could be linked to the exact value of  $J$  at which the approximation breaks down, yet these two  $\Delta_2$  expressions began overfitting at different values of  $J$ . To get a better understanding of the origin of this proposed breakdown, codes were written in Mathematica<sup>®</sup> from Wolfram Research to produce the rotational energy levels for the  $v_1 = 1$  level using the numerical diagonalization (source code in Appendix C) and approximate energy level expressions. The difference between the location of the energy levels calculated by each code was obtained. This comparison showed that the  $J_{1,J-1}$  approximate energy levels deviated from the diagonalization energy level by  $0.02 \text{ cm}^{-1}$  at  $J = 18$ . When the  $J_{3,J-2}$

energy levels where compared in a similar fashion, the deviation reached  $0.02\text{ cm}^{-1}$  for  $J > 22$  where the  $0.02\text{ cm}^{-1}$  difference was chosen as the maximum allowed error in the energy level calculation since the error in a transition formed between two energy levels should not be larger than the resolution of the spectrometer.

The overfitting witnessed in these two particular  $\Delta_2$  plots may result from a fit to data that cannot be approximated or a bad expansion coefficient for each of these energy levels in Polo's publication.<sup>13</sup> Since all other  $\Delta_2$  fits did not show any overfitting and the only significant difference in the approximate energy levels is in the expansion coefficients which are used to predict the implications of asymmetry, the error might be in one of these quoted expansion coefficients.

## ***5.2 Global Fitting Routine***

The goal of any spectroscopic research is to report the rotational and possibly the centrifugal distortion constants that explain the rotation of a molecule from the correctly assigned spectrum. This research is not any different. To obtain these physical constants, a computer code was written to find the parameters that would replicate the data obtained from the spectral assignments up to  $J = 40$ .

### **5.2.1 Approach**

A computer program written to accomplish this task requires a procedure to calculate the energy levels as a function of the parameters that represent the rotational constants and a procedure to find the best set of these parameters which can then be reported as the rotational constants. The choice of the procedure used to calculate the energy levels is

driven by the molecule, while the procedure to find the best set of parameters must be written to find the minimum of a surface that is described by the set of parameters.

Finding the set of parameters that result in a minimum value for the height of a surface is far from a trivial problem. The number of dimensions of the surface is defined by the number of rotational constants required to describe the rotation of the molecule plus one dimension for the height of the surface. For ONBr the centrifugal distortion constants are required which increases the number of required parameters to nine. Therefore, when the height of the surface is included, the procedure must find a minimum on a ten dimensional surface. The relationship of these nine dimensions is unknown which implies a simultaneous change in two parameters may be required to approach the minimum of the surface.

The difficulty described above has a calculus-based solution. At a given point P, there is a corresponding height to the surface. When all points of this surface height are connected, a contour is created with a shape that is dependent on the function which describes the surface. When the gradient of the function is taken at P, the vector obtained will be perpendicular to the contour and point in the direction of the steepest ascent. To find the local minimum of the surface near P, the components of the gradient vector are multiplied by  $\lambda$ , a previously determined step size, and this scaled vector is subtracted from the coordinates describing point P thereby going in the direction of steepest descent. This process continues iteratively until the gradient no longer produces changes in the surface height within the bounds of the accuracy required.

### 5.2.2 Implementation

The global fitting routine to determine the best spectroscopic constants was coded in Mathematica<sup>®</sup> by Wolfram Research. This language was chosen by virtue of the numerous built-in functions that utilize robust and proven algorithms to solve both numerical and analytical mathematics problems. Also, the ability to debug the code as it was written was agreeable. The final, documented code appears in Appendix C.

The two procedures required by this computer program were chosen to aid in computational efficiency and memory usage. The procedure to calculate the energy levels was based on the approximation to the energy levels. Even though this theory was only valid over a subset of the observed transitions, the diagonalization procedure presents a problem with numerous numerical difficulties. To find the best set of parameters to replicate the data, the function FindMinimum was used. This function calls an algorithm which uses a gradient method to calculate the rate of steepest descent and requires input guesses to begin the search for the nearest local minimum.<sup>18</sup> The actual minimization was done on the value of the sum square error at point P where the sum square error is defined by:

$$SSE = \sum_{i=1}^N (TO_i - TC_i)^2 \quad (5.1)$$

where  $SSE$  is the sum square error,  $TO_i$  and  $TC_i$  are the  $i^{\text{th}}$  observed and calculated transitions, respectively, and  $N$  is the number of observed transitions. By minimizing the  $SSE$ , the rotational parameters used to generate the calculated transitions were forced to the values that best replicated the observed transitions. Once the gradient found caused

less than a  $1 \times 10^{-4}$  change in the SSE, the routine ended and the SSE and rotational constants defining the minimum were output. From the output SSE, the quality of the fit could be determined by finding the standard deviation of the data by:

$$\sigma = \sqrt{\frac{SSE}{N-2}} \quad (5.2)$$

where  $\sigma$  is the standard deviation and  $SSE$  and  $N$  are defined as in (5.1).

The minimization of the sum square error for the rotational transitions of ONBr with the constraint that the parameters were physically realistic proved to be a very trying task. To eliminate some of the difficulty, the distortion parameters  $R_5$  and  $R_6$  were constrained such that these values would equal the published  $\delta_k$  value by solving the appropriate transformation in (2.26) for  $R_6$  in terms of  $R_5$  and  $\delta_k$ . Even with this constraint to reduce the parameters, the initial method employed to find the physical local minimum was dependent on results from previous minimizations. This method involved finding the minimum of a hypersurface, a slice of the surface obtained by holding parameters fixed. Upon the completion of each minimization, the previously obtained values were input as the initial guesses and the dimension of the hypersurface was expanded by one by allowing another parameter to vary. This procedure worked well for a hypersurface with less than seven dimensions, however, the ability to find the local minimum on the seven dimensional hypersurface became extremely guess dependent. With this characteristic, the addition of dimensions seemed to create a stiff problem. To compensate for this apparent stiffness, two initial guesses were used for each parameter where the second initial guess was calculated by adding no more than a tenth of a percent to the first guess.

The value of the second guess did not influence the location of the minimum found, only the ability of the code to eliminate the stiffness. With the addition of these guesses, all nine parameters could be minimized by using physically realistic values for the initial guesses.

To verify the code, a subset of the  $v_1 = 0 \rightarrow v_1 = 1$  data was used as the observed data list.

This subset contained transitions between energy levels that could be calculated by the approximate equations. The results of this validation appear in Table 5-1.

**Table 5-1.** Molecular constants for  $\text{ON}^{79}\text{Br}$  for the  $v_1$  fundamental band as published and determined by this research. All rotational parameters, band origins, and  $\sigma$ 's in  $\text{cm}^{-1}$ . Standard errors in units of the last quoted digit are given in parentheses for the constants.

	$v_1 = 0^{\text{a)}}$	$v_1 = 1$	
		Diagonalization <sup>a)</sup>	Approximation
$\nu_0$	N/A	1798.751285(53)	1798.753081
$\mathcal{A}$	2.85229541	2.826284(3)	2.825820
$\mathcal{B}$	0.125002273	0.12552047(15)	0.12550206
$\mathcal{C}$	0.119628555	0.12006208(13)	0.12007743
$\Delta_J (10^{-8})$	9.514889	9.62636(123)	9.51681
$\Delta_{JK} (10^{-6})$	-1.89878	-1.8999(9)	-1.9467
$\Delta_K (10^{-4})$	1.60979	1.5769(4)	1.4638
$\delta_J (10^{-9})$	5.26711	5.3859(157)	2.9732
$\delta_K (10^{-7})$	6.6250 <sup>b)</sup>		
$\epsilon (10^{-4})$	4.9210232	5.0471816	5.0196430
transitions	N/A	890	447
$\sigma$	N/A	0.00063	0.00341

<sup>a)</sup> Observations and values obtained by Esposti *et al.*<sup>4</sup>

<sup>b)</sup> Common value for the ground and  $v_1 = 1$  states.



The minimized parameters obtained are similar to those published by Esposti *et al* with the exception of the band origin and the some of the distortion constants.<sup>4</sup> Since the code used to obtain this set of spectroscopic constants was different and the computation was not done on the complete  $v_1 = 0 \rightarrow v_1 = 1$  data set, the minimized values were not expected to be identical to the published constants, however, the standard deviation, although within the resolution,  $0.0045 \text{ cm}^{-1}$ , is considerably higher than the published deviation. The residuals of the fit were investigated to see if any information could be gained about the maximum J value that could be approximated. If the approximation had broken down, the residuals would exhibit a trend when the asymmetry approximation was no longer valid; no trend was apparent.

### ***5.3 Determination of the Valid Range of J and the Rotational Constants***

When the global fitting routine was implemented to determine the rotational parameters describing the spectral assignment of the  $v_1 = 0 \rightarrow v_1 = 2$  transition, the existence of many local minima on the ten dimensional surface prompted the need for physically realistic values as initial guesses. Since the values of the  $\Delta_2$  plots did not follow the trend between the  $v_1 = 0$  and  $v_1 = 1$  rotational parameters, a method to generate a new set of initial guess was sought. The harmonic approximation was invoked to determine these physically realistic guesses.

In the harmonic approximation, all the vibrational levels are separated by the same distance. This implies that all the rotational parameters for a particular vibrational level will have values that follow a linear trend as the vibrational level is changed. Even

though this approximation cannot explain anharmonicity or dissociation, these phenomena do not need to be considered for the low vibrational levels studied by this research.

Due to the spacing in the vibrational levels, any rotational parameter that is vibrationally dependent, the A, B, and C (representation free) parameters, for example, will exhibit a trend. In the harmonic approximation, the difference between the values of a parameter for the second vibrational level and the first vibrational level will be identical to the difference of the first level and ground level values for the same parameter.

With the harmonically approximated values as the initial guesses, the code was implemented on the set of observed transitions with  $J \leq 40$ . The values obtained for the rotational constants appears in Table 5-2.

**Table 5-2.** Rotational parameters obtained from fit to observed transitions for  $J \leq 40$ . Rotational parameters, band origin, and  $\sigma$  are given in  $\text{cm}^{-1}$  and  $\epsilon$  is unitless.

Constant	$\nu_0$	$\mathcal{A}$	$\mathcal{B}$	$\mathcal{C}$	$\Delta_J (10^{-8})$	$\Delta_{JK} (10^{-7})$
$\nu_1 = 2$	3563.0189	2.80039	0.126434	0.120671	9.644356	6.590861
Constant	$\Delta_K (10^{-4})$	$\delta_J (10^{-8})$	$\delta_K (10^{-7})$	$\epsilon (10^{-4})$	transitions	$\sigma$
$\nu_1 = 2$	3.144468	-2.69033	6.62496	5.38228	434	0.0901

The standard deviation of this fit is close to, but not less than, the resolution of the spectrometer. To determine the primary cause of this high standard deviation, the residuals of the transitions in each of the branches were investigated. All of these residuals exhibited the same type of trend for high J as shown in Figure 5-9.

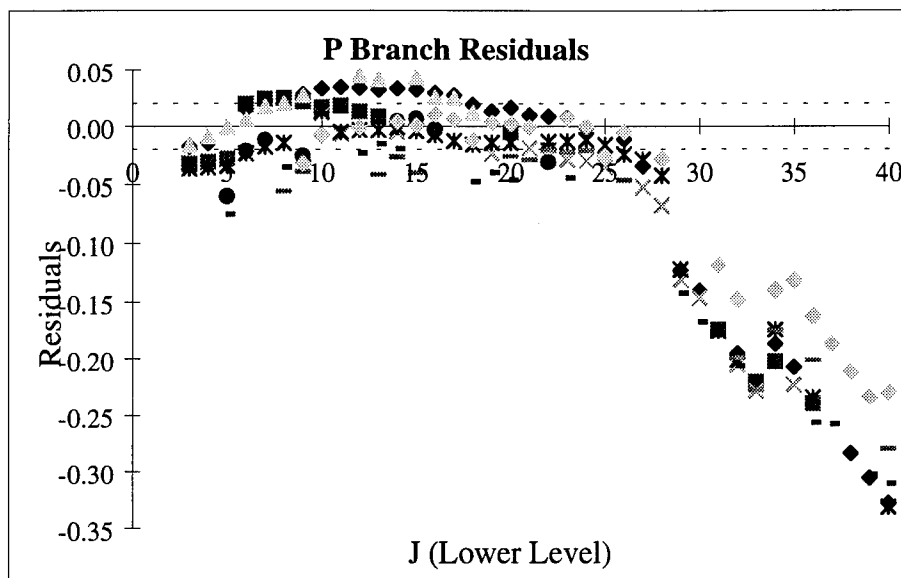


**Figure 5-9.** Residuals of the P branch transitions. Dotted lines represent the resolution bounds and each symbol represents a different combination of  $K_a$  and  $K_c$ .

With the magnitude of the residuals at high  $J$  being so large, the immediate cause of this problem seemed to be linked to the truncation of the power series in  $m$  in the approximation. This situation seems likely since the series converges very slowly with the values of the truncated terms on the order of the resolution.

Another possible cause of the large residuals could be a misassignment of the spectrum. This cause is conceivable since the values obtained for the rotational parameters are not close to the numbers obtained from the  $\Delta_2$  curves. In particular, the values of the  $A$  (representation free) parameter differed by  $0.005 \text{ cm}^{-1}$ . Since the  $A$  parameter is a coefficient in the asymmetry expansion which contains a  $J$  dependence of twelfth order in the series, a change in the value of the  $A$  parameter will drastically change the location of the transitions that fit the trend. With this change of the trend, the assignments that fit the previous  $\Delta_2$  trends would be incorrect for high  $J$ .

To determine the actual cause of the trend for high  $J$ , the constants reported in Table 5-2 were used to calculate the energy levels with the diagonalization code in Appendix C. This code was benchmarked against the calculated transitions published by Esposti *et al* and found to be accurate to within  $5 \times 10^{-4} \text{ cm}^{-1}$ .<sup>4</sup> Transitions corresponding to the observed transitions were calculated from these energy levels and the residuals were obtained. In Figure 5-10 the residuals for the  $J_{0,J}$  transitions in the P branch,  $P(J_{0,J})$ , with  $J \leq 40$  are plotted.

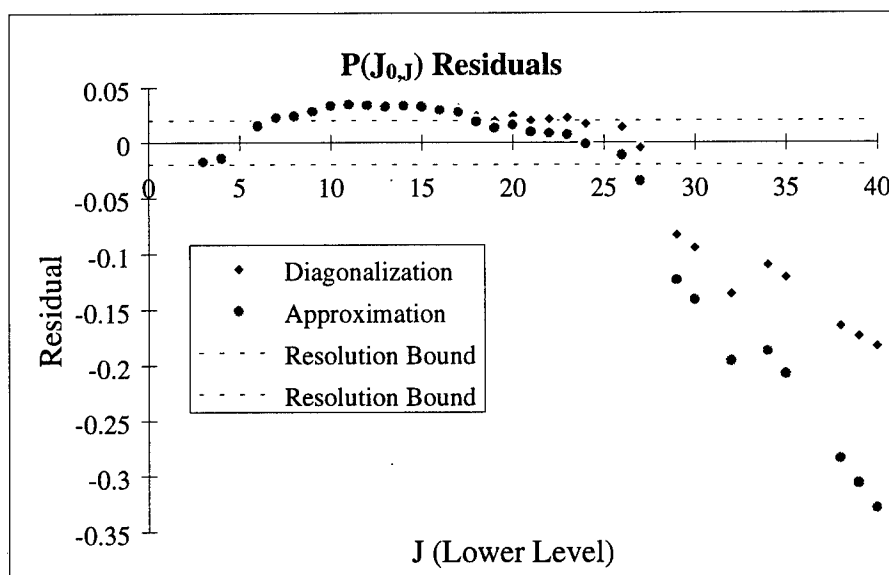


**Figure 5-10.** Residuals of  $J_{0,J}$  transitions for the asymmetry expansion and diagonalization procedures. Rotational parameters used for both methods are found in Table 5-3.

There is a clear deviation in the residuals of the two methods which must result from the breakdown of the asymmetry approximation since any misassignments would effect both sets of residuals. To find the  $J$  value at which this deviation becomes larger than the experimental resolution, the difference of the transitions calculated in the global fit and

the transition calculated by the numerical diagonalization was taken. This difference appears in Figure 5-11.

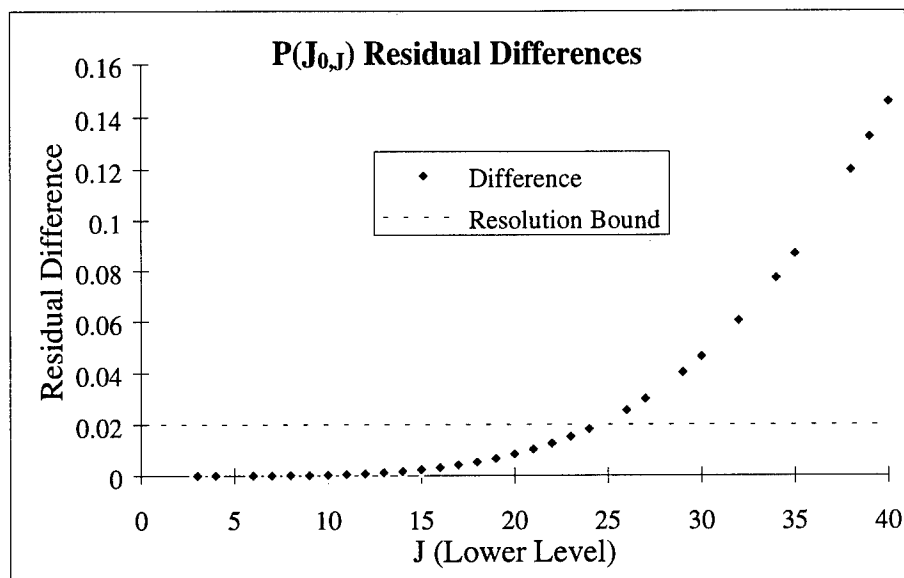


**Figure 5-11.** Difference in the transitions calculated with the diagonalization method and the transitions obtained from the global fit based on the asymmetry approximation method. The smooth trend in this plot clearly shows the dynamic breakdown of the approximation for  $J > 25$ .

From Figure 5-11, the highest  $J$  value that is accurately represented within the experimental resolution is  $J = 24$ . A similar analysis was done for the other sets of transitions of the same  $K_a$  value for all three branches, and all of these residual differences showed roughly the same maximum  $J$  value.

With the valid range of  $J$  known, the asymmetry expansion was used to determine an accurate set of rotational constants for transitions in this range. The previously published constants for the  $v_1 = 0$  and  $v_1 = 1$  levels appear in Table 5-3 with the values obtained from the fit to the set of transitions with  $J \leq 24$ . (For the complete list of transitions, observed and calculated locations, and the residuals of the fit see Appendix D.)

**Table 5-3.** Molecular constants for ON<sup>79</sup>Br. All values are in cm<sup>-1</sup> except the number of transitions. Numbers in parentheses represent the error in the last digit.

	$v_1 = 0^a$	$v_1 = 1^a$	$v_1 = 2$
$v_0$	N/A	1798.751285(53)	3563.03442(92)
$A$	2.85229541	2.826284(3)	2.793526(55)
$B$	0.125002273	0.12552047(15)	0.1264969(56)
$C$	0.119628555	0.12006208(13)	0.1207390(22)
$\Delta_J (10^{-8})$	9.514889	9.62636(123)	16.49(38)
$\Delta_{JK} (10^{-6})$	-1.89878	-1.8999(9)	-2.23(17)
$\Delta_K (10^{-4})$	1.60979	1.5769(4)	1.577(25)
$\delta_J (10^{-9})$	5.26711	5.3859(157)	12.2(29)
$\delta_K (10^{-7})$	6.6250 <sup>b)</sup>		
$\epsilon (10^{-4})$	4.9210232	5.0471816	5.3922(38)
transitions	N/A	890	294
$\sigma$	N/A	0.00063	0.01683

<sup>a)</sup> Observations and values obtained by Esposti *et al.*<sup>4</sup>

<sup>b)</sup> Common value for the ground,  $v_1 = 1$ , and  $v_1 = 2$  states.

The errors quoted in the constants for the  $v_1 = 2$  level were obtained through the use of a Monte Carlo technique that used random numbers whose distribution was described by a Gaussian centered at zero with a standard deviation of 0.0075 cm<sup>-1</sup>. These numbers were added to every point in the observed data set to simulate another collection of rotational transitions, and the best set of constants for the “new” data set were obtained. The distribution of the numerous values for the constants were then used to determine the standard deviation in the value of each constant.

This standard deviation, while lower than the experimental resolution, can be improved by viewing the residuals of the fit. An investigation of these values will show which transitions were misassigned, and the fit can be reaccomplished to refine the values of the constants.

The  $\nu_0$ ,  $A$ ,  $B$ , and  $C$  constants in Table 5-3 are well determined for this small set of transitions may contain some error due to misassignment, but these values can be used to further study the  $\nu_1 = 0 \rightarrow \nu_1 = 2$  transition in ONBr. The distortion constants, however, are not well known since the errors in these constants are quite large.

The size of the errors in the centrifugal distortion constants can be used to understand the physics of the rotating ONBr molecule. The high errors in these constants imply that the molecule is just beginning to distort; the distortion parameters can still be changed dramatically to obtain a low sum square error. Also, earlier in this chapter the centrifugal distortion terms were omitted from the  $\Delta_2$  equations since the inclusion of these terms did not significantly change  $A$ ,  $B$ , and  $C$  (representation free) parameters. These high standard deviations support the assumption to neglect these terms in the  $\Delta_2$  equations used to assign the spectrum.

The constants obtained from the fit are considerably removed from the trend between the  $\nu_1 = 0$  and  $\nu_1 = 1$  constants. This is not surprising since many local minima were found on the ten dimensional surface. The  $\nu_1 = 2$  constants may differ from the previously published vibrational trend since the transitions used to obtain these values was limited to  $J < 25$ . However, the nine constants were determined from 294

transitions with a standard deviation within the experimental resolution. Therefore, the constants for the  $v_1 = 1$  and  $v_1 = 2$  levels should be determined simultaneously using both sets of data with the constraint that the difference in the trend for each constant be no greater than the trend between the band origins of each vibrational transition.

The numbers reported in Table 5-3 show some of the physics of the rotation of the molecule. The asymmetry parameter, for example, has increased for each level. This implies that the molecule has become more asymmetric as the vibrational energy is increased. Undoubtedly, this trend will continue until the molecule dissociates.



## 6. Conclusion

### 6.1 Summary

Nitrosyl bromide (ONBr) is a nearly-prolate asymmetric molecule with an asymmetry parameter,  $\kappa$ , of -0.996. This molecule can be created by combining gaseous  $\text{Br}_2$  and NO in a sample chamber which is allowed to equilibrate under room lights. Equilibrium is reached rapidly under the aforementioned circumstances with only residual amounts of  $\text{Br}_2$  and NO remaining in the cell.

The asymmetric nature of ONBr results in the lack of a quantum mechanical basis in which the rotational Hamiltonian of the molecule is diagonalized. This requires a numerical diagonalization of four tridiagonal matrices to calculate the energy levels of the molecule. Analytical expressions for the energy levels are desirable and can be obtained by using a perturbational technique. These analytical expressions have been used throughout this research.

The validity of the approximation for the energy levels, whose functional form is that of a power series expansion in the asymmetry parameter,  $\epsilon$ , has been checked by numerous methods including a comparison with the numerical diagonalization method. The present research has found that the approximation is valid for  $J \leq 24$  with the exception of the energy levels corresponding to  $J_{1,J-1}$ . By checking the location of these levels as calculated with the approximation against the corresponding levels as calculated with the numerical diagonalization, it appears that an error exists in the numerical expansion coefficients quoted for this J-dependent energy level expression.

The maximum value of  $J$  reported above was determined by comparing the transitions obtained from the global fit and the transitions calculated with the diagonalization procedure. By taking the difference of these two sets of transitions, the issue of a misassigned spectrum became a mute point. The plot of this difference shows a dynamic breakdown of the asymmetry expansion.

The inability of the approximation to represent energy levels for  $J > 25$  occurs because the series expansion in  $m$  must be truncated at the sixth  $J(J + 1)$  term due to the lack of reported expansion coefficients for higher order terms. Although inappropriate for  $J > 25$  for this study, all  $J$  values below this level, with the exception of the case described above, have valid analytical expressions which can be used to assign the spectrum up to the  $J = 24$  level.

The spectral assignment for the  $v_1 = 0 \rightarrow v_1 = 2$  transition in ONBr proved to be a formidable task due to the density of the spectrum. With the resolution obtainable by the FTS employed,  $0.02 \text{ cm}^{-1}$ , the dense spectrum exhibited considerable blending. To make the correct spectral assignments, certain trends between transitions, called second differences, were used. These trends, while applicable for only a small subset of the data, could be used to verify a spectral assignment by fitting the corresponding analytical second difference equation to the data. The spectral assignment was considered correct for a given trend when the parameters of the fit were physically realistic and the residuals of all the data points were within the resolution of the spectrometer.

The set of parameters obtained from these second difference fits were not complete because the values represented local fits to the data set. To obtain a global fit to the data, a computer code was written to find the minimum on a surface created with a dimension for the

sum square error and the each rotational constant. Numerous difficulties arose when this code was implemented. The most difficult of these was the existence of numerous local minima in the region of a local minimum that described a valid set of rotational constants. To guarantee the minimum found would be realistic, initial guesses were made from a harmonic approximation to the rotational constants.

When the dimension of the hypersurface was increased above six, the problem became stiff. This was overcome by calculating a second guess from the first initial guess. These guesses were calculated by adding no more than a tenth of a percent to the initial guess. With these two initial guesses being used, the minimum could be found with the harmonically approximated guesses.

The errors in the reported constants were obtained by introducing random Gaussian noise into the observed data set and then finding the best set of constants for this "new" data. This process was done repetitively until a set of values for each parameter was obtained. The statistics of this set of values were studied with the standard deviations of the set of constants reported as the error in each.

Since the errors in the  $\nu_0$ ,  $A$ ,  $B$ , and  $C$  parameters are small, these numbers have been determined for the  $\nu_1 = 0 \rightarrow \nu_1 = 2$  transition in ONBr and can be used in subsequent investigations of this transition. However, the errors in the centrifugal distortion parameters are too large to merit the use of these values.

All the rotational parameters obtained can be used to explain the physics of the molecule. The asymmetry parameter for each vibrational level in Table 5-3 shows an increasing trend. This implies that the molecule becomes more asymmetric as more energy is

added. Also, the large standard deviations in the centrifugal distortion constants reported in Table 5-3 lead one to believe that the molecule is not considerably distorted as it rotates for  $J \leq 24$ .

## 6.2 *Recommendations for Future Work*

Numerous stones that have been turned by this research have not been investigated. These topics require investigation before the exact role of ONBr in the depletion of the ozone layer or the Br\*/NO energy transfer laser can be understood.

The actual mechanism used to create ONBr is not sufficiently understood. The only rate coefficient published is for the direct creation of ONBr from Br<sub>2</sub> and NO. The reactions used to form ONBr in this experiment involved the photolysis of the Br<sub>2</sub> by room lights and a subsequent reaction of the Br with NO and a third body. These reaction rates were not located by the literature search which accompanied this research.

When the initial spectrum of ONBr was obtained, the amount of absorption was surprising. The cross section for absorption of both the  $\nu_1 = 0 \rightarrow \nu_1 = 1$  and  $\nu_1 = 0 \rightarrow \nu_1 = 2$  transitions have not been reported, so any preliminary calculation of the pressure of ONBr required to obtain an adequate spectrum could not be completed. It was the intent of this research to determine the absorption cross sections for these and other overtones of the  $\nu_1$  stretch frequency, however, theoretical and mathematical difficulties did not allow time for this study.

Since blending is so prevalent in the spectrum, another spectrum of this region taken with a higher resolution should be completed. This would increase the number of spectral

features to assign, however, the features recorded would result from one or possibly two transitions. The limited blending could then lead to an analysis of the intensities of the transitions and a much improved assignment of the spectrum with considerably improved constants. The initial assignment of this spectrum could be done with the second difference equations used by this research for a  $J$  value appropriate for the resolution used to record the spectrum.

Although the approximation is valid for transitions of  $J \leq 24$ , only a small number of the spectral features observed fall into this category. To assign and globally fit all the spectral features, the numerical diagonalization must be used to calculate the energy levels. This requires the writing of a code to perform the necessary diagonalization as a function of the parameters of a minimization procedure. With the completion of this code and a complete assignment of the spectrum, the rotational constants can be improved. If these improved values still do not replicate the slight anharmonic trend expected in the constants, a global fit to the  $v_1 = 0 \rightarrow v_1 = 1$  and  $v_1 = 0 \rightarrow v_1 = 2$  transitions must be completed to generate the appropriate constants for both levels.

## Bibliography

- <sup>1</sup> Solomon, S. "The Mystery of the Antarctic Ozone 'Hole'." *Reviews of Geophysics* 26 (1988): 131-148.
- <sup>2</sup> Johnson, R. O. "Excited Atomic Bromine Energy Transfer and Quenching Mechanisms." Dissertation. Air Force Institute of Technology, 1993.
- <sup>3</sup> Petersen, A. B., L. W. Braveman, and C. Wittig. "H<sub>2</sub>O, NO, and N<sub>2</sub>O Infrared Lasers Pumped Directly and Indirectly by Electronic-Vibrational Energy Transfer." *Journal of Applied Physics* 48 (1977): 230-233.
- <sup>4</sup> Esposti, C. Degli, et al. "High-resolution Fourier Transform Spectroscopy of the  $\nu_1$  Fundamental Band of Nitrosyl Bromide." *Chemical Physics Letters* 214 (1993): 531-535.
- <sup>5</sup> Laane, Jaan, et al. "Vibrational Spectra and Force Constants for Isotopic Species of Nitrosyl Bromide." *Journal of Molecular Spectroscopy* 30 (1969): 485-497.
- <sup>6</sup> Nichols, Nathan L., C. D. Hause, and R. H. Noble. "Near Infrared Spectrum of Nitric Oxide." *Journal of Chemical Physics* 23 (1955): 57-61.
- <sup>7</sup> Olman, M. D., M. Dominic McNelis, and C. D. Hause. "Molecular Constants of Nitric Oxide from the Near Infrared Spectrum." *Journal of Molecular Spectroscopy* 14 (1964): 62-78.
- <sup>8</sup> Guelachvili, G., and K. Narahari Rao, eds. *Handbook of Infrared Standards*. New York: Academic Press, 1986.
- <sup>9</sup> Bransden, B. H. and C. J. Joachain. *Physics of Atoms and Molecules*. New York: Wiley, 1983.
- <sup>10</sup> Watson, James K. G. "Aspects of Quartic and Sextic Centrifugal Effects on Rotational Energy Levels." in *Vibrational Spectra and Structure*. Vol. 6. Ed. James R. Durig. New York: Elsevier, 1977. 1-89.
- <sup>11</sup> Schawlow, A. L., and C. H. Townes. *Microwave Spectroscopy*. New York: McGraw-Hill, 1955.
- <sup>12</sup> Wang, S. C. "On the Asymmetrical Top in Quantum Mechanics." *Physical Review* 34 (1929): 243-252.

- <sup>13</sup> Polo, S. R. "Energy Levels of Slightly Asymmetric Top Molecules." *Canadian Journal of Physics* 35 (1957): 880-885.
- <sup>14</sup> Franklin, Robert E. "High Resolution Fourier Transform Absorption Spectrum of  $^{79}\text{Br}_2 \text{ B}^3\Pi(0_u^+) \leftarrow \text{X}^1\Sigma_g^+$ ." Thesis. Air Force Institute of Technology, 1993.
- <sup>15</sup> Grimely, A. J. and P. L. Houston. "The Photochemistry of Nitrosyl Halides: The  $\text{X} + \text{NOX} \rightarrow \text{X}_2 + \text{NO}(\text{v})$  Reaction ( $\text{X} = \text{Cl}, \text{Br}$ )." *Journal of Chemical Physics* 72 (1980): 1471-1475.
- <sup>16</sup> Hippler, H., et al. *International Journal of Chemical Kinetics* 10 (1978): 155.
- <sup>17</sup> *GRAMS/386 User's Guide*. 1993.
- <sup>18</sup> Wolfram, Stephen. *Mathematica: A System for Doing Mathematics by Computer*. 2nd Ed. New York: Addison-Wesley, 1991.

## Appendix A : Simplification of the Rotational Hamiltonian

With  $k = -J, -J+1, -J+2, \dots, 0, \dots, J-2, J-1, J$ , the Hamiltonian of the system becomes

$$\mathbf{H} = \begin{pmatrix} E_{J,J} & 0 & E_{J,J-2} & \dots & 0 & 0 & \dots & 0 & 0 \\ 0 & E_{J-1,J-1} & 0 & \dots & 0 & 0 & \dots & 0 & 0 \\ E_{J-2,J} & 0 & E_{J-2,J-2} & \dots & 0 & 0 & \dots & 0 & 0 \\ \vdots & \vdots & \vdots & \ddots & \vdots & \vdots & \ddots & \vdots & \vdots \\ 0 & 0 & 0 & \dots & E_{1,1} & 0 & \dots & 0 & 0 \\ 0 & 0 & 0 & \dots & 0 & E_{0,0} & \dots & 0 & 0 \\ 0 & 0 & 0 & \dots & E_{-1,1} & 0 & \dots & 0 & 0 \\ \vdots & \vdots & \vdots & \ddots & \vdots & \vdots & \ddots & \vdots & \vdots \\ 0 & 0 & 0 & \dots & 0 & 0 & \dots & E_{-J+2,-J+2} & E_{-J+2,J} \\ 0 & 0 & 0 & \dots & 0 & 0 & \dots & 0 & 0 \\ 0 & 0 & 0 & \dots & 0 & 0 & \dots & E_{-J+1,-J+1} & 0 \\ 0 & 0 & 0 & \dots & 0 & 0 & \dots & E_{-J,-J+2} & E_{-J,-J} \end{pmatrix} \quad (\text{A.1})$$



where  $E_{k',k}$  denotes the value of  $\langle J, k' | \hat{H}_{\text{rot}}^{(A)} | J, k \rangle$ . Since the ordering of the  $k$  and  $k'$  is degenerate in the calculation of the energy, and  $E_{k,k}$  and  $E_{k\pm 2,k}$  exhibit their  $k$  dependence in even powers of  $k$ ,  $E_{k',k} = E_{-k',k} = E_{k',-k} = E_{-k',-k}$ . With this reduction we need only look at the lower half of the Hamiltonian:

$$\mathbf{H} = \begin{pmatrix} E_{0,0} & 0 & E_{0,2} & 0 & \cdots & 0 & 0 & 0 & 0 \\ 0 & E_{1,1} & 0 & E_{1,3} & \cdots & 0 & 0 & 0 & 0 \\ E_{0,2} & 0 & E_{2,2} & 0 & \cdots & 0 & 0 & 0 & 0 \\ \vdots & \vdots & \vdots & \vdots & \ddots & \vdots & \vdots & \vdots & \vdots \\ \vdots & \vdots & \vdots & \vdots & \ddots & \vdots & \vdots & \vdots & \vdots \\ 0 & 0 & 0 & 0 & \cdots & E_{J-3,J-3} & 0 & E_{J-3,J-1} & 0 \\ 0 & 0 & 0 & 0 & \cdots & 0 & E_{J-2,J-2} & 0 & E_{J-2,J} \\ 0 & 0 & 0 & 0 & \cdots & E_{J-3,J-1} & 0 & E_{J-1,J-1} & 0 \\ 0 & 0 & 0 & 0 & \cdots & 0 & E_{J-2,J} & 0 & E_{J,J} \end{pmatrix} \quad (\text{A.2})$$

By invoking the symmetry of the rotational surface for an asymmetric top, Wang developed the following transformation to convert  $\mathbf{H}$  to a block diagonal form:<sup>10,12</sup>

$$\begin{aligned} |J, 0^+\rangle &= |J, 0\rangle \\ |J, k^+\rangle &= \frac{1}{\sqrt{2}} (|J, k\rangle + |J, -k\rangle) \\ |J, k^-\rangle &= \frac{1}{\sqrt{2}} (|J, k\rangle - |J, -k\rangle) \end{aligned} \quad (2.18)$$

The generalized transformation matrix is, for  $J$  even:

$$\mathbf{T}_e = \begin{pmatrix} \langle J, J | J, 0^+ \rangle & \langle J, J | J, 2^+ \rangle & \cdots & \langle J, J | J, J^- \rangle & \langle J, J | J, 1^+ \rangle & \cdots & \langle J, J | J, (J-1)^- \rangle \\ \langle J, J-1 | J, 0^+ \rangle & \langle J, J-1 | J, 2^+ \rangle & \cdots & \langle J, J-1 | J, J^- \rangle & \langle J, J-1 | J, 1^+ \rangle & \cdots & \langle J, J-1 | J, (J-1)^- \rangle \\ \vdots & \vdots & \cdots & \vdots & \vdots & \cdots & \vdots \\ \langle J, 0 | J, 0^+ \rangle & \langle J, 0 | J, 2^+ \rangle & \cdots & \langle J, 0 | J, J^- \rangle & \langle J, 0 | J, 1^+ \rangle & \cdots & \langle J, 0 | J, (J-1)^- \rangle \\ \vdots & \vdots & \cdots & \vdots & \vdots & \cdots & \vdots \\ \langle J, -J+1 | J, 0^+ \rangle & \langle J, -J+1 | J, 2^+ \rangle & \cdots & \langle J, -J+1 | J, J^- \rangle & \langle J, -J+1 | J, 1^+ \rangle & \cdots & \langle J, -J+1 | J, (J-1)^- \rangle \\ \langle J, -J | J, 0^+ \rangle & \langle J, -J | J, 2^+ \rangle & \cdots & \langle J, -J | J, J^- \rangle & \langle J, -J | J, 1^+ \rangle & \cdots & \langle J, -J | J, (J-1)^- \rangle \end{pmatrix} \quad (\text{A.4})$$

and for J odd:

$$\mathbf{T}_o = \begin{pmatrix} \langle J, J | J, O^+ \rangle & \langle J, J | J, 2^+ \rangle & \dots & \langle J, J | J, (J-1)^- \rangle & \langle J, J | J, 1^+ \rangle & \dots & \langle J, J | J, J^- \rangle \\ \langle J, J-1 | J, O^+ \rangle & \langle J, J-1 | J, 2^+ \rangle & \dots & \langle J, J-1 | J, (J-1)^- \rangle & \langle J, J-1 | J, 1^+ \rangle & \dots & \langle J, J-1 | J, J^- \rangle \\ \vdots & \vdots & \dots & \vdots & \vdots & \dots & \vdots \\ \langle J, 0 | J, O^+ \rangle & \langle J, 0 | J, 2^+ \rangle & \dots & \langle J, 0 | J, (J-1)^- \rangle & \langle J, 0 | J, 1^+ \rangle & \dots & \langle J, 0 | J, J^- \rangle \\ \vdots & \vdots & \dots & \vdots & \vdots & \dots & \vdots \\ \langle J, -J+1 | J, O^+ \rangle & \langle J, -J+1 | J, 2^+ \rangle & \dots & \langle J, -J+1 | J, (J-1)^- \rangle & \langle J, -J+1 | J, 1^+ \rangle & \dots & \langle J, -J+1 | J, J^- \rangle \\ \langle J, -J | J, O^+ \rangle & \langle J, -J | J, 2^+ \rangle & \dots & \langle J, -J | J, (J-1)^- \rangle & \langle J, -J | J, 1^+ \rangle & \dots & \langle J, -J | J, J^- \rangle \end{pmatrix} \quad (\text{A.5})$$

where the even K values in the new basis are followed by the odd K values, and the  $K^+$  term always comes before the  $K^-$  term.

By taking the transpose of the proper unitary transformation matrix and computing the Hamiltonian in the new basis, we find, for

J even:

$$\mathbf{H}'_e = \mathbf{T}_e^\dagger \mathbf{H} \mathbf{T}_e = \begin{pmatrix} E_{0,0} & \sqrt{2}E_{0,2} & 0 & 0 & 0 & 0 & 0 & 0 & 0 & 0 & 0 \\ \sqrt{2}E_{0,2} & \ddots & \ddots & \vdots & \vdots & \vdots & \vdots & \vdots & \vdots & \vdots & 0 \\ 0 & \ddots & E_{J,J} & 0 & 0 & 0 & 0 & 0 & 0 & 0 & 0 \\ 0 & \dots & 0 & E_{2,2} & 0 & 0 & 0 & 0 & 0 & 0 & 0 \\ 0 & \dots & 0 & E_{2,4} & \ddots & \ddots & \ddots & \ddots & \ddots & \ddots & \ddots \\ 0 & \dots & \vdots & 0 & 0 & 0 & 0 & 0 & 0 & 0 & 0 \\ \vdots & \vdots & \vdots & \vdots & \vdots & \vdots & 0 & E_{J,J} & \vdots & \vdots & \vdots \\ \vdots & \vdots & \vdots & \vdots & \vdots & \vdots & E_{1,1} + E_{-1,1} & 0 & \vdots & \vdots & \vdots \\ \vdots & \vdots & \vdots & \vdots & \vdots & \vdots & E_{1,3} & E_{1,3} & \vdots & \vdots & \vdots \\ 0 & \dots & \vdots & \vdots & \vdots & \vdots & 0 & 0 & 0 & 0 & 0 \\ 0 & \dots & \vdots & \vdots & \vdots & \vdots & 0 & 0 & 0 & 0 & 0 \\ 0 & \dots & \vdots & \vdots & \vdots & \vdots & 0 & E_{J-1,J-1} & 0 & 0 & 0 \\ 0 & \dots & \vdots & \vdots & \vdots & \vdots & 0 & 0 & E_{1,1} - E_{-1,1} & E_{1,3} & 0 \\ 0 & \dots & \vdots & \vdots & \vdots & \vdots & 0 & 0 & E_{1,3} & \ddots & \ddots \\ 0 & \dots & \vdots & \vdots & \vdots & \vdots & 0 & 0 & 0 & \ddots & E_{J-1,J-1} \end{pmatrix} \quad (\text{A.6})$$

where the  $\mathbf{H}'_e$  matrix is block diagonal which implies: the term immediately to the left and below the first entry has a value other than zero, terms appear diagonally from these three values to the bottom right corner of the matrix, and the rest of the matrix entries are zero. A similar block diagonal matrix can be obtained for the odd J case such that

$\mathbf{H}'_o = \mathbf{T}_o^\dagger \mathbf{H} \mathbf{T}_o$ . The block diagonal matrices can then be reduced to the four

submatrices shown below for J even.

$$\begin{aligned}
 \mathbf{E}^+ &= \begin{pmatrix} E_{0,0} & \sqrt{2}E_{0,2} & 0 & 0 & \cdots \\ \sqrt{2}E_{0,2} & E_{2,2} & E_{2,4} & 0 & \cdots \\ 0 & E_{2,4} & E_{4,4} & \ddots & \cdots \\ \vdots & \vdots & \ddots & \ddots & \cdots \\ 0 & 0 & \cdots & E_{J-2,J} & E_{J,J} \end{pmatrix} \\
 \mathbf{E}^- &= \begin{pmatrix} E_{2,2} & E_{2,4} & 0 & 0 & \cdots \\ E_{2,4} & E_{4,4} & E_{4,6} & 0 & \cdots \\ 0 & E_{4,6} & E_{6,6} & \ddots & \cdots \\ \vdots & \vdots & \ddots & \ddots & \cdots \\ 0 & 0 & \cdots & E_{J-2,J} & E_{J,J} \end{pmatrix} \\
 \mathbf{O}^+ &= \begin{pmatrix} E_{1,1} + E_{-1,1} & E_{1,3} & 0 & 0 & \cdots \\ E_{1,3} & E_{3,3} & E_{3,5} & 0 & \cdots \\ 0 & E_{3,5} & E_{5,5} & \ddots & \cdots \\ \vdots & \vdots & \ddots & \ddots & \cdots \\ 0 & 0 & \cdots & E_{J-3,J-1} & E_{J-1,J-1} \end{pmatrix} \\
 \mathbf{O}^- &= \begin{pmatrix} E_{1,1} - E_{-1,1} & E_{1,3} & 0 & 0 & \cdots \\ E_{1,3} & E_{3,3} & E_{3,5} & 0 & \cdots \\ 0 & E_{3,5} & E_{5,5} & \ddots & \cdots \\ \vdots & \vdots & \ddots & \ddots & \cdots \\ 0 & 0 & \cdots & E_{J-3,J-1} & E_{J-1,J-1} \end{pmatrix} \tag{A.7}
 \end{aligned}$$

By finding the eigenvalues of each of these submatrices, one has obtained the energies of a particular rotational level. These levels can be labeled by the quantum

numbers  $J$ ,  $K_a$ , and  $K_c$  where  $K_a + K_c = J$  or  $J+1$ .<sup>10</sup> This collection of quantum numbers can be written as  $J_{K_a, K_c}$  and for this representation,  $I^\Gamma$ , the energy levels in order of increasing energy are:<sup>10</sup>

$$\begin{aligned}
 E^+ &: J_{0,J}, J_{2,J-2}, J_{4,J-4}, J_{6,J-6}, \dots \\
 E^- &: J_{2,J-1}, J_{4,J-3}, J_{6,J-5}, J_{8,J-7}, \dots \\
 O^+ &: J_{1,J-1}, J_{3,J-3}, J_{5,J-5}, J_{7,J-7}, \dots \\
 O^- &: J_{1,J}, J_{3,J-2}, J_{5,J-4}, J_{7,J-6}, \dots
 \end{aligned}
 \tag{A.8}$$

## Appendix B : Second Difference Plots and Residuals

Below are the  $\Delta_2$  plots and corresponding residuals generated for the spectral assignment. The plots used in the body of the paper will not be reproduced here, but note how all  $\Delta_2$  fits but one work up to  $J = 40$ .

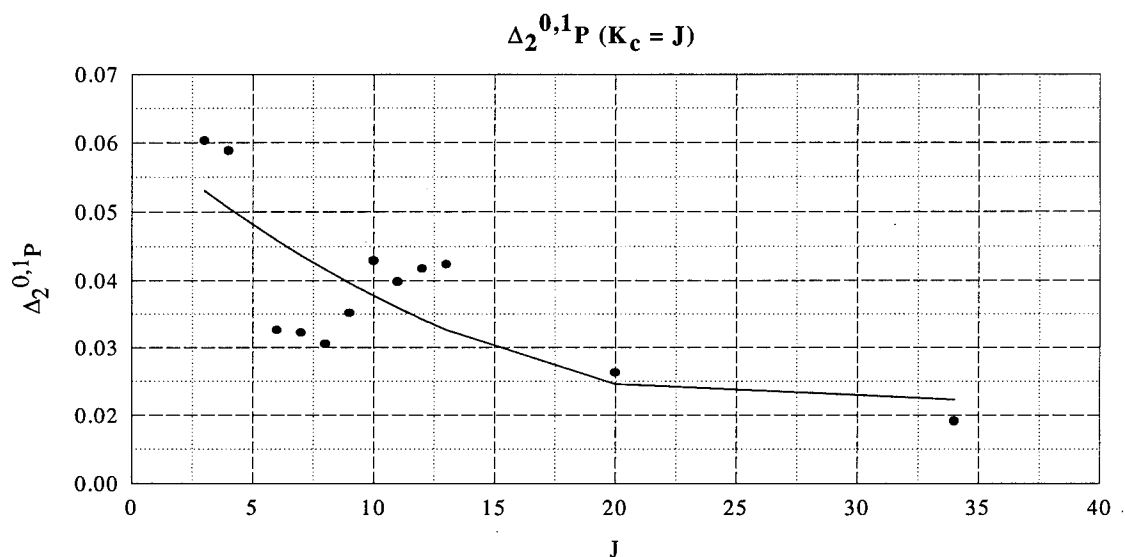


**Figure B-1.** Second difference for the trend from  $J_{0,J}$  to  $J_{1,J}$ . Blending is the cause of the scattering of the locations in the region from  $J = 6$  to  $J = 13$ .

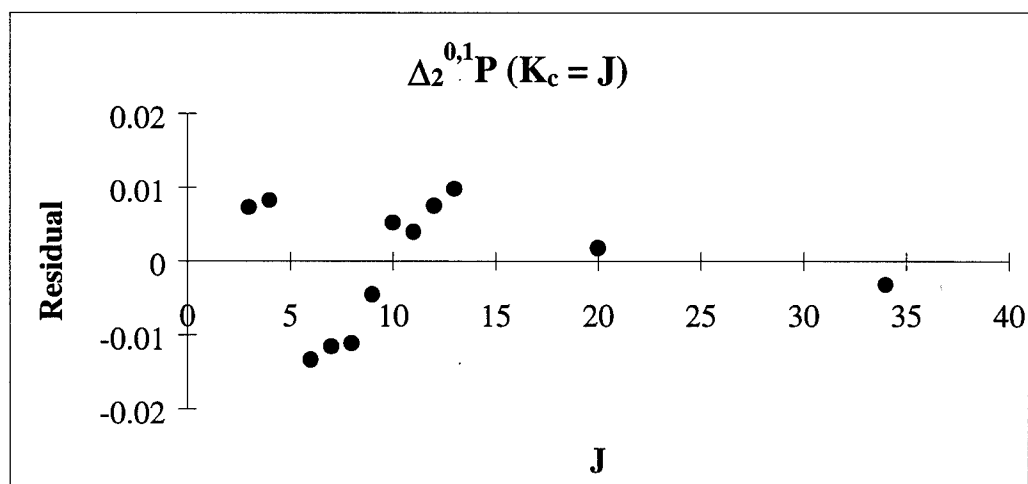


**Figure B-2.** Residuals of fit above. Even though the transition differences in the  $J = 6$  to  $J = 13$  range looked bad, the residuals are still within the resolution.

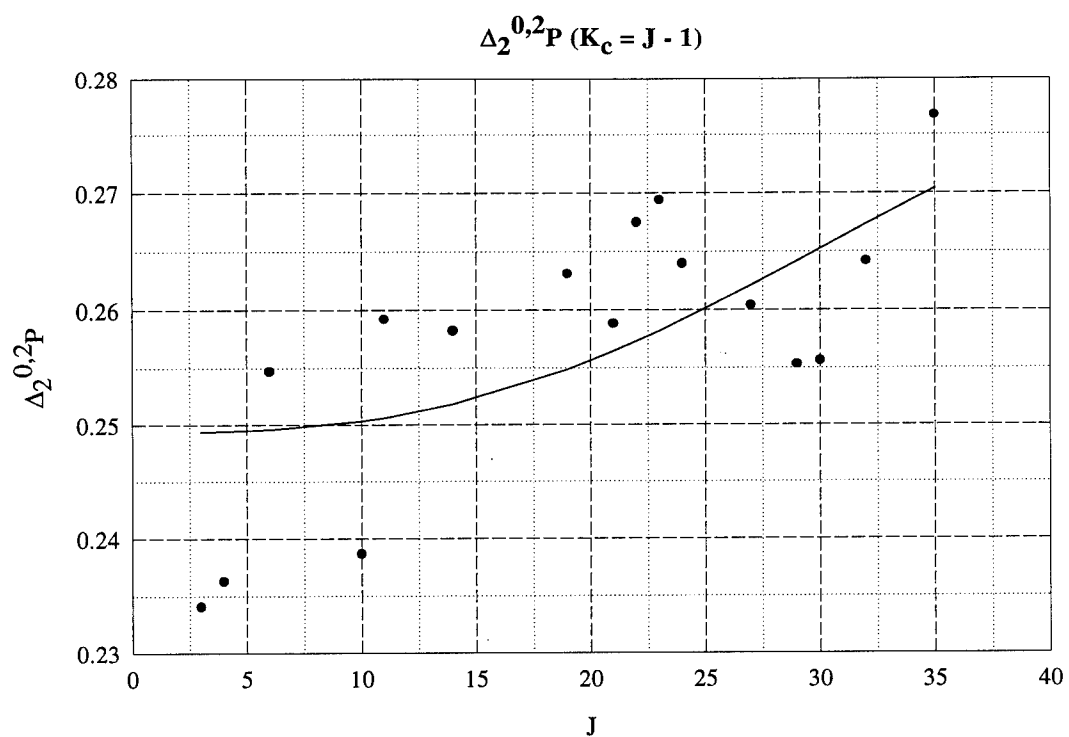


**Figure B-3.** Second difference for the trend from  $J_{0,J}$  to  $J_{2,J-1}$ . Once again, the effects of blending can be seen in the assignments.

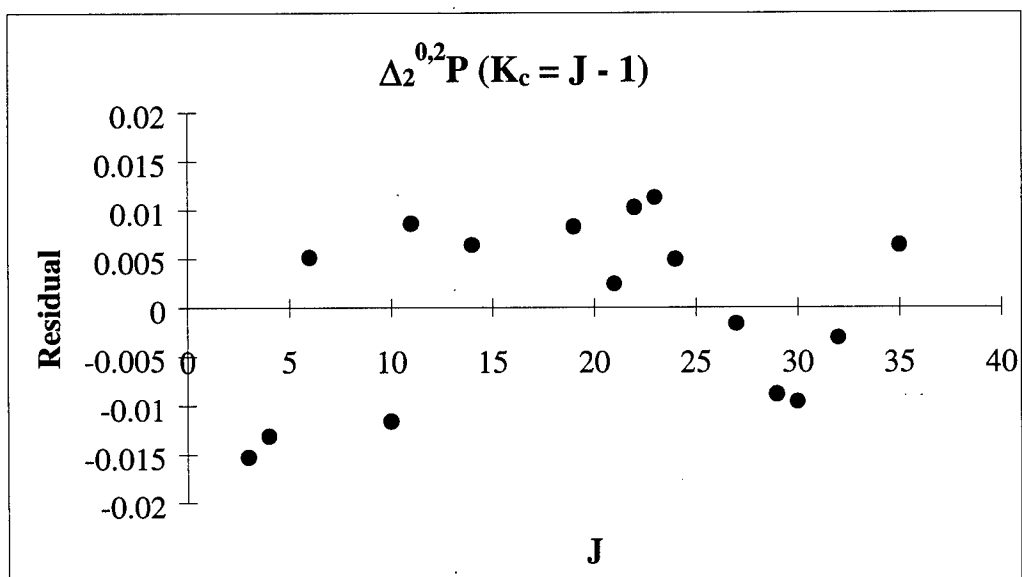


**Figure B-4.** Residuals of second difference fit above.

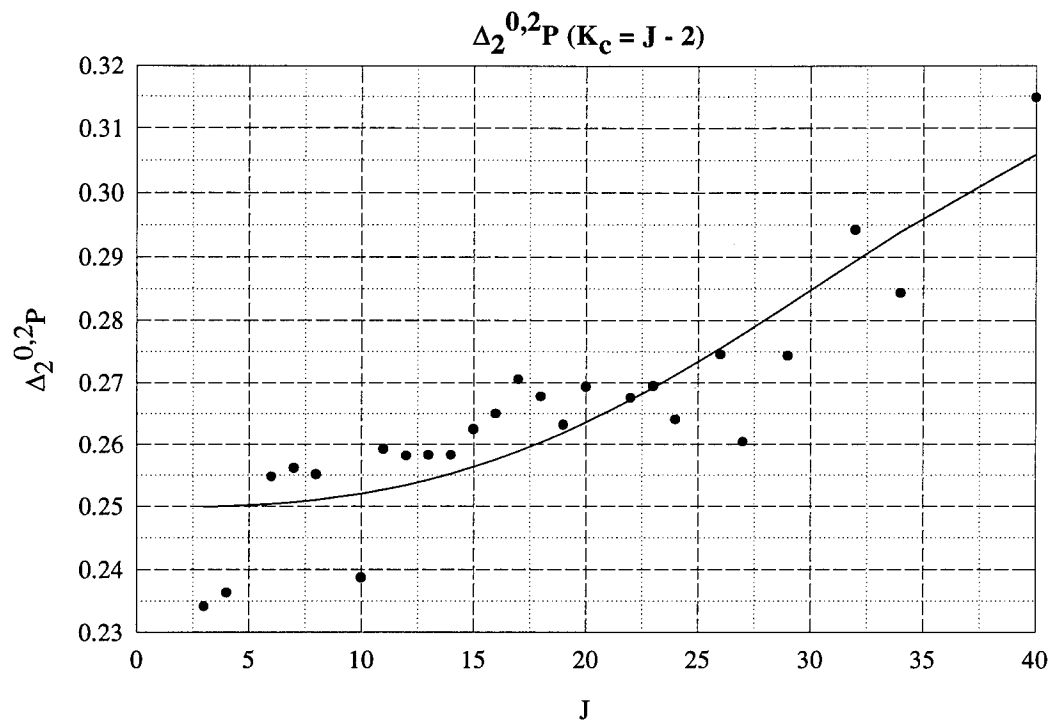


**Figure B-5.** Second difference for the trend from  $J_{0,J}$  to  $J_{2,J-2}$ .

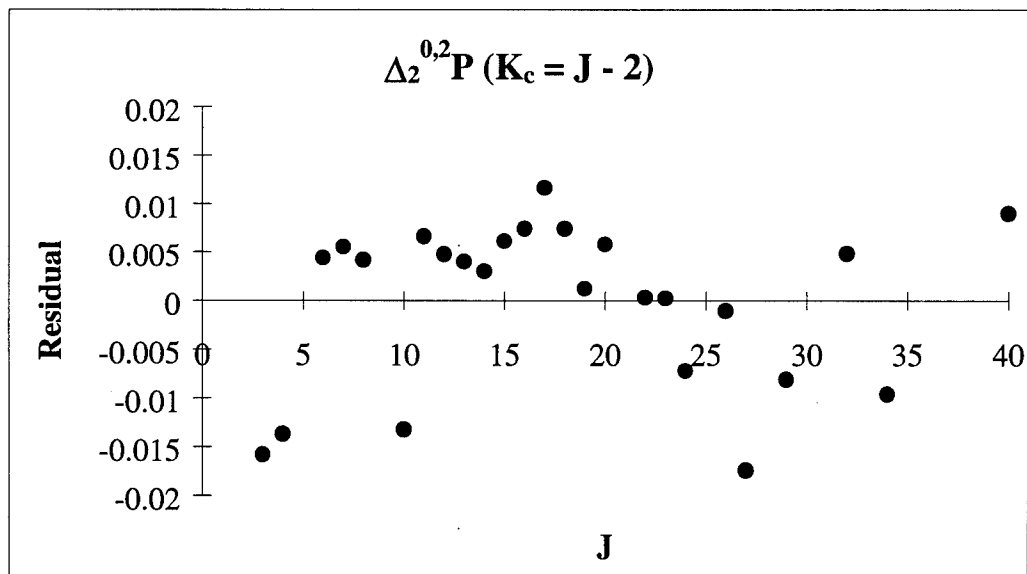


**Figure B-6.** Residuals of the  $J_{0,J}$  to  $J_{2,J-2}$  trend.



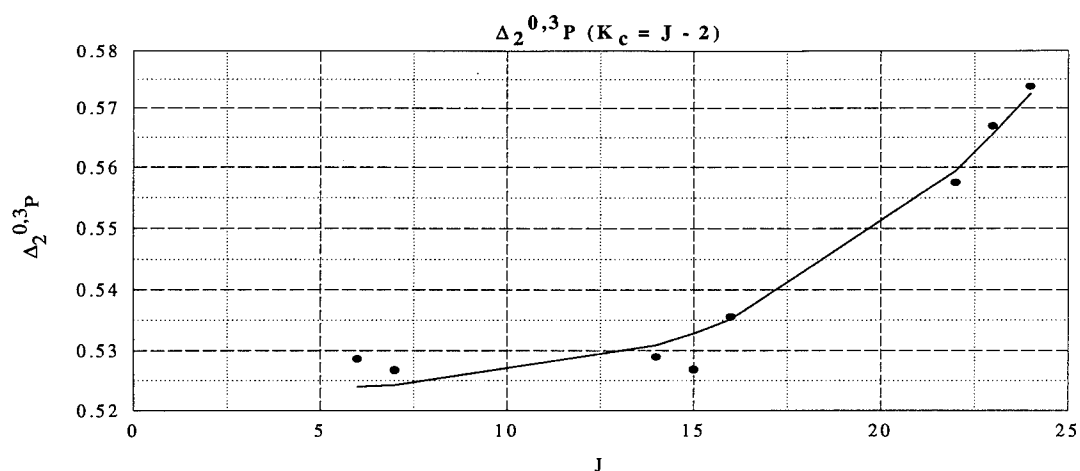


**Figure B-7.** Second difference from  $J_{0,J}$  to  $J_{3,J-2}$  in the P branch. Note the ability to fit these transitions for the reduced range of  $J$ .

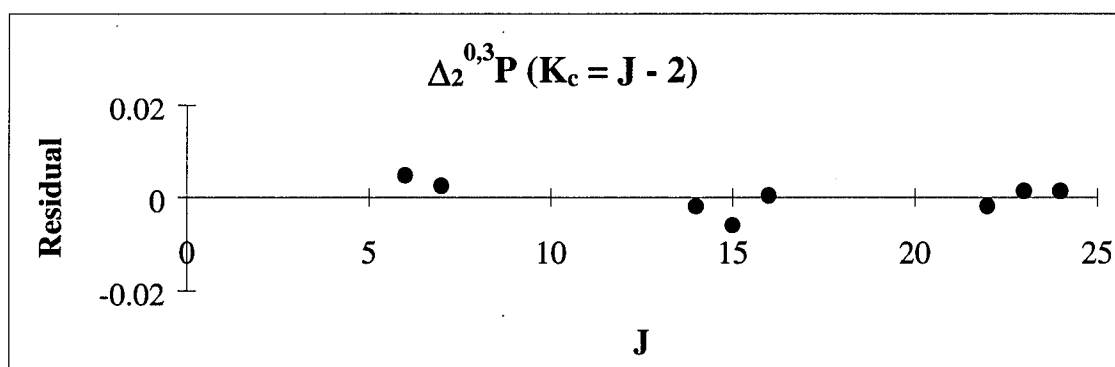


**Figure B-8.** Residuals from the fit above.

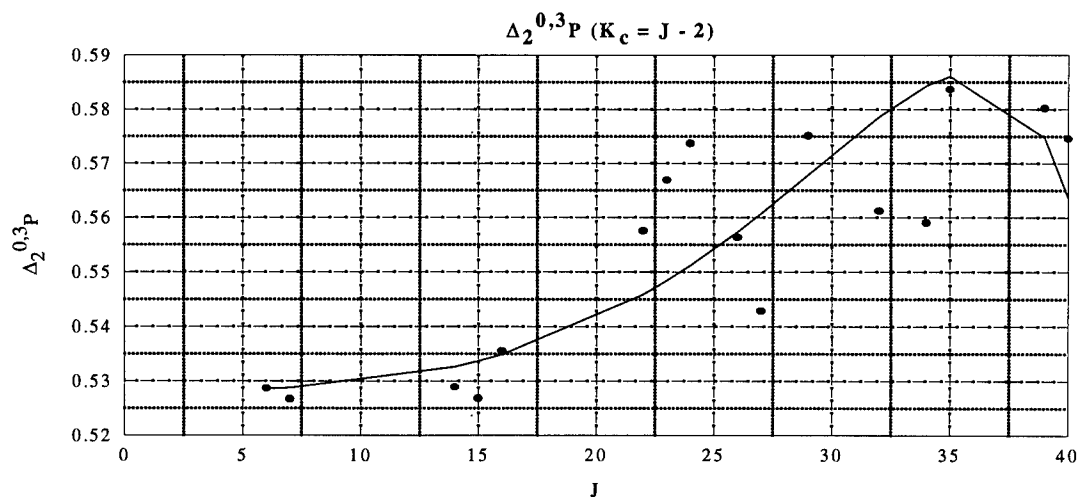


**Figure B-9.** Break down of the asymmetry approximation occurs for this trend above  $J = 22$ . The transitions that were fit in Figure B-7 in the region between  $J = 20$  and  $J = 25$  are not fit well.

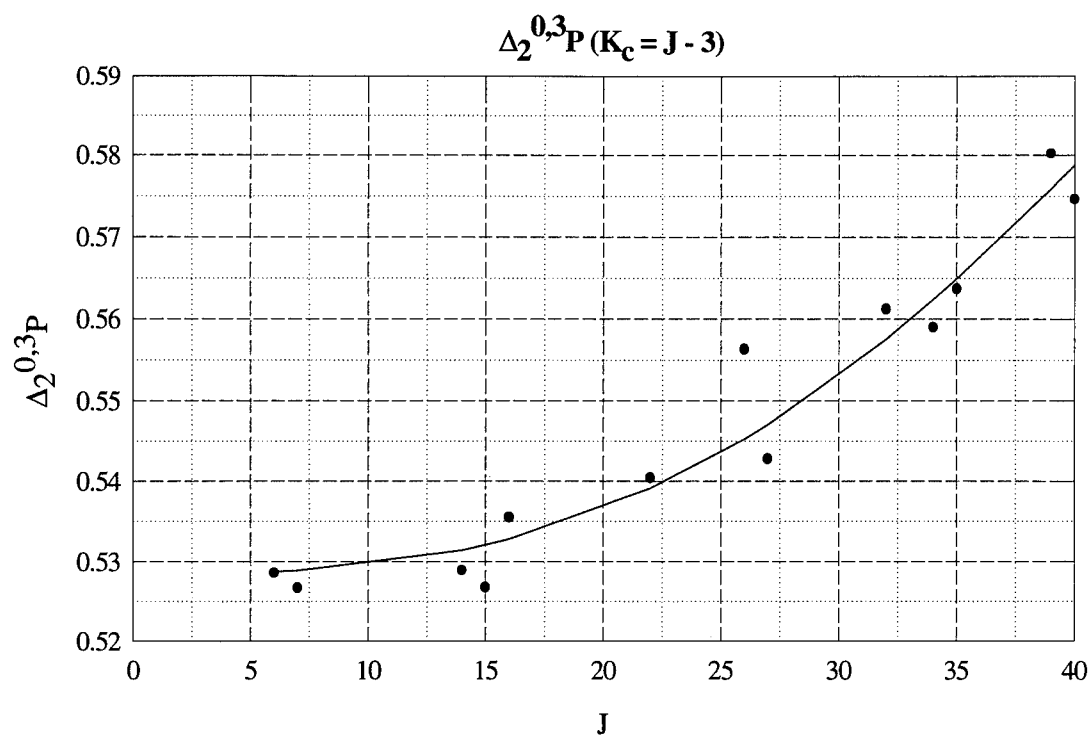


**Figure B-10.** Trend from  $J_{0,J}$  to  $J_{3,J-3}$ .

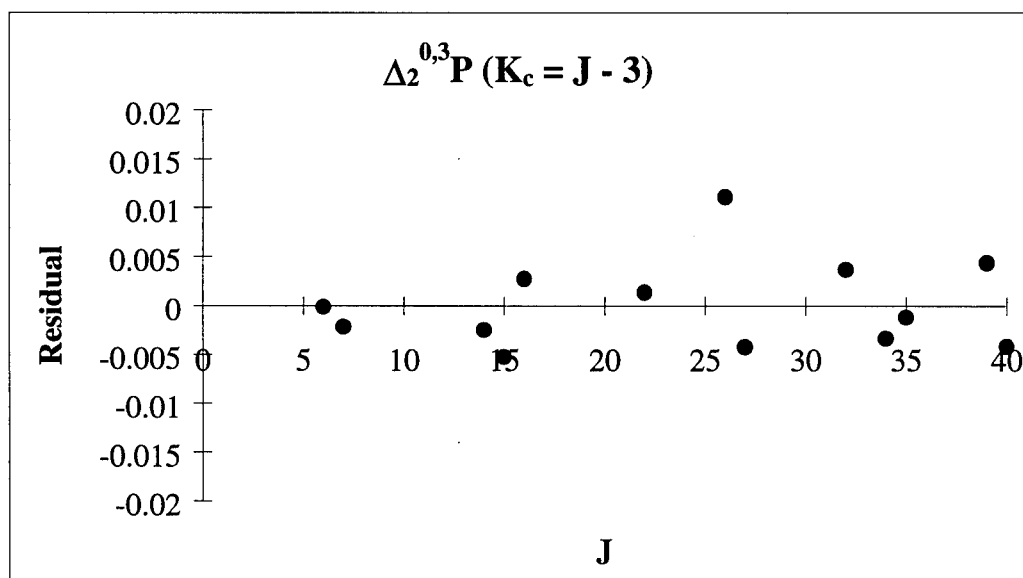


**Figure B-11.** Residuals for the trend fit above.

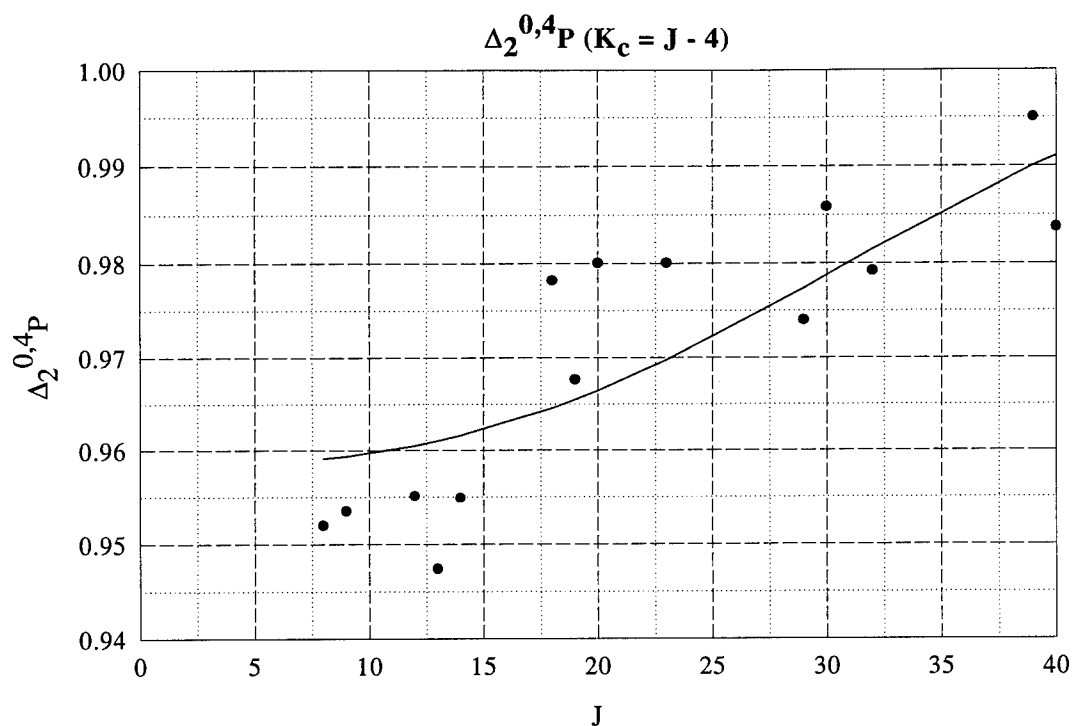


**Figure B-12.** Difference in assignments for the  $J_{0,J}$  and  $J_{4,J-4}$  levels.

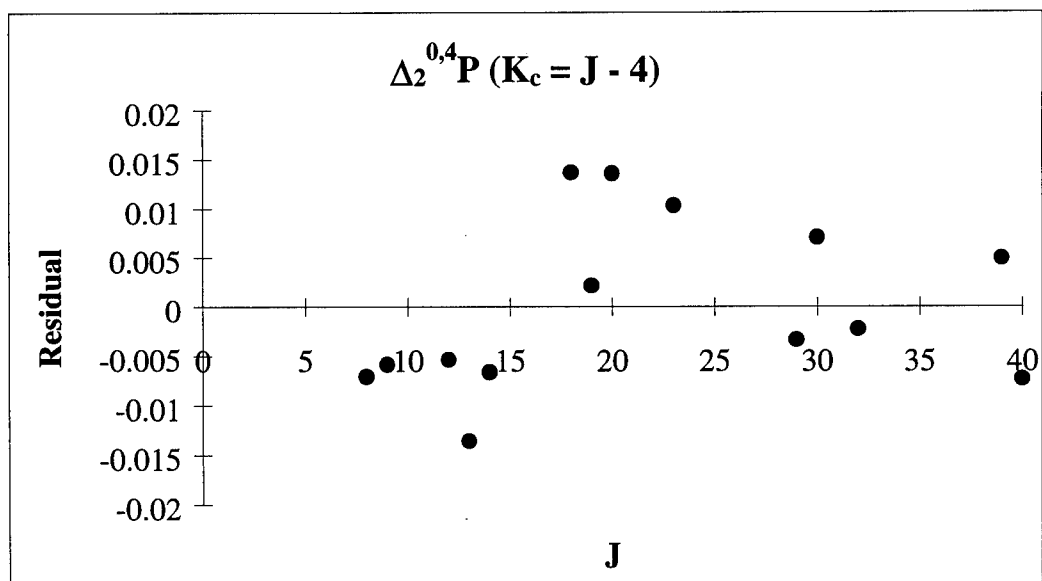


**Figure B-13.** Distance from the fit to the differences in the transitions used above.

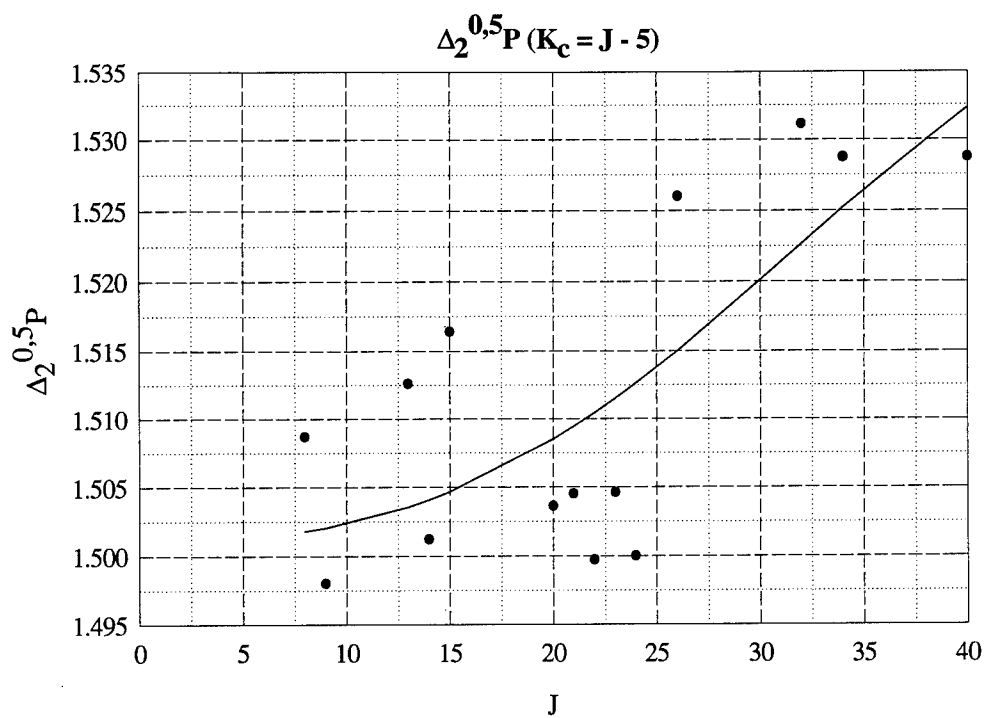


**Figure B-14.** Trend from  $J_{0,J}$  to  $J_{5,J-5}$ .

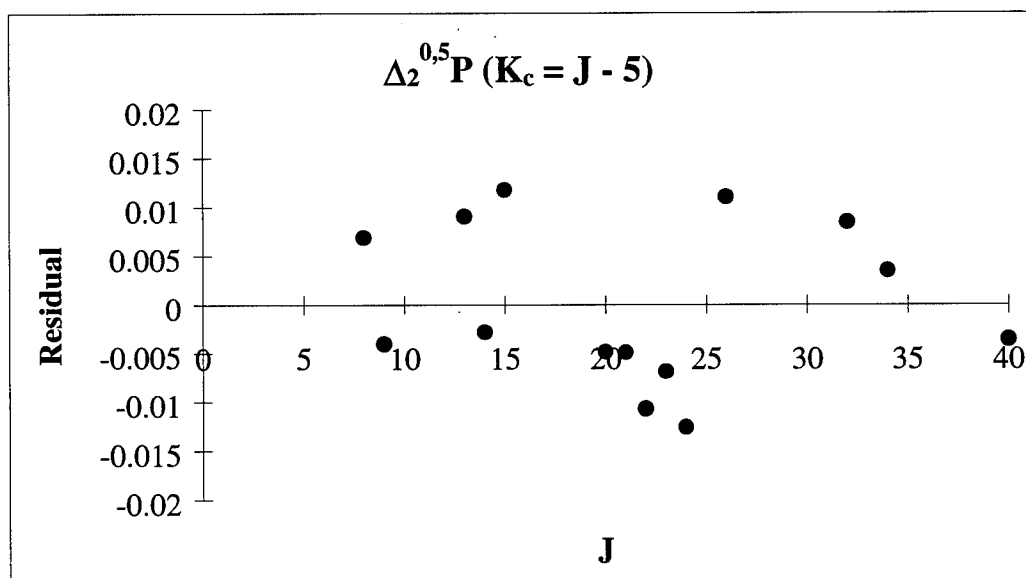


**Figure B-15.** Residuals from above fit.

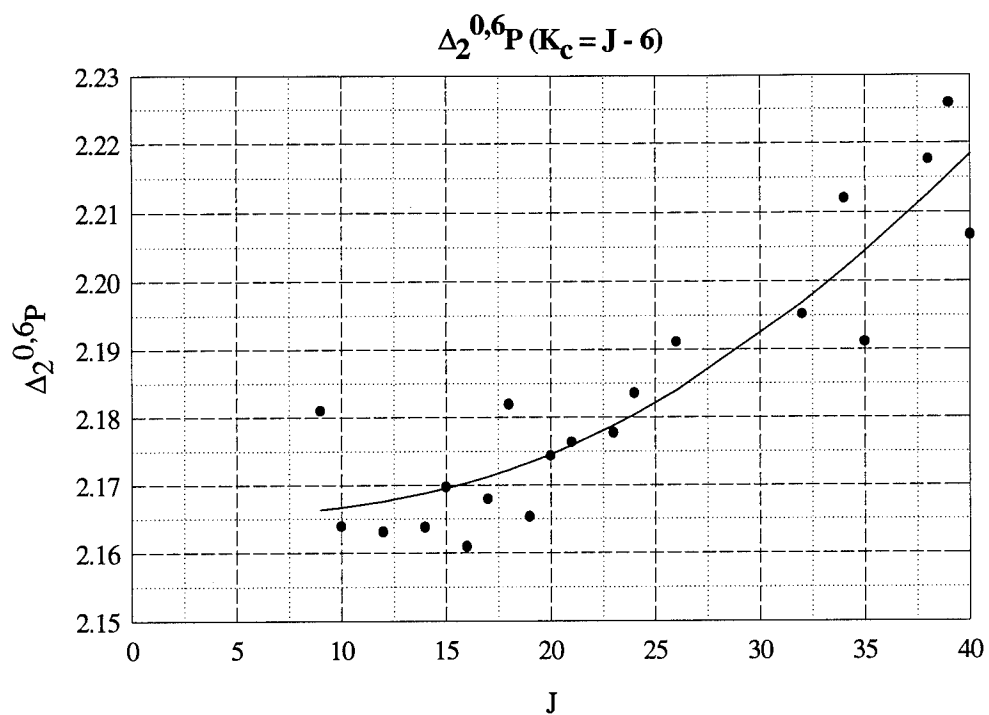


**Figure B-16.** Fit for the  $J_{0,J}$  to  $J_{6,J-6}$  trend.

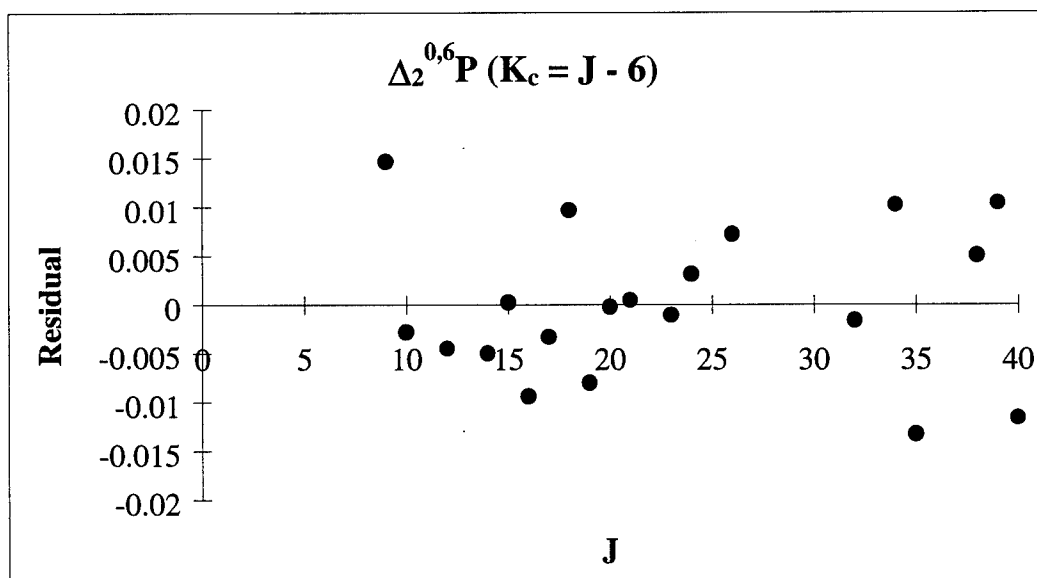


**Figure B-17.** Residuals for the above fit.

## Appendix C : Mathematica® Codes

Below is the Mathematica® code written to generate the energy levels for any

vibrational level of an asymmetric top in the  $\bar{\Gamma}$  representation.

```
(*Diagonalization Procedure*)

(*Rules to calculate energy levels*)
ekk[j_, kp_, k_, lev_] := 0.5*((B[lev]+Cv[lev]) j (j+1)) +
  (A[lev]-0.5*(B[lev]+Cv[lev])) k^2 - Dj[lev] j^2 (j+1)^2 -
  Djk[lev] j (j+1) k^2 - Dk[lev] k^4 + Fj j^3 (j+1)^3 +
  Fjk j^2 (j+1)^2 k^2 + Fkj j (j+1) k^4 + Fk k^6;
ekm2k[j_, kp_, k_, lev_] := (0.25*(B[lev]-Cv[lev]) - dj[lev] j (j+1) -
  0.5*dk*(kp^2+k^2) + fj j^2 (j+1)^2 + 0.5*fjk j (j+1) (kp^2+k^2) +
  0.5*fk*(kp^4+k^4)) Sqrt[(j (j+1) - k (k-1))*(j (j+1) - (k-1) (k-2))];*)

(*Rules required*)
uprElim[n_] := If[EvenQ[n],n,n-1];
uprOlim[n_] := If[EvenQ[n],n-1,n];
ka[n_] := If[EvenQ[n],n/2,(n-1)/2];
kc[n_] := If[EvenQ[n],j-ka[n]+1,j-ka[n]];
kmax[n_] := If[EvenQ[n],n/2,(n-1)/2];
omax[n_] := If[EvenQ[n],kmax[n],kmax[n]+1];

(*J=1 Energy Level Calculation*)
enercalc[lev] = Array[ener[lev],{70,70,70}];
j=1;
lev=0;

j1matrix[lev] = {{ekk[j,1,1,lev], 0, ekm2k[j,-1,1,lev]},
  {0, ekk[j,0,0,lev], 0},
  {ekm2k[j,-1,1,lev], 0, ekk[j,1,1,lev]}};
j1vals[lev] = Eigenvalues[j1matrix[lev]];
j1sort[lev] = Sort[Flatten[j1vals[lev]]];
For[i=1,i<=(2 j + 1),i++,ener[lev][j,ka[i],kc[i]] = j1sort[lev][[i]]];
Clear[j]

Do[{eposdi[lev] = Table[ekk[j,k,k,lev],{k,0,uprElim[j],2}],
  eposoff[lev] = Table[If[k-2>0,N[ekm2k[j,k-2,k,lev]],
    N[Sqrt[2] ekm2k[j,k-2,k,lev]]],{k,2,uprElim[j],2}],
  epos[lev] = Table[Switch[r-s,-1,eposoff[lev][[r]],0,eposdi[lev][[r]],
    1,eposoff[lev][[s]],_,0],{r,kmax[j]+1},{s,kmax[j]+1}],
  enegdi[lev] = Table[ekk[j,k,k,lev],{k,2,uprElim[j],2}],
  enegoff[lev] = Table[If[k-2>0,N[ekm2k[j,k-2,k,lev]],
    N[Sqrt[2] ekm2k[j,k-2,k,lev]]],{k,4,uprElim[j],2}],
  eneg[lev] = Table[Switch[r-s,-1,enegoff[lev][[r]],0,enegdi[lev][[r]],
    1,enegoff[lev][[s]],_,0],{r,kmax[j]},{s,kmax[j]}],
  oposdi[lev] = Table[If[k>1,ekk[j,k,k,lev],(ekk[j,k,k,lev]+
    ekm2k[j,k-2,k,lev])],{k,1,uprOlim[j],2}],
  oposoff[lev] = Table[N[ekm2k[j,k-2,k,lev]],{k,3,uprOlim[j],2}],
  opos[lev] = Table[Switch[r-s,-1,oposoff[lev][[r]],0,oposdi[lev][[r]],
    1,oposoff[lev][[s]],_,0],{r,omax[j]},{s,omax[j]}],
  onegdi[lev] = Table[If[k>1,ekk[j,k,k,lev],(ekk[j,k,k,lev]-
    ekm2k[j,k-2,k,lev])],{k,1,uprOlim[j],2}],
  onegoff[lev] = Table[N[ekm2k[j,k-2,k,lev]],{k,3,uprOlim[j],2}],
  oneg[lev] = Table[Switch[r-s,-1,onegoff[lev][[r]],0,onegdi[lev][[r]],
    1,onegoff[lev][[s]],_,0],{r,omax[j]},{s,omax[j]}],
  jevals[lev] = Table[{Eigenvalues[epos[lev]],Eigenvalues[eneg[lev]],
    Eigenvalues[opos[lev]],Eigenvalues[oneg[lev]]}],
  enerlevs[lev] = Sort[Flatten[jevals[lev]]],
  }, {j,2,70}];
```

The Mathematica<sup>®</sup> code below was used to determine the best rotational constants for the assigned spectrum. To compare the energy levels, the lines of code prior to the line which calculates the transitions between the energy levels was used with the appropriate  $v_1 = 1$  constant values for the parameters entered. The minimization parameters represent the following constants:

$$p1 \Rightarrow v_0, p2 \Rightarrow A, p3 \Rightarrow B, p4 \Rightarrow C, p5 \Rightarrow \Delta_J, p6 \Rightarrow \Delta_{JK}, p7 \Rightarrow \Delta_K, p8 \Rightarrow \delta_J, \text{ and } p9 \Rightarrow R_5.$$

```
(*Mathematica commands to minimize rotational parameters for an asymmetric*)
(*triatomic molecule from transitions contained in a data file. This code*)
(*uses an approximation for the energy levels that was published by Polo*)
(*in Can. J. of Phys. 35, (1957): 880-885. For nitrosyl bromide - the*)
(*molecule for which this code was written - this approximation breakdown*)
(*above J = 25 for most cases. It has been determined that the energy level*)
(*equations do not properly predict the Ka = 1, Kc = J-1 for J > 18 and the*)
(*Ka = 3, Kc = J-2 for J > 22. Two guesses are required for the parameters,*)
(*however, the second set of guesses are determined from the first set of*)
(*guesses read in from an external file called "Guesses."*)

(*All values are in cm-1.*)

MHztoWave = 10^6 * 3.336*10^(-11); (*Conversion from MHz to cm-1*)

(*Lower Level Coefficients*)
A[0] = 85500.4620*MHztoWave;
B[0] = 3747.07053*MHztoWave;
Cv[0] = 3585.98785*MHztoWave;
Dj[0] = 2.852185*10^(-3)*MHztoWave;
Djk[0] = -5.69179*10^(-2)*MHztoWave;
Dk[0] = 4.8255*MHztoWave;
dj[0] = 1.57887*10^(-4)*MHztoWave;

(*Asymmetry parameter.*)
eps[p2_, p3_, p4_] := (p3 - p4)/(2 (2 p2 - p3 - p4));

(*Constraint on r6 value.*)
r6[p2_, p3_, p4_, p9_] = (-3.31248*10^(-7) - p9) eps[p2, p3, p4];

(*Standard deviation rule.*)
standev[sumsqerr_, numtrans_] := Sqrt[sumsqerr/(numtrans - 2)];

(*Rules containing the appropriate expansion coefficient for the different*)
(*energy levels.*)
ck[j_, ka_, kc_] := Which[ka == 0, 0, ka == 1 && kc == j, -3/2,
ka == 1 && kc == j-1, 3/2, ka == 2 && kc == j-1, -3/2,
ka == 2 && kc == j-2, -3/2, ka == 3 && kc == j-2, -3/2,
ka == 3 && kc == j-3, 3/2, ka == 4 && kc == j-3, -3/2,
ka == 4 && kc == j-4, -3/2, ka == 5 && kc == j-4, -3/2,
ka == 5 && kc == j-5, 3/2, ka > 5, -3/2];

cj1[j_, ka_, kc_] := If[ka == 1, If[kc == j, -1, 1], 0];

cj2[j_, ka_, kc_] := Which[ka == 0, -1/2, ka == 1 && kc == j, -1/8,
ka == 1 && kc == j-1, 1/8, ka == 2 && kc == j-1, -1/12,
```

```

ka == 2 && kc == j-2, 5/12, ka == 3 && kc == j-2, 1/16,
ka == 3 && kc == j-3, -1/16, ka == 4, 1/30,
ka == 5 && kc == j-4, 1/48, ka == 5 && kc == j-5, -1/48,
ka > 5, 1/(2 (ka^2 - 1))];

cj3[j_,ka_,kc_] := Which[ka == 0, 0, ka == 1 && kc == j, 1/64,
ka == 1 && kc == j-1, -1/64, ka == 2, 0,
ka == 3 && kc == j-2, -1/64, ka == 3 && kc == j-3, 1/64,
ka == 4, 0, ka == 5, 0, ka > 5, 0];

cj4[j_,ka_,kc_] := Which[ka == 0, 7/128, ka == 1 && kc == j, -1/1536,
ka == 1 && kc == j-1, 1/1536, ka == 2 && kc == j-1, 5/13824,
ka == 2 && kc == j-2, -763/13824, ka == 3 && kc == j-2, 13/20480,
ka == 3 && kc == j-3, -13/20480, ka == 4 && kc == j-3, -317/864000,
ka == 4 && kc == j-4, 433/864000, ka == 5 && kc == j-4, 11/774144,
ka == 5 && kc == j-5, -11/774144,
ka > 5, ((5 ka^2 + 7)/(32 (ka^2-1)^3 (ka^2-4)))]];

cj5[j_,ka_,kc_] := Which[ka == 0, 0, ka == 1 && kc == j, -11/36864,
ka == 1 && kc == j-1, 11/36864, ka == 2, 0,
ka == 3 && kc == j-2, 5/16384, ka == 3 && kc == j-3, -5/16384,
ka == 4, 0, ka == 5 && kc == j-4, -1/147456,
ka == 5 && kc == j-5, 1/147456, ka > 5, 0];

cj6[j_,ka_,kc_] := Which[ka == 0, -29/2304, ka == 1, 0,
ka == 2 && kc == j-1, -289/79626240,
ka == 2 && kc == j-2, 1002401/79626240, ka > 2, 0];

(*Rigid rotor energy level calculation rule which uses the coefficients in the*)
(*rules above.*)
erig[j_,ka_,kc_,p2_,p3_,p4_] := 0.5 (p3+p4) j (j+1) +
(p2 - 0.5 (p3+p4)) ka^2 + (p2 - 0.5 (p3+p4))*
(ka^2 ck[j,ka,kc] (eps[p2,p3,p4])^2 +
j (j+1) cj1[j,ka,kc] eps[p2,p3,p4] +
j^2 (j+1)^2 cj2[j,ka,kc] (eps[p2,p3,p4])^2 +
j^3 (j+1)^3 cj3[j,ka,kc] (eps[p2,p3,p4])^3 +
j^4 (j+1)^4 cj4[j,ka,kc] (eps[p2,p3,p4])^4 +
j^5 (j+1)^5 cj5[j,ka,kc] (eps[p2,p3,p4])^5 +
j^6 (j+1)^6 cj6[j,ka,kc] (eps[p2,p3,p4])^6);

(*Energy calculation to correct for the influence of first order centrifugal*)
(*distortion correction. The actual energy is calculated using the*)
(*distortion equation required for the particular energy level.*)
edist[j_,ka_,kc_,p2_,p3_,p4_,p5_,p6_,p7_,p8_,p9_] := Which[
ka == 0, zero[j,p2,p3,p4,p5,p8,p9],
ka == 1 && kc == j, oneup[j,p2,p3,p4,p5,p6,p7,p8,p9],
ka == 1 && kc == j-1, onelow[j,p2,p3,p4,p5,p6,p7,p8,p9],
ka == 2 && kc == j-1, twoup[j,p2,p3,p4,p5,p6,p7,p8,p9],
ka == 2 && kc == j-2, twolow[j,p2,p3,p4,p5,p6,p7,p8,p9],
ka == 3 && kc == j-2, threeup[j,p2,p3,p4,p5,p6,p7,p8,p9],
ka == 3 && kc == j-3, threelow[j,p2,p3,p4,p5,p6,p7,p8,p9],
ka > 3, over3[j,ka,p2,p3,p4,p5,p6,p7,p8,p9]];

(*Equations to describe the centrifugal distortion influence for different*)
(*cases of the k values of the energy level to be calculated.*)
zero[j_,p2_,p3_,p4_,p5_,p8_,p9_] := (- 4 r6[p2,p3,p4,p9] +
8 p9 eps[p2,p3,p4]) j (j+1) + (- p5 -
(4 p9 + 2 p8) eps[p2,p3,p4]) j^2 (j+1)^2 +
(p8 eps[p2,p3,p4]) j^3 (j+1)^3;

oneup[j_,p2_,p3_,p4_,p5_,p6_,p7_,p8_,p9_] := (- p7 + 10 r6[p2,p3,p4,p9] -
30 p9 eps[p2,p3,p4]) + (- p6 - 4 r6[p2,p3,p4,p9] - 2 p9 +
(3 r6[p2,p3,p4,p9] + 20 p9 + 3 p8) eps[p2,p3,p4]) j (j+1) +
(- p5 + p8 - (2 r6[p2,p3,p4,p9] + (5/2) p9 +
2 p8) eps[p2,p3,p4]) j^2 (j+1)^2 + ((1/4) (r6[p2,p3,p4,p9] +
p8) eps[p2,p3,p4]) j^3 (j+1)^3;

```



```

onelow[j_,p2_,p3_,p4_,p5_,p6_,p7_,p8_,p9_] := (- p7 + 10 r6[p2,p3,p4,p9] -
30 p9 eps[p2,p3,p4]) + (- p6 - 4 r6[p2,p3,p4,p9] + 2 p9 +
(- 3 r6[p2,p3,p4,p9] + 20 p9 + 3 p8) eps[p2,p3,p4]) j (j+1) +
(- p5 - p8 - (- 2 r6[p2,p3,p4,p9] + (5/2) p9 +
2 p8) eps[p2,p3,p4]) j^2 (j+1)^2 + ((1/4) (- r6[p2,p3,p4,p9] +
p8) eps[p2,p3,p4]) j^3 (j+1)^3;

twoup[j_,p2_,p3_,p4_,p5_,p6_,p7_,p8_,p9_] := (- 16 p7 + 40 r6[p2,p3,p4,p9] -
240 p9 eps[p2,p3,p4]) + (-4 p6 - 2 r6[p2,p3,p4,p9] + (60 p9 +
12 p8) eps[p2,p3,p4]) j (j+1) + (- p5 - r6[p2,p3,p4,p9] -
((10/3) p9 + 3 p8) eps[p2,p3,p4]) j^2 (j+1)^2 +
((1/6) p8 eps[p2,p3,p4]) j^3 (j+1)^3;

twolow[j_,p2_,p3_,p4_,p5_,p6_,p7_,p8_,p9_] := (- 16 p7 + 40 r6[p2,p3,p4,p9] -
240 p9 eps[p2,p3,p4]) + (-4 p6 - 6 r6[p2,p3,p4,p9] + (52 p9 +
12 p8) eps[p2,p3,p4]) j (j+1) + (- p5 + r6[p2,p3,p4,p9] +
((2/3) p9 - p8) eps[p2,p3,p4]) j^2 (j+1)^2 +
(-(5/6) p8 eps[p2,p3,p4]) j^3 (j+1)^3;

threeup[j_,p2_,p3_,p4_,p5_,p6_,p7_,p8_,p9_] := (- 81 p7 + 90 r6[p2,p3,p4,p9] -
990 p9 eps[p2,p3,p4]) + (-9 p6 - 4 r6[p2,p3,p4,p9] +
(-3 r6[p2,p3,p4,p9] + 116 p9 + 27 p8) eps[p2,p3,p4]) j (j+1) +
(- p5 + (4 r6[p2,p3,p4,p9] - (7/4) p9 -
2 p8) eps[p2,p3,p4]) j^2 (j+1)^2 + ((-1/4) r6[p2,p3,p4,p9] -
(1/8) p8) eps[p2,p3,p4]) j^3 (j+1)^3;

threelow[j_,p2_,p3_,p4_,p5_,p6_,p7_,p8_,p9_] := (- 81 p7 + 90 r6[p2,p3,p4,p9] -
990 p9 eps[p2,p3,p4]) + (-9 p6 - 4 r6[p2,p3,p4,p9] +
(3 r6[p2,p3,p4,p9] + 116 p9 + 27 p8) eps[p2,p3,p4]) j (j+1) +
(- p5 + (-4 r6[p2,p3,p4,p9] - (7/4) p9 -
2 p8) eps[p2,p3,p4]) j^2 (j+1)^2 + ((1/4) r6[p2,p3,p4,p9] -
(1/8) p8) eps[p2,p3,p4]) j^3 (j+1)^3;

over3[j_,ka_,p2_,p3_,p4_,p5_,p6_,p7_,p8_,p9_] := (- ka^4 p7 +
10 ka^2 r6[p2,p3,p4,p9] - 10 ka^2 (ka^2 + 2) p9 eps[p2,p3,p4]) +
(- ka^2 p6 - 4 r6[p2,p3,p4,p9] + (4 (3 ka^2 + 2) p9 +
3 ka^2 p8) eps[p2,p3,p4]) j (j+1) + (- p5 - (2 ((ka^2-2)/(ka^2-1)) p9 +
2 p8) eps[p2,p3,p4]) j^2 (j+1)^2 +
(- (1/(ka^2-1)) p8 eps[p2,p3,p4]) j^3 (j+1)^3;

(*Energy level calculation including first order centrifugal distortion terms.*)
energy[j_,ka_,kc_,p2_,p3_,p4_,p5_,p6_,p7_,p8_,p9_] :=
erig[j,ka,kc,p2,p3,p4] +
edist[j,ka,kc,p2,p3,p4,p5 + 2 r6[p2,p3,p4,p9],p6 - 12 r6[p2,p3,p4,p9],
p7 + 10 r6[p2,p3,p4,p9],p8,p9];

(*Calculation of transitions between upper level - with minimization*)
(*parameters - and lower level - constants held fixed to microwave data.*)
(*See Esposti, et. al. in Chem. Phys. Letters, 214, 6, (1993): 531 - 535.*)
transcalc[ju_,kau_,kcu_,jl_,kal_,kcl_,p1_,p2_,p3_,p4_,p5_,p6_,p7_,p8_,p9_] :=
SetPrecision[p1 + energy[ju,kau,kcu,p2,p3,p4,p5,p6,p7,p8,p9] -
energy[jl,kal,kcl,A[0],B[0],Cv[0],Dj[0],Djk[0],Dk[0],dj[0],0],7];

(*Module to call for the calculation of the transitions between the levels*)
(*with the minimization parameters being passed as the upper level constants.*)
(*This module appends each calculated transition to a table, tCalc, which is*)
(*created with a leading entry of 0. Upon completion of the calculation of*)
(*the theoretical transitions corresponding to observed transitions, the*)
(*leading 0 is not present in tCalculated since the "Rest" command drops the*)
(*first entry of the table. This table, tCalculated, is returned to the*)
(*program from the module.*)
f[p1_,p2_,p3_,p4_,p5_,p6_,p7_,p8_,p9_] := Module[{tCalc = {0}},
Do[
AppendTo[tCalc, transcalc[tObs[[i,1]],tObs[[i,2]],tObs[[i,3]],
tObs[[i,4]],tObs[[i,5]],tObs[[i,6]],p1,p2,p3,p4,p5,p6,p7,p8,p9]],
{i,1,transmax}];
tCalculated = Rest[tCalc];

```

```

Return[tCalculated];
];

(*Function which returns the sum squared error, SSE, of the observed minus the*)
(*calculated transitions.*)
sse[tEx_, tMeas_] := Apply[Plus, (tEx-tMeas)^2];

(*Function to be minimized. Note that the tenth dimension of the surface is*)
(*the SSE and not the height.*)
g[p1_, p2_, p3_, p4_, p5_, p6_, p7_, p8_, p9_, tEx_] :=
  sse[tEx, f[p1, p2, p3, p4, p5, p6, p7, p8, p9]];

(*Command to read in and properly form observed data list.*)
tObs = Partition[Flatten[ReadList["/home/reptiles1/twiest/test", Number,
  RecordLists->True, RecordSeparators->{"", " "}], 7];
transmax = Dimensions[tObs][[1]];
tObserved = Last[Transpose[tObs]];

(*To do error analysis by a Monte Carlo technique, change the line above to:*)
(*  tObserv = Last[Transpose[tObs]]; *)
(*and add the following lines of code: *)
(*  (*Commands to generate a set of random numbers whose*) *)
(*  (*distribution can be described by a Gaussian centered*) *)
(*  (*at zero with a standard deviation of 0.0075.*/) *)
(*  <<Statistics`NormalDistribution` *)
(*  gausDist = NormalDistribution[0, 0.0075]; *)
(*  ranvals = Table[Random[gausDist], {i, 1, transmax}]; *)
(*  tObserved = tObserv + ranvals; *)

(*Initial guesses. Only one set is required in the data set as the second set*)
(*is obtained from the first. The numbers added to form the second set need*)
(*not be in the direction of the minimum.*/)
guessvals = ReadList["/home/reptiles1/twiest/Guesses", Number];
p1ges = guessvals[[1]];
p1ges2 = p1ges + 0.03;
p2ges = guessvals[[2]];
p2ges2 = p2ges + 0.01;
p3ges = guessvals[[3]];
p3ges2 = p3ges + 0.001;
p4ges = guessvals[[4]];
p4ges2 = p4ges + 0.001;
p5ges = guessvals[[5]];
p5ges2 = p5ges + 1*10^(-9);
p6ges = guessvals[[6]];
p6ges2 = p6ges + 1*10^(-7);
p7ges = guessvals[[7]];
p7ges2 = p7ges + 1*10^(-5);
p8ges = guessvals[[8]];
p8ges2 = p8ges + 1*10^(-10);
p9ges = guessvals[[9]];
p9ges2 = p9ges + 1*10^(-7);

(*Initial calculation to determine how bad the initial guesses are. This*)
(*calculation uses only the guesses read in from the "Guesses" file. The*)
(*actual determination is done by calculating the SSE and the standard*)
(*deviation.*/)
f[p1ges, p2ges, p3ges, p4ges, p5ges, p6ges, p7ges, p8ges, p9ges];
rinit = sse[tObserved, tCalculated];
initstd = standev[rinit, transmax];

(*Minimization function which uses the Steepest Descent method to find a local*)
(*minimum.*/)
h[tEx_] := SetPrecision[FindMinimum[g[p1, p2, p3, p4, p5, p6, p7, p8, p9, tEx],
  {p1, p1ges, p1ges2}, {p2, p2ges, p2ges2}, {p3, p3ges, p3ges2},
  {p4, p4ges, p4ges2}, {p5, p5ges, p5ges2}, {p6, p6ges, p6ges2},
  {p7, p7ges, p7ges2}, {p8, p8ges, p8ges2}, {p9, p9ges, p9ges2},
  MaxIterations -> 30, WorkingPrecision->16, AccuracyGoal -> 4,

```

```

PrecisionGoal -> 4, Compiled->True],10];

(*Print statements output to file that show the initial guesses read into the*)
(*memory, the initial SSE, and the initial standard deviation.*)
Print["Command file name: ZAMFtest"]
Print["Transition file name: test"]
Print["Guess file name: Guesses"]
Print["Number of transitions = ",transmax]
Print["p1 guess = ",p1ges]
Print["p2 guess = ",p2ges]
Print["p3 guess = ",p3ges]
Print["p4 guess = ",p4ges]
Print["p5 guess = ",p5ges]
Print["p6 guess = ",p6ges]
Print["p7 guess = ",p7ges]
Print["p8 guess = ",p8ges]
Print["p9 guess = ",p9ges]
Print["Initial r6 value = ",r6[p2ges,p3ges,p4ges,p9ges]]
Print["Initial SSE = ",rinit]
Print["Initial Standard Deviation = ",initsd]

(*Minimization call with time stamping to determine the efficiency of the*)
(*procedure. The final minimized values are entered into the table "params"*)
(*and the centrifugal distortion constant, detltak, is calculated as a check*)
(*to guarantee that the constraint on p9 and r6 has been met.*)
Date[]
r = h[tObserved];
Date[]
params = Rest[r];
minp1 = p1 /. params[[1,1]];
minp2 = p2 /. params[[1,2]];
minp3 = p3 /. params[[1,3]];
minp4 = p4 /. params[[1,4]];
minp5 = p5 /. params[[1,5]];
minp6 = p6 /. params[[1,6]];
minp7 = p7 /. params[[1,7]];
minp8 = p8 /. params[[1,8]];
minp9 = p9 /. params[[1,9]];
delk = (-2 minp9 - 2 (1/eps[minp2,minp3,minp4]) r6[minp2,minp3,minp4,minp9]);

(*Commands to print the performance of the minimization procedure.*)
Print[" "]
Print["| Minimization Performance |"]
Print[" "]
Print["Final Sum Square Error = ",r[[1]]]
Print["with an accuracy of ",Accuracy[r[[1]]]," digits and a precision of ",
Precision[r[[1]]]," digits."]
Print["Final Standard Deviation = ",standev[r[[1]],transmax]]
Print["with an accuracy of ",Accuracy[standev[r[[1]],transmax]]," digits and a
precision of ",Precision[standev[r[[1]],transmax]]," digits."]

(*Commands to print out the minimized parameters, the accuracy and precision*)
(*of those numbers, and to transform the minimized parameters to the*)
(*values that should be reported.*)
Print[" "]
Print["| Minimized Parameters |"]
Print[" "]
Print["Parameter 1 = ",minp1,"; Accuracy: ",Accuracy[minp1]," Precision: ",
Precision[minp1]]
Print["Parameter 2 = ",minp2,"; Accuracy: ",Accuracy[minp2]," Precision: ",
Precision[minp2]]
Print["Parameter 3 = ",minp3,"; Accuracy: ",Accuracy[minp3]," Precision: ",
Precision[minp3]]
Print["Parameter 4 = ",minp4,"; Accuracy: ",Accuracy[minp4]," Precision: ",
Precision[minp4]]
Print["Parameter 5 = ",minp5,"; Accuracy: ",Accuracy[minp5]," Precision: ",
Precision[minp5]]

```

```

Print["Parameter 6 = ",minp6,"; Accuracy: ",Accuracy[minp6]," Precision: ",
Precision[minp6]]
Print["Parameter 7 = ",minp7,"; Accuracy: ",Accuracy[minp7]," Precision: ",
Precision[minp7]]
Print["Parameter 8 = ",minp8,"; Accuracy: ",Accuracy[minp8]," Precision: ",
Precision[minp8]]
Print["Parameter 9 = ",minp9,"; Accuracy: ",Accuracy[minp9]," Precision: ",
Precision[minp9]]
Print["_____"]
Print["|      Constant Values in the      |"]
Print["|              Final Form              |"]
Print["_____"]
Print["Final asymmetry parameter = ",eps[minp2,minp3,minp4]]
Print["A = ", (minp2 + 2 minp5)]
Print["B = ", (minp3 + 2 minp5 + minp6 - 2 p8ges - 2 delk)]
Print["C = ", (minp4 + 2 minp5 + minp6 + 2 p8ges + 2 delk)]
Print["Deltaj value = ", minp5]
Print["Deltajk value = ", minp6]
Print["Deltak value = ", minp7]
Print["deltaj value = ", minp8]
Print["deltak value = ", delk]

(*These commands will list the data by the six quantum numbers for the*)
(*transition, the observed transition location, the corresponding calculated*)
(*transition location, and the difference of the observed minus the calculated*)
(*transitions.*)
trtObs = Transpose[tObs];
AppendTo[trtObs,tCalculated];
AppendTo[trtObs,tObserved-tCalculated];
Print["_____"]
Print["|      Residuals      |"]
Print["_____"]
diff = Transpose[trtObs]

```

## Appendix D : List of Transitions

Number	Upper Level ( $\nu = 2$ )			Lower Level ( $\nu = 0$ )			Locations		Difference
	$J$	$K_a$	$K_c$	$J$	$K_a$	$K_c$	Observed	Calculated	
1	2	0	2	3	0	3	3562.2749	3562.308	-0.03348
2	3	0	3	4	0	4	3562.0408	3562.072	-0.03082
3	5	0	5	6	0	6	3561.6036	3561.606	-0.00240
4	6	0	6	7	0	7	3561.3811	3561.377	0.00396
5	7	0	7	8	0	8	3561.1555	3561.151	0.00459
6	8	0	8	9	0	9	3560.9355	3560.927	0.00818
7	9	0	9	10	0	10	3560.7187	3560.706	0.01234
8	10	0	10	11	0	11	3560.5006	3560.488	0.01258
9	11	0	11	12	0	12	3560.2831	3560.272	0.01079
10	12	0	12	13	0	13	3560.0674	3560.059	0.00818
11	13	0	13	14	0	14	3559.8569	3559.849	0.00816
12	14	0	14	15	0	15	3559.6468	3559.641	0.00592
13	15	0	15	16	0	16	3559.4375	3559.436	0.00186
14	16	0	16	17	0	17	3559.2319	3559.233	-0.00112
15	17	0	17	18	0	18	3559.0222	3559.033	-0.01083
16	18	0	18	19	0	19	3558.8179	3558.836	-0.01779
17	19	0	19	20	0	20	3558.625	3558.641	-0.01599
18	20	0	20	21	0	21	3558.4253	3558.449	-0.02368
19	21	0	21	22	0	22	3558.2335	3558.26	-0.02618
20	22	0	22	23	0	23	3558.044	3558.073	-0.02913
21	23	0	23	24	0	24	3557.8503	3557.889	-0.03907
22	2	1	2	3	1	3	3562.2146	3562.256	-0.04161
23	3	1	3	4	1	4	3561.982	3562.022	-0.03996
24	4	1	4	5	1	5	3561.7526	3561.79	-0.03770
25	5	1	5	6	1	6	3561.571	3561.561	0.00977
26	6	1	6	7	1	7	3561.3489	3561.335	0.01414
27	7	1	7	8	1	8	3561.125	3561.111	0.01411
28	8	1	8	9	1	9	3560.9004	3560.89	0.01075
29	9	1	9	10	1	10	3560.6758	3560.671	0.00476
30	10	1	10	11	1	11	3560.4608	3560.455	0.00571
31	11	1	11	12	1	12	3560.2414	3560.242	-0.00040
32	12	1	12	13	1	13	3560.025	3560.031	-0.00619
33	19	1	19	20	1	20	3558.5987	3558.634	-0.03539
34	2	1	1	3	1	2	3562.2146	3562.24	-0.02574
35	3	1	2	4	1	3	3561.982	3562.001	-0.01897
36	4	1	3	5	1	4	3561.7526	3561.764	-0.01162
37	5	1	4	6	1	5	3561.5235	3561.53	-0.00658
38	6	1	5	7	1	6	3561.3024	3561.299	0.00385
39	7	1	6	8	1	7	3561.075	3561.07	0.00541

40	8	1	7	9	1	8	3560.8544	3560.843	0.01123
41	11	1	10	12	1	11	3560.2035	3560.179	0.02461
42	12	1	11	13	1	12	3559.982	3559.962	0.01966
43	14	1	13	15	1	14	3559.556	3559.536	0.01974
44	15	1	14	16	1	15	3559.328	3559.327	0.00135
45	16	1	15	17	1	16	3559.12	3559.119	0.00075
46	17	1	16	18	1	17	3558.902	3558.914	-0.01200
47	2	2	1	3	2	2	3562.0408	3562.068	-0.02730
48	3	2	2	4	2	3	3561.8045	3561.831	-0.02679
49	4	2	3	5	2	4	3561.571	3561.597	-0.02609
50	5	2	4	6	2	5	3561.3489	3561.365	-0.01660
51	9	2	8	10	2	9	3560.48	3560.465	0.01491
52	10	2	9	11	2	10	3560.2414	3560.246	-0.00503
53	13	2	12	14	2	13	3559.5987	3559.606	-0.00702
54	18	2	17	19	2	18	3558.5548	3558.588	-0.03298
55	20	2	19	21	2	20	3558.1665	3558.198	-0.03113
56	21	2	20	22	2	21	3557.966	3558.006	-0.04013
57	22	2	21	23	2	22	3557.7746	3557.817	-0.04237
58	23	2	22	24	2	23	3557.5863	3557.63	-0.04384
59	2	2	0	3	2	1	3562.0408	3562.068	-0.02726
60	3	2	1	4	2	2	3561.8045	3561.831	-0.02671
61	4	2	2	5	2	3	3561.571	3561.597	-0.02593
62	5	2	3	6	2	4	3561.3489	3561.365	-0.01633
63	6	2	4	7	2	5	3561.125	3561.136	-0.01109
64	7	2	5	8	2	6	3560.9004	3560.909	-0.00909
65	9	2	7	10	2	8	3560.48	3560.464	0.01612
66	10	2	8	11	2	9	3560.2414	3560.245	-0.00342
67	11	2	9	12	2	10	3560.025	3560.028	-0.00323
68	12	2	10	13	2	11	3559.8092	3559.814	-0.00488
69	13	2	11	14	2	12	3559.5987	3559.602	-0.00365
70	14	2	12	15	2	13	3559.3844	3559.393	-0.00859
71	15	2	13	16	2	14	3559.1726	3559.186	-0.01337
72	16	2	14	17	2	15	3558.9614	3558.981	-0.01983
73	17	2	15	18	2	16	3558.7545	3558.779	-0.02424
74	18	2	16	19	2	17	3558.5548	3558.578	-0.02363
75	19	2	17	20	2	18	3558.3557	3558.38	-0.02454
76	21	2	19	22	2	20	3557.966	3557.99	-0.02391
77	22	2	20	23	2	21	3557.7746	3557.798	-0.02299
78	23	2	21	24	2	22	3557.5863	3557.607	-0.02074
79	4	3	2	5	3	3	3561.269	3561.297	-0.02785
80	5	3	3	6	3	4	3561.075	3561.065	0.00977
81	6	3	4	7	3	5	3560.8544	3560.836	0.01821
82	8	3	6	9	3	7	3560.388	3560.386	0.00212
83	13	3	11	14	3	12	3559.328	3559.305	0.02336

84	14	3	12	15	3	13	3559.12	3559.096	0.02412
85	15	3	13	16	3	14	3558.902	3558.89	0.01242
86	21	3	19	22	3	20	3557.676	3557.701	-0.02539
87	4	3	1	5	3	2	3561.269	3561.297	-0.02789
88	5	3	2	6	3	3	3561.075	3561.065	0.00971
89	6	3	3	7	3	4	3560.8544	3560.836	0.01812
90	8	3	5	9	3	6	3560.388	3560.386	0.00196
91	13	3	10	14	3	11	3559.328	3559.305	0.02292
92	14	3	11	15	3	12	3559.12	3559.096	0.02361
93	15	3	12	16	3	13	3558.902	3558.89	0.01185
94	21	3	18	22	3	19	3557.6931	3557.702	-0.00921
95	4	4	0	5	4	1	3560.8544	3560.877	-0.02247
96	7	4	3	8	4	4	3560.2035	3560.19	0.01371
97	8	4	4	9	4	5	3559.982	3559.966	0.01605
98	11	4	7	12	4	8	3559.328	3559.31	0.01822
99	12	4	8	13	4	9	3559.12	3559.096	0.02387
100	13	4	9	14	4	10	3558.902	3558.885	0.01702
101	17	4	13	18	4	14	3558.044	3558.065	-0.02102
102	18	4	14	19	4	15	3557.8503	3557.866	-0.01576
103	19	4	15	20	4	16	3557.645	3557.669	-0.02445
104	22	4	18	23	4	19	3557.064	3557.093	-0.02939
105	7	5	2	8	5	3	3559.6468	3559.65	-0.00354
106	8	5	3	9	5	4	3559.4375	3559.427	0.01097
107	12	5	7	13	5	8	3558.5548	3558.557	-0.00214
108	13	5	8	14	5	9	3558.3557	3558.346	0.00983
109	14	5	9	15	5	10	3558.1304	3558.137	-0.00690
110	19	5	14	20	5	15	3557.1214	3557.131	-0.00957
111	20	5	15	21	5	16	3556.9208	3556.937	-0.01600
112	21	5	16	22	5	17	3556.7338	3556.745	-0.01113
113	22	5	17	23	5	18	3556.5394	3556.555	-0.01590
114	23	5	18	24	5	19	3556.3503	3556.368	-0.01759
115	8	6	2	9	6	3	3558.7545	3558.768	-0.01330
116	9	6	3	10	6	4	3558.5548	3558.547	0.00822
117	11	6	5	12	6	6	3558.12	3558.112	0.00815
118	13	6	7	14	6	8	3557.6931	3557.687	0.00582
119	14	6	8	15	6	9	3557.4771	3557.479	-0.00166
120	15	6	9	16	6	10	3557.2766	3557.273	0.00387
121	16	6	10	17	6	11	3557.064	3557.069	-0.00515
122	17	6	11	18	6	12	3556.8403	3556.868	-0.02770
123	18	6	12	19	6	13	3556.6526	3556.669	-0.01667
124	19	6	13	20	6	14	3556.4507	3556.473	-0.02220
125	20	6	14	21	6	15	3556.249	3556.279	-0.02989
126	22	6	16	23	6	17	3555.8663	3555.898	-0.03146

127	23	6	17	24	6	18	3555.6668	3555.711	-0.04377
128	6	0	6	5	0	5	3564.537	3564.556	-0.01939
129	9	0	9	8	0	8	3565.369	3565.351	0.01759
130	10	0	10	9	0	9	3565.626	3565.621	0.00469
131	12	0	12	11	0	11	3566.1774	3566.168	0.00907
132	13	0	13	12	0	12	3566.4638	3566.445	0.01841
133	14	0	14	13	0	13	3566.749	3566.725	0.02420
134	16	0	16	15	0	15	3567.3	3567.291	0.00940
135	17	0	17	16	0	16	3567.575	3567.577	-0.00195
136	18	0	18	17	0	17	3567.8676	3567.866	0.00200
137	19	0	19	18	0	18	3568.162	3568.157	0.00545
138	20	0	20	19	0	19	3568.4468	3568.45	-0.00300
139	22	0	22	21	0	21	3569.0757	3569.043	0.03242
140	23	0	23	22	0	22	3569.3547	3569.344	0.01113
141	24	0	24	23	0	23	3569.6808	3569.646	0.03453
142	4	1	4	3	1	3	3563.9507	3563.968	-0.01700
143	5	1	5	4	1	4	3564.21	3564.222	-0.01242
144	7	1	7	6	1	6	3564.7257	3564.74	-0.01382
145	8	1	8	7	1	7	3564.9988	3565.002	-0.00311
146	9	1	9	8	1	8	3565.2755	3565.267	0.00863
147	11	1	11	10	1	10	3565.814	3565.805	0.00950
148	13	1	13	12	1	12	3566.349	3566.353	-0.00351
149	15	1	15	14	1	14	3566.919	3566.911	0.00801
150	16	1	16	15	1	15	3567.1886	3567.194	-0.00560
151	17	1	17	16	1	16	3567.4908	3567.48	0.01071
152	20	1	20	19	1	19	3568.3606	3568.354	0.00650
153	21	1	21	20	1	20	3568.6412	3568.651	-0.00980
154	23	1	23	22	1	22	3569.2747	3569.253	0.02136
155	24	1	24	23	1	23	3569.5628	3569.559	0.00391
156	5	1	4	4	1	3	3564.2516	3564.251	0.00100
157	6	1	5	5	1	4	3564.497	3564.514	-0.01669
158	7	1	6	6	1	5	3564.775	3564.779	-0.00435
159	8	1	7	7	1	6	3565.052	3565.048	0.00445
160	9	1	8	8	1	7	3565.319	3565.318	0.00074
161	10	1	9	9	1	8	3565.587	3565.591	-0.00444
162	14	1	13	13	1	12	3566.69	3566.708	-0.01812
163	16	1	15	15	1	14	3567.2634	3567.28	-0.01676
164	17	1	16	16	1	15	3567.575	3567.569	0.00558
165	18	1	17	17	1	16	3567.8676	3567.861	0.00684
166	6	2	5	5	2	4	3564.3182	3564.317	0.00163
167	8	2	7	7	2	6	3564.844	3564.845	-0.00055
168	9	2	8	8	2	7	3565.1134	3565.112	0.00108
169	10	2	9	9	2	8	3565.369	3565.383	-0.01360
170	11	2	10	10	2	9	3565.6682	3565.655	0.01285



171	12	2	11	11	2	10	3565.919	3565.931	-0.01156
172	16	2	15	15	2	14	3567.072	3567.056	0.01650
173	17	2	16	16	2	15	3567.3365	3567.343	-0.00614
174	18	2	17	17	2	16	3567.6452	3567.632	0.01311
175	19	2	18	18	2	17	3567.9288	3567.924	0.00498
176	20	2	19	19	2	18	3568.2167	3568.218	-0.00110
177	22	2	21	21	2	20	3568.854	3568.812	0.04159
178	24	2	23	23	2	22	3569.448	3569.416	0.03232
179	6	2	4	5	2	3	3564.3182	3564.317	0.00131
180	8	2	6	7	2	5	3564.844	3564.845	-0.00130
181	9	2	7	8	2	6	3565.1134	3565.113	0.00000
182	10	2	8	9	2	7	3565.369	3565.384	-0.01506
183	11	2	9	10	2	8	3565.6682	3565.657	0.01091
184	12	2	10	11	2	9	3565.919	3565.933	-0.01405
185	13	2	11	12	2	10	3566.2243	3566.211	0.01297
186	15	2	13	14	2	12	3566.794	3566.775	0.01867
187	16	2	14	15	2	13	3567.072	3567.061	0.01102
188	17	2	15	16	2	14	3567.369	3567.349	0.02001
189	18	2	16	17	2	15	3567.6452	3567.639	0.00587
190	22	2	20	21	2	19	3568.854	3568.823	0.03143
191	24	2	22	23	2	21	3569.478	3569.426	0.05190
192	4	3	2	3	3	1	3563.4948	3563.499	-0.00400
193	5	3	3	4	3	2	3563.742	3563.756	-0.01447
194	6	3	4	5	3	3	3564.0266	3564.017	0.00988
195	8	3	6	7	3	5	3564.537	3564.545	-0.00791
196	11	3	9	10	3	8	3565.369	3565.356	0.01280
197	12	3	10	11	3	9	3565.626	3565.632	-0.00562
198	14	3	12	13	3	11	3566.1774	3566.19	-0.01242
199	15	3	13	14	3	12	3566.4638	3566.473	-0.00874
200	16	3	14	15	3	13	3566.749	3566.758	-0.00863
201	17	3	15	16	3	14	3567.0339	3567.045	-0.01116
202	18	3	16	17	3	15	3567.3365	3567.335	0.00170
203	19	3	17	18	3	16	3567.6452	3567.627	0.01840
204	20	3	18	19	3	17	3567.9288	3567.921	0.00778
205	4	3	1	3	3	0	3563.4948	3563.499	-0.00397
206	5	3	2	4	3	1	3563.742	3563.756	-0.01442
207	6	3	3	5	3	2	3564.0266	3564.017	0.00997
208	8	3	5	7	3	4	3564.537	3564.545	-0.00768
209	11	3	8	10	3	7	3565.369	3565.356	0.01346
210	12	3	9	11	3	8	3565.626	3565.631	-0.00475
211	14	3	11	13	3	10	3566.1774	3566.188	-0.01098
212	15	3	12	14	3	11	3566.4638	3566.471	-0.00695
213	16	3	13	15	3	12	3566.749	3566.755	-0.00643
214	17	3	14	16	3	13	3567.0339	3567.042	-0.00850

215	18	3	15	17	3	14	3567.3365	3567.332	0.00488
216	19	3	16	18	3	15	3567.6452	3567.623	0.02216
217	20	3	17	19	3	16	3567.9288	3567.917	0.01218
218	8	4	4	7	4	3	3564.121	3564.125	-0.00434
219	9	4	5	8	4	4	3564.3835	3564.393	-0.00981
220	10	4	6	9	4	5	3564.675	3564.664	0.01120
221	11	4	7	10	4	6	3564.923	3564.937	-0.01379
222	12	4	8	11	4	7	3565.2327	3565.212	0.02043
223	13	4	9	12	4	8	3565.5081	3565.49	0.01789
224	14	4	10	13	4	9	3565.7726	3565.771	0.00201
225	15	4	11	14	4	10	3566.0412	3566.053	-0.01219
226	16	4	12	15	4	11	3566.349	3566.339	0.01043
227	18	4	14	17	4	13	3566.9124	3566.916	-0.00355
228	20	4	16	19	4	15	3567.527	3567.502	0.02452
229	21	4	17	20	4	16	3567.809	3567.799	0.00992
230	22	4	18	21	4	17	3568.131	3568.098	0.03314
231	23	4	19	22	4	18	3568.4157	3568.399	0.01694
232	24	4	20	23	4	19	3568.7286	3568.702	0.02686
233	10	5	5	9	5	4	3564.121	3564.125	-0.00386
234	11	5	6	10	5	5	3564.3835	3564.398	-0.01438
235	12	5	7	11	5	6	3564.675	3564.673	0.00163
236	13	5	8	12	5	7	3564.9627	3564.951	0.01138
237	14	5	9	13	5	8	3565.2327	3565.232	0.00101
238	15	5	10	14	5	9	3565.5081	3565.514	-0.00635
239	16	5	11	15	5	10	3565.814	3565.8	0.01443
240	18	5	13	17	5	12	3566.3996	3566.377	0.02281
241	19	5	14	18	5	13	3566.69	3566.669	0.02119
242	20	5	15	19	5	14	3566.9713	3566.963	0.00825
243	21	5	16	20	5	15	3567.2634	3567.259	0.00392
244	22	5	17	21	5	16	3567.575	3567.558	0.01696
245	23	5	18	22	5	17	3567.8676	3567.859	0.00890
246	7	6	1	6	6	0	3562.6702	3562.663	0.00737
247	8	6	2	7	6	1	3562.9358	3562.928	0.00737
248	11	6	5	10	6	4	3563.742	3563.74	0.00155
249	15	6	9	14	6	8	3564.8824	3564.858	0.02444
250	16	6	10	15	6	9	3565.1459	3565.143	0.00250
251	18	6	12	17	6	11	3565.735	3565.721	0.01368
252	19	6	13	18	6	12	3566.0412	3566.014	0.02745
253	22	6	16	21	6	15	3566.9124	3566.904	0.00791
254	24	6	18	23	6	17	3567.527	3567.509	0.01788
255	1	1	0	1	1	1	3562.979	3562.982	-0.00338
256	3	1	2	3	1	3	3563.022	3563.023	-0.00051
257	4	1	3	4	1	4	3563.052	3563.055	-0.00262
258	6	1	5	6	1	6	3563.1354	3563.143	-0.00750

259	9	1	8	9	1	9	3563.339	3563.335	0.00352
260	10	1	9	10	1	10	3563.4141	3563.416	-0.00161
261	11	1	10	11	1	11	3563.4948	3563.504	-0.00917
262	13	1	12	13	1	13	3563.685	3563.705	-0.01951
263	6	2	4	6	2	5	3562.844	3562.849	-0.00544
264	8	2	6	8	2	7	3562.883	3562.889	-0.00648
265	10	2	8	10	2	9	3562.9358	3562.941	-0.00507
266	11	2	9	11	2	10	3562.979	3562.971	0.00803
267	13	2	11	13	2	12	3563.052	3563.04	0.01173
268	18	2	16	18	2	17	3563.289	3563.27	0.01904
269	3	3	0	3	3	1	3562.5217	3562.51	0.01197
270	4	3	1	4	3	2	3562.5217	3562.52	0.00157
271	5	3	2	5	3	3	3562.5217	3562.533	-0.01140
272	9	3	6	9	3	7	3562.601	3562.61	-0.00925
273	11	3	8	11	3	9	3562.6702	3562.664	0.00665
274	4	4	0	4	4	1	3562.0892	3562.1	-0.01109
275	5	4	1	5	4	2	3562.0892	3562.113	-0.02413
276	7	4	3	7	4	4	3562.15	3562.147	0.00282
277	8	4	4	8	4	5	3562.15	3562.168	-0.01796
278	10	4	6	10	4	7	3562.2146	3562.217	-0.00257
279	12	4	8	12	4	9	3562.2749	3562.276	-0.00158
280	17	4	13	17	4	14	3562.477	3562.468	0.00923
281	18	4	14	18	4	15	3562.5217	3562.513	0.00850
282	22	4	18	22	4	19	3562.745	3562.718	0.02724
283	5	5	0	5	5	1	3561.571	3561.574	-0.00304
284	7	5	2	7	5	3	3561.6036	3561.608	-0.00429
285	10	5	5	10	5	6	3561.666	3561.678	-0.01175
286	12	5	7	12	5	8	3561.7526	3561.737	0.01580
287	17	5	12	17	5	13	3561.933	3561.926	0.00670
288	6	6	0	6	6	1	3560.9355	3560.931	0.00423
289	7	6	1	7	6	2	3560.9355	3560.95	-0.01408
290	8	6	2	8	6	3	3560.972	3560.97	0.00154
291	12	6	6	12	6	7	3561.075	3561.08	-0.00453
292	13	6	7	13	6	8	3561.125	3561.113	0.01191
293	15	6	9	15	6	10	3561.201	3561.188	0.01339
294	20	6	14	20	6	15	3561.4323	3561.416	0.01646

### *Vita*

Second Lieutenant Todd E. Wiest was born November 30, 1969 in Sunbury, Pennsylvania. He graduated from Line Mountain High School in Herndon, Pennsylvania in 1988, and upon graduation, Todd received a Reserve Officer Training Corps (ROTC) scholarship. He attended college at Wilkes University, Wilkes - Barre, Pennsylvania where he was a member of ROTC Detachment 752. In January of 1993, Todd graduated from college and was commissioned. While awaiting an active duty assignment, he worked as a consultant on a lens defect detection system at Wilkes University. His initial active duty assignment was to the Air Force Institute of Technology where he entered the School of Engineering to study Engineering Physics in June, 1993. Upon graduation, Todd will be reassigned to Rome Laboratory, Griffiss AFB, Rome, New York.

Permanent Address:

RD 1, Box 1636

Herndon, PA 17830

REPORT DOCUMENTATION PAGE			Form Approved OMB No. 0704-0188	
Public reporting burden for this collection of information is estimated to average 1 hour per response, including the time for reviewing instructions, searching existing data sources, gathering and maintaining the data needed, and completing and reviewing the collection of information. Send comments regarding this burden estimate or any other aspect of this collection of information, including suggestions for reducing this burden, to Washington Headquarters Services, Directorate for Information Operations and Reports, 1215 Jefferson Davis Highway, Suite 1204, Arlington, VA 22202-4302, and to the Office of Management and Budget, Paperwork Reduction Project (0704-0188), Washington, DC 20503.				
1. AGENCY USE ONLY (Leave blank)		2. REPORT DATE December 1994		3. REPORT TYPE AND DATES COVERED Masters Thesis
4. TITLE AND SUBTITLE HIGH RESOLUTION FOURIER TRANSFORM SPECTROSCOPY OF THE FIRST OVERTONE OF THE N-O STRETCH IN NITROSYL BROMIDE				5. FUNDING NUMBERS
6. AUTHOR(S) Todd E. Wiest, Second Lieutenant, USAF				
7. PERFORMING ORGANIZATION NAME(S) AND ADDRESS(ES) Air Force Institute of Technology Wright-Patterson AFB OH 45433-6583				8. PERFORMING ORGANIZATION REPORT NUMBER AFIT/GAP/ENP/94D-11
9. SPONSORING/MONITORING AGENCY NAME(S) AND ADDRESS(ES) The Philips Laboratory (PL/LID) Dr. Ernest A. Dorko Kirtland AFB NM 87117-6008				10. SPONSORING/MONITORING AGENCY REPORT NUMBER
11. SUPPLEMENTARY NOTES				
12a. DISTRIBUTION / AVAILABILITY STATEMENT  Approved for public release; distribution unlimited				12b. DISTRIBUTION CODE
13. ABSTRACT (Maximum 200 words)  Infrared Fourier transform spectroscopy of the first overtone of the nitric oxide (NO) bond stretch in nitrosyl bromide (ONBr) has been performed at a resolution of $0.02 \text{ cm}^{-1}$ to obtain the rotational parameters of the $v_1 = 2$ energy level. Roughly 1000 transitions have been observed for rotational levels up to $J = 80$ and $K_a = 7$ . The calculation of the complete set of rotational energy levels of this asymmetric molecule requires the numerical diagonalization of four, tridiagonal matrices for each $J$ . From a non-linear least squares fit of observed transitions with $J \leq 40$ using an approximation for the energy levels, the maximum $J$ value accurately approximated was determined to be twenty-four. The fit was reaccomplished for $J \leq 24$ and the following rotational parameters were obtained: $v_0 = 3563.03442 \pm 0.00092$ , $A = 2.793526 \pm 0.000055$ , $B = 0.1264969 \pm 0.0000056$ , $C = 0.1207390 \pm 0.0000022$ , $\Delta_J = (1.649 \pm 0.038) \times 10^{-7}$ , $\Delta_{JK} = (-2.23 \pm 0.17) \times 10^{-6}$ , $\Delta_K = (1.577 \pm 0.025) \times 10^{-4}$ , and $\delta_J = (1.22 \pm 0.29) \times 10^{-8} \text{ cm}^{-1}$ . The Monte Carlo analysis suggests the need to use higher $J$ levels to determine the distortion constants.				
14. SUBJECT TERMS Fourier Transform Spectroscopy, Nitrosyl Bromide, Asymmetric Molecule, Rotational Spectrum, Perturbation Techniques				15. NUMBER OF PAGES 116
				16. PRICE CODE
17. SECURITY CLASSIFICATION OF REPORT Unclassified		18. SECURITY CLASSIFICATION OF THIS PAGE Unclassified		19. SECURITY CLASSIFICATION OF ABSTRACT Unclassified
				20. LIMITATION OF ABSTRACT UL